Fermi National Accelerator Laboratory

FERMILAB-TM-2060

An RF Separated Kaon Beam from the Main Injector: Superconducting Aspects

D.A. Edwards

Fermi National Accelerator Laboratory
P.O. Box 500, Batavia, Illinois 60510

November 1998

Operated by Universities Research Association Inc. under Contract No. DE-AC02-76CH03000 with the United States Department of Energy

An RF Separated Kaon Beam from the Main Injector: Superconducting Aspects

J. D. Fuerst, M. S. McAshan
Cryogenic Department, Beams Division

Y. Terechkine
Engineering, Technical Division

R. N. Coleman, T. R. Kobilarcik, H. B. White
External Beams Department, Beams Division

M. H. Foley
Mechanical Support Department, Beams Division

H. T. Edwards, W. H. Hartung, K. P. O. Koepke, M. Kuchnir
Photoinjector/SCRF Group, Beams Division

T. W. Koeth, G. B. Thomson
Physics Department, Rutgers University

J. E. Dey
RF and Instrumentation Department, Beams Division

J. Doornbos
TRIUMF

D. A. Edwards, Editor
Deutsches Elektronen-Synchrotron DESY

October 19, 1998

Contents

1 Introduction

1.1 Main Injector Context

The Fermilab Main Injector will produce intense extracted beams of protons of momentum 120 GeV/c for fixed target experiments. This is the first time such beams will be available, and they will make possible new types of experiments in kaon physics. A high flux of secondary kaons will occur at a momentum of 22-25 GeV/c, which is a fine range for making pure $K^{\pm}$ beams by the technique of RF-separation. The charged kaon beams can be used for studies of rare decays of K^{+} and K^{-} mesons, and can be used to make neutral kaon beams as well. In the interaction of $K^{\pm}$ mesons with matter charge exchange scattering forms about 20% of the total cross section, and in such scattering events a K^{+} (K^{-}) beam will produce an almost pure K^{0} ($\overline{K}^{0}$) meson beam. This is a valuable characteristic for experiments that study $K_L - K_S$ interference.

The Main Injector cycle time will be three seconds, and the slow extracted beam spill will be of one second duration within that. This high duty factor requires that a separated beam employ superconducting RF technology to bring power demands within reason: hundreds of watts as opposed to many megawatts. In addition, with the operation of the Main Injector, fixed target experiments may operate simultaneously with the operation of collider experiments, a capability which did not exist during the Main Ring era.

1.2 Basic Separator Principle

The idea of RF separated kaon beams has been around for a long time.[1.1] Using conventional (room-temperature) RF, such beams were built at ANL, BNL and CERN. A superconducting version was in use at CERN some 20 years ago.

The principle is as follows. The primary proton beam strikes a thick target, and the emerging hadrons pass through a momentum selection stage. The particles then are primarily a mix of protons, pions, and kaons of the same momentum but of differing speeds. Speed selection is accomplished by two RF stations that are designed to provide transverse deflection. The resonant frequency, the relative phase, and the distance between the stations are selected so that kaons will be transmitted to the users, while pions and protons will be rejected.

Because of the relatively short charged kaon lifetime, 12 ns in its restframe, it is desirable to keep the beam line short. So one designs for a phase difference between pions and kaons at the second deflection station of …=2. At the energies of interest here, the pion speed will be very close to that of light. Expressed in terms of the product of the frequency, f, of the separator system, and the distance, L, between the deflection stations this condition is:

$$f L = c°^{2}_{K}=2 \tag{1.1}$$

where c is the speed of light and $°_K$ is the Lorentz factor of the kaon. In the same spirit, the condition that pions and protons differ in phase by 2… so that they will be deflected in the same direction is

$$f L = 2c°^{2}_{p} \tag{1.2}$$

A consequence of these (approximate) relations is that the kaon and proton masses should differ by a factor of two, as is fortunately close to being the case.

Once a decision is made on the desired kaon energy, the frequency-length product is fixed. Since neither the frequency nor the length is easily changed after construction, the phase relationships are valid for only one energy. So a question arises about the energy range over which the phase relationships are adequately satisfied. At this writing, the two experiments that have expressed interest in a separated kaon beam in their present design differ in energy: 22 and 25 GeV.

[1.1] See references at end of Sec. 3

1.3 Comments on Superconducting RF

The application of superconducting RF to particle accelerators has grown rapidly since the beginning of effort in this direction at the Stanford High Energy Physics Laboratory in 1965. Today there are about 500m of structures installed in a variety of accelerators througout the world.

The progress in higher accelerating gradient structures at Cornell, DESY, KEK, Saclay, and Jefferson Laboratory is impressive, and it is desirable to exploit this development here. Only six or so years ago, design gradients were at about the 5 MeV/m level; today, at DESY, a significant number of multi-cell cavities perform above 20 MeV/m and one has exceeded 30 MeV/m. (The limit for solid niobium cavities is about 55 MeV.)

Improvements in cavity shape have played some role in the gradient improvement, but the main reason is attention to material quality, care in cavity fabrication, and painstaking processing procedures.

The material of interest is niobium sheet. The residual resistance ratio (the ratio of the room temperature resistivity to that just above the superconducting state) is a measure of the material purity. Over recent years, niobium with a residual resistivity ratio in excess of 300 has become available, in contrast to the value of 30 typical of impure niobium The importance of elimination of inclusions has led to detailed examination of the sheet after rolling.

The predominant cavity shaping technique is deep drawing of half-cells, following by electron beam welding of a number of half-cells into a multicell cavity. The welding environment is critical to avoid impurity absorption into the niobium and to insure high quality circumferential welds, especially at the equators of the cells where the surface current flows transverse to the welds.

Following fabrication, processing is carried out to improve thermal conductivity by high temperature vacuum gettering employing titanium. Surfaces are treated to remove potential field emitters, such as particulate matter which adheres to the inner suface of the resonator. To date, this activity has been generally carried out at or near the site of use. Much of the infrastructure has become widespread and readily available from commercial sources due to the microelectronic and pharmaceutical industries, for example, cleanrooms and ultrapure water.

Processing is apt to be an iterative process. Initial RF tests are carried out in a vertical dewar, for ease of test assembly. If cavity performance is deemed inadequate, it is returned for further processing. If adequate in the vertical test, the cavity is enclosed in a permanent helium vessel, requiring further electron beam welds, tested horizontally and a number of such assemblies are installed in a single cryostat.

1.4 Scope of this Report

This report is intended to focus on the superconducting aspects of a potential separated kaon beam facility for the Main Injector, and most of this document reflects that emphasis. However, the RF features cannot be divorced from the overall beam requirements, and so the next section is devoted to the latter subject. The existing optics design that meets the needs of the two proposed experiments is outlined, and its layout at Fermilab is shown. The frequency and deflection gradient choices present implementation difficulties, and the section closes with some commentary on these issues.

Sec. 3 provides an introduction to cavity design considerations, and, in particular carries forward the discussion of resonator shape and frequency selection. The R&D program is the subject of Sec. 4. Provisional parameter choices will be summarized. Initial steps toward cavity fabrication based on copper models have been taken. The next stages in cavity fabrication will be reviewed in some detail. The infrastructure needs and availability will be discussed.

Sec. 5 discusses what may be characterized as the ingredients of a point design. At this writing, some aspects are clear and some are not. The basic systems are reasonably clear and are described. The final section presents a cost and schedule estimate for both the R&D and production phase. Some supporting material and elaboration is provided in the Appendices.

2 Beam Requirements

2.1 The CP/T and CKM Experiments

The CP/T and CKM experiments have been proposed to use the Main Injector 120 GeV/c extracted beam and an RF-separated K^+ beam at 25 and 22 GeV/c respectively. The aims of the CP/T experiment are to perform studies of CP violation in K^0 meson decays and to test the conservation of CPT symmetry with sensitivity at the Planck scale. The CKM experiment aims to measure the branching ratio for the rare decay $K^+ \to \ldots^+ \nu\bar{\nu}$, from which the magnitude of the Cabbibo, Kobayashi, Maskawa (CKM) matrix element V_{td} can be determined. The aim of the CKM experiment is to collect 100 events, from which the magnitude of V_{td} can be calculated to 10% total uncertainty.

In the CP/T experiment the function of the RF-separated K^+ beam is to make a beam of pure K^0 mesons by charge exchange scattering. This maximizes the $K_L - K_S$ interference from which the CP and CPT tests are made. In the CKM experiment the function of RF-separation is to reduce the flux of unwanted pions and protons in the secondary beam. An unseparated beam made in this way contains about 10 times more pions and 3 times more protons than kaons. Using the unseparated beam would reduce the interference seen in the CP/T experiment by about an order of magnitude. The rate of pions and protons would swamp the detectors of the CKM experiment. Neither experiment can be performed without the RF-separated K^+ beam.

The CP/T experiment needs a flux of $2.4 \times 10^8 K^+$ per spill in a focus of radus 0.5 cm at the charge exchange target, and can handle about 10% impurities in the beam. The CKM experiment needs a flux of 3×10^7. Initially, CKM specified a single parallel beam (divergence less than ± 100 μrad) of kaons entering the experiment. However, recently this has been re-evaulated and there may be advantages to less parallism and exploiting the phase space hole (discussed below in Sec. 2.2). Essentially CKM might use two beams in its detector. The CKM experiment can handle up to 30% impurities.

Although at this time no further proposals have been submitted to the Laboratory to use the RF-separated K^+ beam, other kaon experiments could be done here, and the beam could be modified to produce antiprotons as well.

2.2 Existing Optics Design

Jaap Doornbos of TRIUMF designed an RF-separated K^+ beam as part of the plans for the KAON accelerator proposed for TRIUMF[2.1]. He modified his design for the specific needs of the CP/T and CKM experiments, and is a member of the CP/T collaboration. Fig. 2.1 shows a plan view of the beam line, and indicates how the CPT and CKM experiments could share the same K^+ beam. What is shown is a version of the design that uses two RF cavity stations, and would work only over a very restricted range of momenta. By adding a third RF cavity between the two shown in the figure a much wider set of momenta can be accommodated with good purity. Either of these designs produces a beam after the stopper which is quite pure, but which has a hole in its phase space due to the particles removed by the stopper. The addition of another RF cavity after the stopper, which is run in the opposite phase (for kaons) from the second RF cavity shown in the figure, would have the effect of reducing the size of this phase space hole. It would produce a small spot size at the target for CP/T, and a smaller beam envelope for CKM. Fig. 2.2 shows (for the CP/T branch of the beam) the beam line optical elements and beam size in x and y, as a function of z. The first quadrupoles collect the K^+'s and focus them in x at a point between bending magnets B2 and B3,

[2.1] J. Doornbos, RF Separated Kaon and Antiproton Beam for Momenta from 10 to 20 GeV/c at KAON, Saturne Rapport Interne LNS/GT/92-12. J. Doornbos and P. Pile designed the (electrostatically) separated K^+ beam for Brookhaven experiment E787 as well. See TRIUMF design notes TRI-DN-97-24 and TRI-DN-97-25. In E787 design they were very careful in minimizing aberrations, and by this approach were able to improve the purity of the E787 beam by a factor of 18. This same approach has been very successful in the design of the Fermilab beam also.

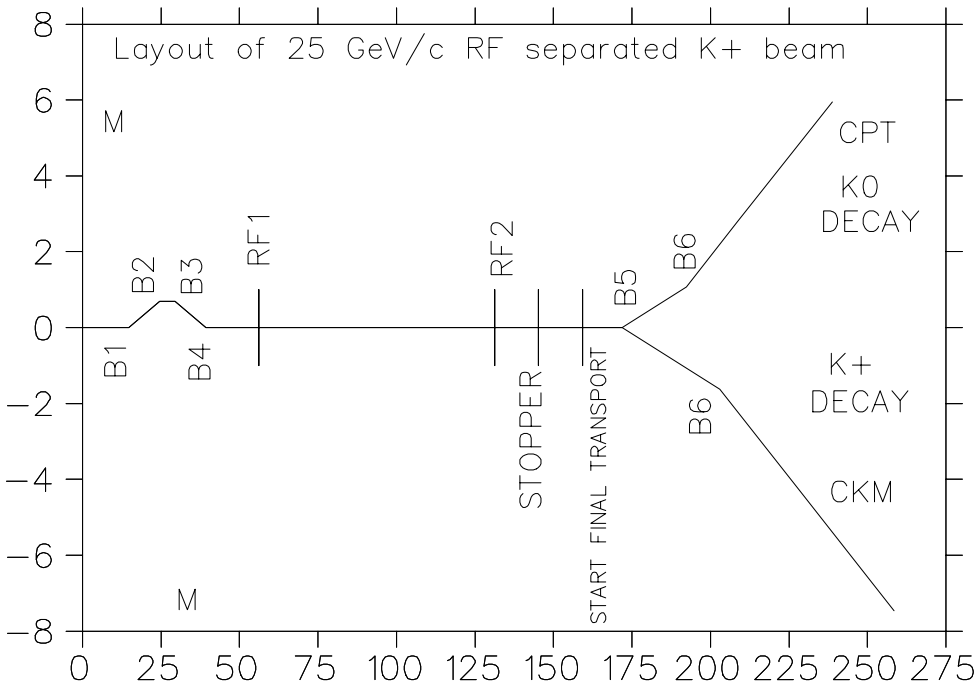

Figure 2.1: Plan View of the K^+ Beam

where a momentum slit selects the central momentum and momentum width of the beam. The proton dump is located after the first bending magnet. The quadrupoles before the first RF cavity transform the large y' acceptance into a small divergence (0.6 mrad) so the 1.2 mrad kick of the first RF cavity dominates the particles' angles. Two (-1) matrix quadrupole strings follow which give a net (+1) transformation, and the second RF cavity (RF2) is run at opposite phase (for pions) from the first. The next quadrupoles transform y' into y at the stopper. After that the beam is cleaned up with bending magnets and (for the CP/T experiment) focused on the K^0 production target. The spot size at the target is about 5 mm in diameter. The CKM branch of the beam uses quadrupoles to reduce the divergence of the beam, and achieves the CKM experiment's divergence goals. To do this the acceptance of the beam at the production target must be reduced, and the beam intensity is lower by about an order of magnitude, but this also falls within the experiment's requirements. This is a highly symmetric design which minimizes higher order aberrations. Using the TRIUMF Monte Carlo program REVMOC, which has been tested to give identical results to DECAY TURTLE, the acceptance of the beam has been calculated, taking into account kaon decays. Fig. 2.3 shows the y coordinate of pions and kaons at the location of the stopper for the CP/T experiment. It can be seen from the figure that the physical size of the stopper should be about 16 mm ($\pm$8 mm), and that about half of the kaons are transported past it. With 5×10^{12} protons per pulse at 120 GeV/c striking the target at 0 mrad, a flux of 2.4×10^8 kaons per pulse results, which is what the CP/T experiment requires.

2.3 Estimates of Achievable Rejection Ratio

The prediction of TRANSPORT and REVMOC is that the beam will have a clean trajectory. One might expect that the main source of backgrounds would be interactions in the stopper. This expectation using the Doornbos design, was tested by experimenters in the Rutgers University

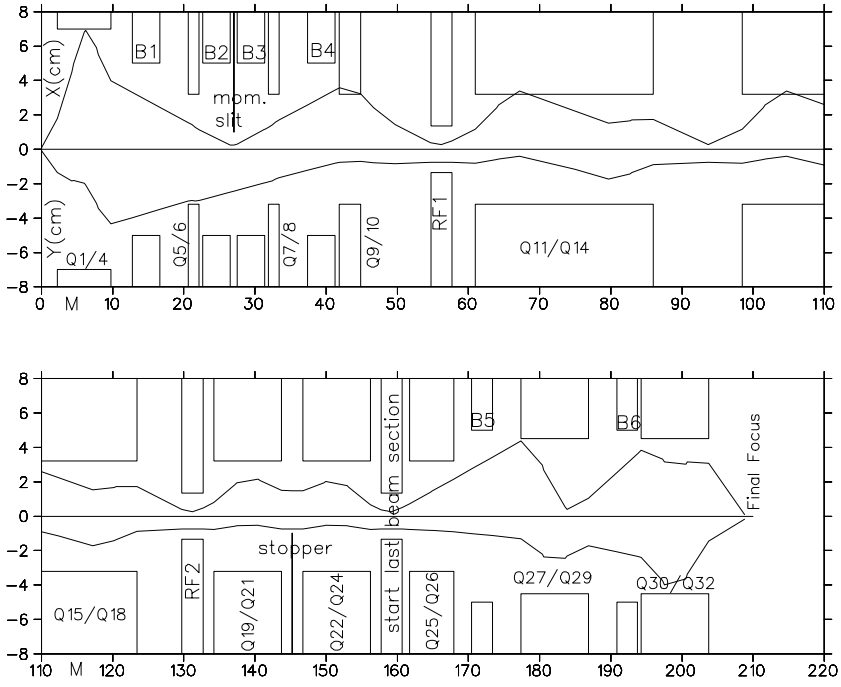

Figure 2.2: K^+ Beam Line Elements and Beam Sizes

group for the CP/T configuration by putting the stopper and the magnets following it, in a GEANT simulation and using the phase space of pions, protons, and kaons determined from REVMOC as the input parameters of beam particles. Very little background resulted from pions hitting the stopper, probably because they are heading into the material, but kaons that just clip the edge did produce pions of only slightly lower energy that were closer to the beam phase space. They were few in number, and can be removed by collimators just before the B5 bending magnet.

Continued GEANT studies of the beam indicate that two additional sources of backgrounds have been found. One comes from scattering in the vicinity of the first RF cavity. This produces about 2% background in the beam, which is well within the needed cleanliness. The other comes from pions in the tails of the beam which pass through the material of the second RF cavity and hence do not see all of its field. These pions number about 1% of kaons. These GEANT calculations are not yet complete, but the results so far are quite promising.

2.4 Contribution from Fermilab External Beams Group

The first beam design under study included components that fit the expectations for specific RF frequencies, beam geometries and magnet strengths. As a cost reduction practice, the Fermilab external beams department has earmarked available magnets and conventional beam components that could be used for this beam. The magnets are listed in Table 2.1 and a plan view of the beam layout for the Meson Area in Fig. 2.4. The reference optics using these existing magnets and beam components as input, are being studied by members of the external beams department, namely Tom Kobilarcik, Richard Coleman and others, as well as J. Doornbos of TRIUMF. Using these existing Fermilab magnets in another GEANT simulation, R. Coleman also investigated backgound contamination of the K^+ beam. This simulation of the CKM configuration finds that excellent beam purity is possible (the ratio of non-kaon hadrons to all charged particles ≈a few percent) as long as

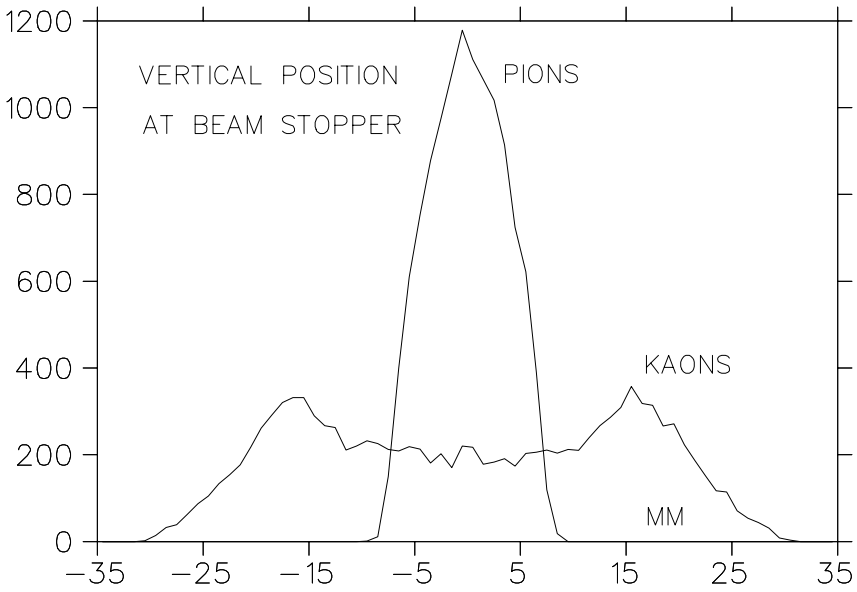

Figure 2.3: y Coordinate of Pions and Kaons at the Stopper

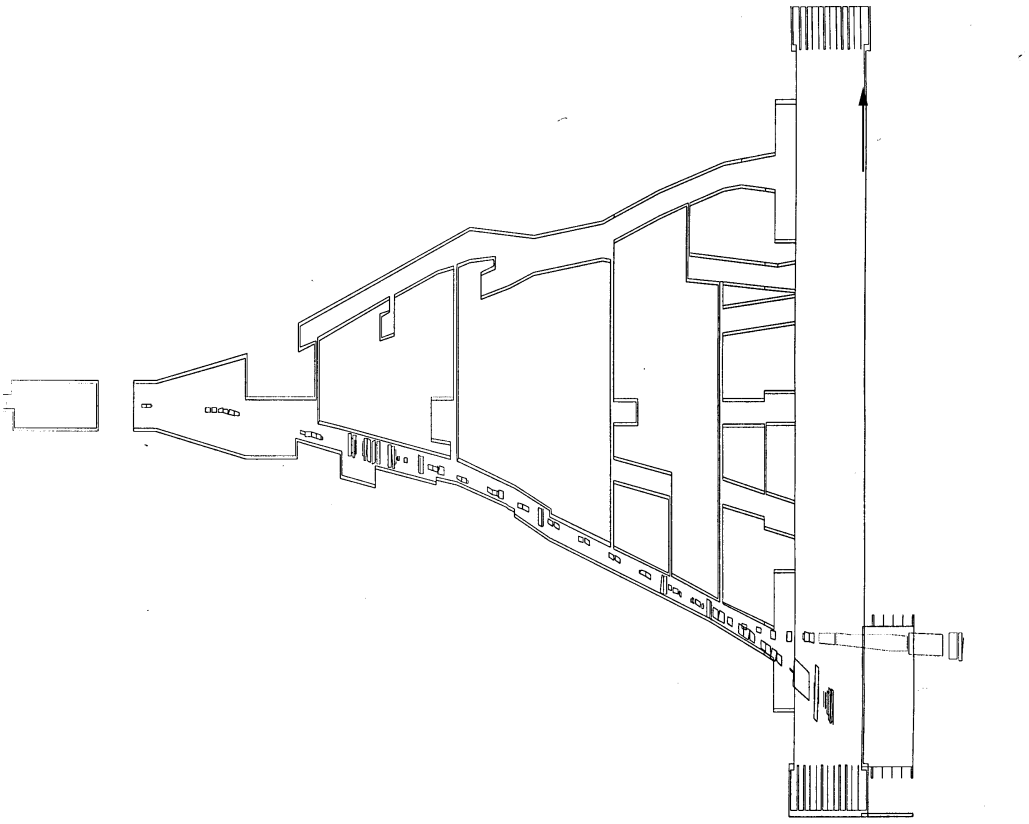

Figure 2.4: Beam layout in the Meson East area. The element distribution is that for the lowest (S-band) frequency possibility.

the beam stopper is made sufficiently wide. Muon contamination is of order 10% of the kaon beam at the CKM experiment.

These results are consistent with the results of previous RF-separated beams, for example the CERN u3-4 beams. Tab. 2.2 and Tab. 2.3 list a few of the characteristics of previously built RF separated beams.

Constraints imposed by the frequency of the RF cavities, the length of the beam line, desired beam charactieristics, and utilizing existing facilities will contribute to the final design.

2.5 Comments on RF Implementation

A study of the implications of the design above for superconducting RF led to the conclusions that the frequency choice of 5.8 GHz was too high and that the deflection gradient strength of 10 MV/m was too large. The reasoning and calculations will be detailed in the next two sections; here only the highlights are presented.

Regarding frequency, there are several arguments. It is desirable to capitalize on the R&D effort of recent years, and not stray farther than necessary from designs that have sucessfully minimized the risk of multipacting. A 5.8 GHz design with an iris adequate for beam transmission would be far from the TESLA proportions. In a more quantitative vein, the scaling of surface resistivity with frequency leads to increase in both RF power and cryogenic capacity. Further, this same growth of surface resistivity with frequency leads to a heat transfer instability in the neighborhood of 5.8 GHz. A frequency of 3.9 GHz was selected for the near-term R&D effort.

Regarding deflection gradient, the difficulty is that the maximum surface magnetic field for a deflecting mode is higher than that for the accelerating mode of equal strength as measured in MV/m. The choice of 10 MV/m corresponds in peak magnetic field to a TESLA cavity operating at 42 MV/m. TESLA cavities are now, after six years of intense effort, achieving 25 MV/m with some reliability. It may be possible to offset the implied reduction in deflection strength by a reduction in the secondary beam phase space. The spot size on the production target used in the design is considerably larger than that regularly achieved in targetting for anti-proton production. A similar capability in targetting for the kaon beam could reduce the maximum transverse kick required at a deflection station, provided a suitable revision in the post-target beam optics were possible.

The complete layout associated with the existing design would require four deflection stations to provide a range of kaon energies and to provide phase space recombination after the stopper. A more compact arrangement insofar as distribution of RF and cryogens that satisfies the same desires may be accomplished by a two-station version with two transverse-degree-of-freedom deflection. Some elaboration of this remark may be found in Appendix A.1. Again, for this change to be advantageous, a compatible beam optics would need to be devised.

Table 2.1: Available Fermilab Magnets

Magnet	Quantity	Type	Field/Gradient
Q11	2	10Q36	5.0
Q12	3	8Q32	3.9
Q13	2	10Q36	2.9
B1	8	4-9-39	15.0
B2	4	BM105	16.2
Q31	1	3Q60	3.0
Q32	1	3Q60	1.9
Q41	8	3Q120	1.7
Q51	4	3Q60	3.0
Q52	2	3Q120	2.7
Q61	1	4Q120	2.7
Q62	1	4Q120	1.9
B5	2	6-3-120	14.3
AQ11	2	4Q120	2.3
AQ12	1	4Q120	2.9
AQ21	1	4Q120	1.5
AQ22	1	4Q120	2.9
AQ23	1	4Q120	2.5
BQ11	2	3Q120	0.8
BQ21	1	4Q120	0.4
BQ22	1	4Q120	1.0
BQ23	1	4Q120	0.8

Table 2.2: RF Separated Beams

Beam/ Period	Proton Energy (GeV)	Secondary Energy type (GeV)	Pulse Length/ Power	Fill /cycle time	Beam Length (m)	Target to RF (m)	Intercavity Length (m)	RF to Expt (m)
AGS North area to 80in BC/ 1965	25	12.8 $K^{\pm}$ 9.0 $K^{\pm}$ 7.4 $K^{\pm}$ 14.0-18.5 $\pi^{\pm}$	2.7 μsec/ 14MW	0.5 μsec/ 2.5 sec	129	50	40	39
CERN U3 Jan 1965	19-20	14-16 $K^{\pm}$ 16-18 $\pi^{\pm}$ ~ 13 $\overline{p}$	8.0 μsec/ 10-12MW	0.5 μsec/ 1 sec	167	58	50	59
CERN U4 Jun 1967	19-20	7-16 $K^{\pm}$,$\pi^{\pm}$ 7-18 $\overline{p}$	8.0 μsec/ 10-12MW	0.5 μsec/ 1 sec	167	NA	22 25	NA
CERN S1 Fall 1977 Super-Conducting	200	37 $\overline{p}$ 26 $\overline{p}$ $K^{\pm}$, $\overline{p}$			234	77	83	74
Proposed FNAL- 2002	120	22-25 $K^{\pm}$	1 sec $\sim$ 300W	NA 3 sec	207 CPT 225 CKM	57	75	75 CPT 93 CKM

Table 2.3: RF Separated Beams, cont.

Beam/ Period	Cavity Type/ Number	Cavity Mode	Cavity Length (m)	Cavity Field MV/m	Acc'pt Angle at Tgt Horz (mrad)	Acc'pt Angle at Tgt Vert (mrad)	Solid Angle (μster)	Δp/p %
AGS North area to 80in BC/ 1965	S-Band 2 cavities	$\pi/2$ HEM11	3	6	~ 1	~ 1	6.6	± 1.2
CERN U3 Jan 1965	S-Band 2 cavities	$\pi/2$ HEM11	Two 3 m	7	± 7.5	± 5	150	$\pm .25$
CERN U4 Jun 1967	S-Band 3 cavities	$\pi/2$ HEM11	Added 3rd 2 m	7	± 7.5	± 5	150	$\pm .25$
CERN S1 Fall 1977 Super-Conducting	S-Band 2 cavities	$\pi/2$	2.74	1.2 - 1.4	± 8	± 2	64	± 2.0
Proposed FNAL- 2002 Super-Conducting	C-Band 2 cavities	π	~ 2	10	± 7	± 4.5	126	$\sim \pm 2.0$

3 Superconducting Cavity Principles

3.1 Deflecting Modes

Pillbox Modes

The transverse momentum imparted to a particle passing at a constant velocity through a localized region of time-harmonic electromagnetic field can be given as [4]:

$$\vec{p} = -ev\int_{t_1}^{t_2} \vec{\nabla}_T \frac{i}{\omega} E_z dt \tag{3.1}$$

Here v is the particle velocity taken to be in the z direction ($z = z_0 + vt$) and E_z is the longitudinal component of the electric field which may be a function of the transverse variables, z and t. Thus in a resonator it is the transverse gradient of the axial electric field that provides the transverse force in a deflection mode while it is the field itself that provides the longitudinal force in an accelerator mode.

Table 3.1: Monopole and Dipole TM Fields in the Cylindrical Pillbox (see also [1])

	TM010	**TM1n0**
1.	$E_z = E_0 J_0(k_0 r)$	$E_z = E_0 J_1(k_n r)\cos\phi$
2.	$H_\phi = -i\frac{E_0}{Z_0} J_0'(k_0 r)$	$H_\phi = -i\frac{E_0}{Z_0} J_1'(k_n r)\cos\phi$
3.	$H_r = 0$	$H_r = -i\frac{E_0}{Z_0}\frac{J_1(k_n r)}{k_n r}\sin\phi$
4.	$\vec{\nabla}_T E_z = \hat{r} E_0 k J_0'(k_0 r)$	$\vec{\nabla}_T E_z = E_0(\hat{r} k_n J_1'(k_n r)\cos\phi - \hat{\phi}\frac{J_1(k_n r)}{r}\sin\phi)$
5.	$\frac{i}{\omega}\vec{\nabla}_T E_z\Big\|_{r=0} = 0$	$\frac{i}{\omega_n}\vec{\nabla}_T E_z\Big\|_{r=0} = \hat{x}\frac{iE_0}{2c}$
6.	$V_L = E_0 LT$	$V_T = \frac{E_0 LT}{2}$
7.	$k_0 a = \frac{\omega_0}{c} a = u_{01} = 2.40483$	$k_n a = \frac{\omega_n}{c} a = u_{1n} : u_{11} = 3.83171$
8.	$U = E_0^2 \frac{\varepsilon_0}{2}\pi a^2 L J_1^2(u_{01})$	$U = E_0^2 \frac{\varepsilon_0}{4}\pi a^2 L J_1'^2(u_{1n})$
9.	$G_1 = Z_0 \frac{u_{01}}{2}\left(\frac{1}{a/L + 1}\right)$	$G_1 = Z_0 \frac{u_{1n}}{2}\left(\frac{1}{a/L + 1}\right)$
10.	$G_2 = \frac{4Z_0}{u_{01}^2 J_1^2(u_{01})}$	$(G_2)' = \frac{2Z_0}{u_{1n}^2 J_1'^2(u_{1n})}$

In the situation where deflection in one plane is required, cavity fields of dipole symmetry must be produced. In order to see how this works the monopole and dipole TM modes of the cylindrical pillbox are compared in Table 3.1.

The fields of the TM010 mode are familiar. The electric lines are parallel to the z axis, and the magnetic lines form circles about it. The dipole modes have no electric field on the axis, but instead have 2n regions of electric field located along the x- axis. The magnetic lines form loops around the electric lines. Figure 3.1 illustrates the field lines of the TM110 mode, and Table 3.2 gives field values in several locations in the cell.

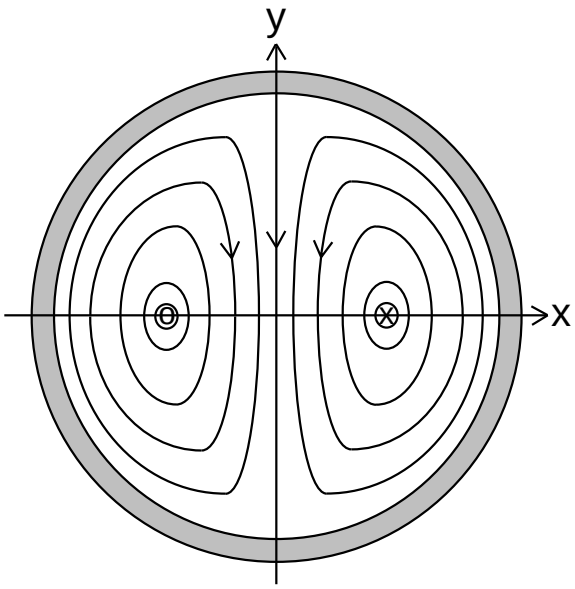

Figure 3.1 TM110 Magnetic Field Shape

Line 4 of Table 3.1 gives the transverse gradient of E_z and line 5 the value of this gradient on the axis. Line 6 defines two voltages, the accelerating voltage for the TM010 mode,

$$V_L = \int_{-L/2}^{L/2} E_z \cos(\frac{c}{v} kz) dz \tag{3.2}$$

and the transverse kick voltage for the TM1n0

$$V_T = p\frac{c}{e} = \frac{-i}{k}\int_{-L/2}^{L/2} \nabla_T E_z \cos(\frac{c}{v} kz) dz \tag{3.3}$$

where the transverse momentum is given by equation (3.1) above. Here k = ω/c, and the phase of the particle has taken to give the largest voltage. The quantity T is the transit-time factor.[3]

$$T = \frac{\lambda v}{\pi L c} \sin \frac{\pi L c}{\lambda v}$$

Here L is the cell length, and λ is the free-space wavelength of the fields. For the case v = c and L = λ/2, T has the value 2/π.

Table 3.2: Peak Field Locations in the TM010 and TM110 Mode Pillbox

TM010	**TM110**
Peak Electric Field:	
$E_z = E_0$ at r = 0	$E_z = \pm 0.58187 E_0$ at x/a = ±0.48051
Peak Magnetic Field:	
$H_\phi = .58187 E_0/Z_0$ at r/a = 0.76562	$H_r = -0.50000 E_0/Z_0$ at r = 0
	$H_\phi = 0.41944 E_0/Z_0$ at x/a = ±0.91826

Line 7 of the table gives the resonance condition which sets the cell radius a. The quantity u_{xy} is the y^{th} root of J_x. Line 8 is the stored energy, and lines 9 and 10 are the two geometrical factors [3] of the resonator. These factors, which depend only on mode and cavity proportion, are independent of frequency scaling and materials properties. G_1 is defined as the product of the cavity Q and the surface resistance of the wall so that:

$$Q \equiv \frac{\omega U}{P} = \frac{G_1}{R_s}$$

where P is the power dissipated in the cavity wall.

G_2 is a factor of the shunt impedance, and in order to define it, some cavity voltage must be chosen. Here r is the shunt impedance per unit length, and the unprimed quantities refer to the acceleration voltage while the primed quantities refer to the transverse voltage.

$$\frac{r}{Q} \equiv \frac{V_L^2}{PL} = \frac{G_2 T^2}{\lambda} \quad and \quad \left(\frac{r}{Q}\right)' \equiv \frac{V_T^2}{PL} = \frac{(G_2)' T^2}{\lambda} \tag{3.4}$$

The G factors are useful in making explicit the scaling of the various quantities associated with a resonator. It is clear from the above that Q is independent of frequency but scales as $1/R_s$, and r/Q scales as ω. However, because T is not defined in a perfectly general way and because r/Q can be easily determined without determining T, in practice G_2 is rarely used.

Table 3.3 contains some numerical values for pillbox resonator quantities.

Table 3.3: Values for Pillbox Resonator Quantities for the case v = c and L = λ/2

	TM010	**TM110**	**TM120**
λ	2.6127a	1.6398a	0.89560a
G_1, Ω	256.6	325.2	408.7
G_2, Ω	966.8		
$(G_2)'$, Ω		316.4	170.0
3.9 Ghz: λ = 0.07687 m;			
a, m	0.02942	0.04688	0.08583
r/Q, Ω/m	5097		
(r/Q)', Ω/m		1668	896.3

The G_1 increase with n toward a limit at high n of 591.8 Ω, but the $(G_2)'$ decrease indefinitely as n increases. This is easily understandable, since the higher modes have a lot of useless field at large cell radii.

Multi-Cell Structures

The first RF deflector [5,6] was a single rectangular cell operating in the equivalent of the TM110 described above. More extensive applications require the use of coupled structures; and if these are to be superconducting, they will operate with a standing wave.

The electromagnetic field with dipole symmetry, harmonic in time, in a region with cylindrically symmetric boundary conditions can be expressed in the following way.

$$\begin{aligned} \vec{E}(r,\phi,z,t) &= \hat{r}E_r(r,z)\cos\phi + \hat{\phi}E_\phi(r,z)\sin\phi + \hat{z}E_z(r,z)\cos\phi \\ \vec{H}(r,\phi,z,t) &= \hat{r}H_r(r,z)\sin\phi + \hat{\phi}H_\phi(r,z)\cos\phi + \hat{z}H_z(r,z)\sin\phi \end{aligned} \tag{3.5}$$

This form is complete but it is not unique, and of the six scalar functions in these expressions, only two are independent. This is the form in which the fields are determined in the code URMEL[29,30]. For a standing wave structure, E_z will be periodic in z and in a cylindrical sub-region around the z axis, with a suitable choice of reference plane, it can be represented by a Fourier cosine series:

$$E_z(r,\phi,z,t) = e^{i\omega t}\cos\phi\sum_{i=1}^{\infty} E_i J_1(k_i r)\cos(\beta_i z) \quad where \quad \beta_i = \frac{2\pi i}{2L}$$

Here the periodicity has been taken to be 2L. This E_z must satisfy the scalar Helmholtz equation, which leads to the requirement

$$k_i^2 = k^2 - \beta_i^2$$

For the case $L = \lambda/2$ it can be seen that the first value of k_i is zero and the rest imaginary. In this situation it can be shown [7,8] that the complete form for E_z becomes:

$$E_z(r,\phi,z,t) = e^{i\omega t}\cos\phi\left(E_1\frac{r}{r_0}\cos(\frac{2\pi z}{\lambda}) + \sum_{i=2}^{\infty} E_i\frac{I_1(k_i r)}{I_1(k_i r_0)}\cos(\beta_i z)\right)$$

where now both the k_i and the hyperbolic Bessel functions can be taken as real. The quantity r_0 here is taken as the iris diameter of the structure, but another smaller value could be used. This is the largest diameter for which this representation of the field is valid.

In computing voltage integrals from this function, again for v = c, there will be terms like $\cos(2\pi z/\lambda)\cos(2\pi nz/\lambda)$. A familiar argument shows that for any n except 1, the result of such an integral is periodic and will be zero for whole periods and average to zero in the limit of long structures. Thus only the first term contributes to such an integral, and we have for a single cell:

$$\vec{p} = -\frac{e}{c}\frac{i}{kr_0}E_1\vec{\nabla}_T r\cos\phi\int_{-\lambda/2}^{\lambda/2}\cos^2(\frac{2\pi z}{\lambda})dz = \frac{e}{c}\frac{-i}{kr_0}E_1\frac{\lambda}{4}\hat{x} \tag{3.6}$$

This is a remarkable result. The transverse momentum kick for the round iris is independent of r. Also we have:

$$V_L = E_1\frac{r}{r_0}\cos\phi\int_{-\lambda/2}^{\lambda/2}\cos^2(\frac{2\pi z}{\lambda})dz = E_1\frac{\lambda}{4}\frac{r}{r_0}\cos\phi \tag{3.7}$$

and finally for the extended structure:

$$V_T = \frac{1}{kr_0}V_L(r = r_0, \phi = 0) \quad and \quad \left(\frac{r}{Q}\right)' = \frac{1}{(kr_0)^2}\frac{r}{Q} \tag{3.8}$$

This analysis shows how to find two important properties of a deflecting structure, the deflection voltage and the shunt impedance associated with it, from the table of fields and the derived quantities produced by a computer code such as URMEL. After working it out, it seems obvious that the deflection voltage for a standing wave should be derived from the Fourier transform of E_z. What is not so obvious is the uniformity of the deflection over the aperture of the structure. This is can be accepted as a gift.

Another argument from the symmetry of the deflection fields in a cylindrical boundary has to do with the location of field maxima. The field expressions, (3.5) above have the ϕ variation in the form:

$$F \equiv (E\ or\ H)^2 = A^2\sin^2\phi + B^2\cos^2\phi$$

So that

$$\frac{\partial F}{\partial\phi} = 2(A^2 - B^2)\sin\phi\cos\phi$$

It is clear that if the fields are not uniform in ϕ, ($A^2 \neq B^2$), then the extrema must be at $\phi = 0,\ \pi/2,\ldots$ This makes it easier to find peak fields in computer output.

3.2 Prior Art

The Karlsruhe - CERN RF Separator

The first generation of particle separators were constructed at Brookhaven and at CERN. These systems employed traveling-wave copper waveguide, and operated at the low duty factor implied by the high peak power required. The designers of these system chose and optimized an iris-loaded guide operating in the TM11-like mode [9]. It was very early recognized, however, that a superconducting separator operating with a long pulse would have a more general usefulness [10], and about 1967 a collaboration began for design and construction of such a device [16,17]. The completed system began operation late in 1977 [14, 25]. Some of the parameters of the superconducting waveguides are listed in Table 3.4 below.

Table 3.4: Some Design and Measured Parameters of the Karlsruhe - CERN RF Separator [14]

Type of Accelerating Structure	Standing Wave	
Operating Frequency	2865	MHz
Iris Opening	40	mm
Cell Diameter, Elliptical	122.5 x 128.3	mm
Group Velocity, v_g/c	-0.03	±.001
{Cavity Coupling, k	0.0382	}
Mode	π/2, uniform periodic	
G_1		138 Ω
(r/Q)'	765	Ω/m
Design Rs	280	nΩ
Effective Deflector Length	2.74	m
Number of Cells/Deflector	104	
Mean Deflecting Field, E_0	2	MV/m
E_{peak}/E_{def}	5.54	
B_{peak}/E_{def}	15.5	mT/(MV/m)
Working Temperature	1.8	K
	RF 1	RF 2
Unloaded Q	2.1e+09	2.2e+09
Loaded Bandwidth	≈10 Hz	≈100 Hz
RF Dissipation in 1 Deflector at 1.4 MV/m	7	W
Heat Losses of Cryostat at 1.8 K	13	W

The system consists of 2 resonators separated by 90 m. Each resonator is assembled from 5 sub-sections of 19 or 22 cells each. Each sub-section is separately processed and the final assembly of each resonator is completed by demountable seals in unexcited cells. The sub-section length is determined by the length of the available furnace for UHV heat treatment.

Each of the two resonators has an off-center coax adjustable coupler in the center sub-section and monitor couplers in the two end sub-sections. There are coarse mechanical plunger tuners in each of the two middle sub sections, and fine mechanical plunger tuners in each of the two end sub sections. The operating frequency is locked to one of the resonators. Each resonator has Kapton windows in the beam line to protect the cavities from contamination [14,22, 24, 25]. The deflection is in the vertical plane.

Each sub-section is made rigid by welded-on longitudinal bars around the circumference, and limited cell-by-cell tuning was done by dimpling. Field flatness was not easy to achieve, and repeated measurements together with second order perturbation calculations and inclusion of next-nearest neighbor coupling in the model was necessary to get satisfactory results.

The highest peak magnetic field achieved during the development for the separator was 85 mT at a Q_0 of 2.5e+09 in a four-cell test structure. The best 20 cell sub-structures operated at 40 mT and the worst at 20 mT [21, 22, 14].

There is a large amount of information in the literature about the design of this system and about structure fabrication and processing. For a review see [14]. Much of this is not of current interest, but there are several themes that are important here. These will be discussed in the paragraphs below.

Cavity Design

"Systematic measurements for standing wave disc-loaded structures show that for a given disk opening and mode there exists an optimum disk thickness such that B_{peak}/E_{def} or E_{peak}/E_{def} is a minimum. Furthermore, it has been found that the maximum deflection field is limited by B_{peak} and not E_{peak}" [16]. This is an important recognition, clearly stated. Measurements of the peak fields are shown in Figure 3.2 [15].

Calculations together with measurements give the behavior of the cell-to-cell coupling and shunt impedance with disk opening. This is shown together with several other parameters in Figure 3.3 [11]. This figure shows that a deflecting structure can operate with either a reverse wave for $2a/\lambda$ near 0.4 or a forward wave for values near 0.6. The peak fields are higher and the shunt impedance is lower for operation in the forward-wave region, but the advantages for application to a separator of large aperture at a given frequency was noted in [16]. It had been already noted that the dispersion curve for this forward- wave deflecting structure is not monotonic due, presumably, to the admixture of TE-like modes [10], and this is given as a reason[19] for choosing the backward-wave deflector. The problem that this brings in a standing-wave resonator remain to be determined.

We note that the normalized shunt inpedance presented in Figure 3.3 can be represented in terms of the G parameters in the following way:

$$r'(Wilson) \equiv \frac{\lambda R_s r_t}{Z_0^2} = \frac{G_1 G_2 T^2}{Z_0^2}$$

Structure Design

The first parameter list published for the deflector [17] begins with a guide 2.83 m long in a 2 to 1 biperiodic $\pi/2$ mode. The mode is chosen for its insensitivity to dimensional errors, and the biperiodic symmetry for its lower peak magnetic field. The even lower peak field of the π-mode is recognized, but at the cost of a large iris thickness (25 mm, presumably with a lowered cell-to-cell coupling). The biperiodic configuration was found difficult to analyze and slow to develop, and a singly-periodic design was adopted instead [18]. The final cell dimensions are given in reference [18].

For mode stabilization the outer diameter of the cell is made elliptical while the iris remains round. The goal is to raise the frequencies in the passband of the unwanted modes. Because of the perturbations associated with the tuners, the shift is made sufficient to raise the orthogonal π-mode frequency is shifted to be higher than the wanted $\pi/2$ mode frequency. This is a shift of 50 Mhz [19].

There is an important mention in reference [19] about the possibility of replacement of the long single structure by five short independent π-mode structures. The development of this kind of resonator for separator use at Rutherford Lab is noted [13]. This is rejected without detailed discussion, and we are aware of no compelling case in the literature against the use of short π-mode deflectors.

In this regard we note that both of the long deflectors failed to operate at the design goal of 2 MV/m producing a total deflection of 7.12 MV rather than the 11 MV aimed for. However, if the 10 sub-sections had been operated independently at their respective gradient limits, a total of 10.45 MV [14] would have been produced.

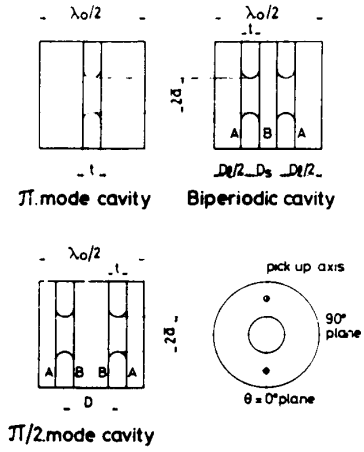

FIG. 1. Geometry of the measured models. $\lambda_0 = 10.5$ cm, $t = 10$ mm, $D = 26.25$ mm, $D_t = 2D_s$.

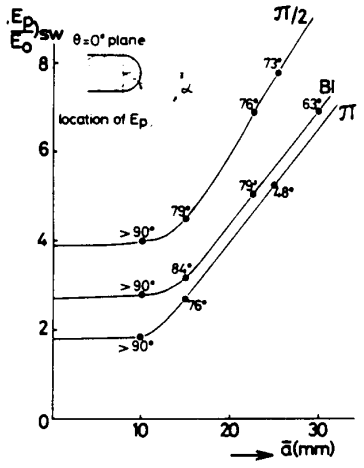

FIG. 2. E_p/E_0 under standing wave condition (sw) as a function of (rounded) disk opening. The location of E_p is indicated by the angle α.

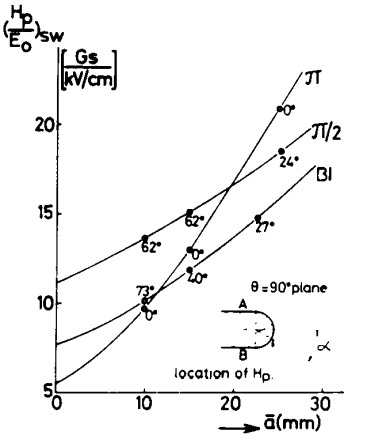

FIG. 3. H_p/E_0 under standing wave condition (sw) as a function of (rounded) disk opening. The location of H_p is indicated by the angle α.

Figure 3.2: Measurements of peak fields in a disk-loaded deflector. From Reference [15]

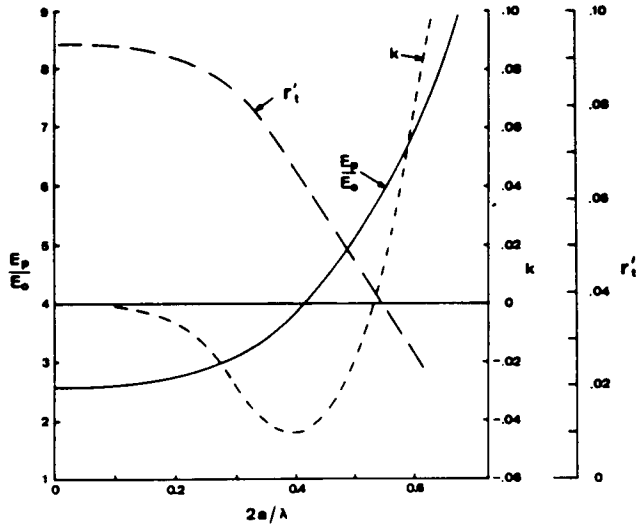

Figure 3.3: Several properties for typical separator structure. From Reference [11]

This is an application of the so-called area argument. This goes as follows: The characteristics of a superconducting surface varies on some characteristic scale. Performance of a superconducting cell is limited by its worst spot. Thus small cells tend to have higher limiting fields than larger cells and single cells tend to have higher limits than multi-cell structures. This situation is of course confused by many systematic effects, frequency dependence, and design and processing variation. Nonetheless, overall there are many instances in which this trend is apparent.

Multipacting

The first test cells for the separator showed strong multipacting levels which could be overcome by processing from a few to 50 hours [18,19]. This was hypothesized to occur in the end half-cells of the test structures, and subsequent structures were built with full-length end cells. Test structures of this design showed little or no multipacting [20]. In a series of tests to study the effects of gas exposure, test cavities required typically 24 hours of processing to get through multipacting barriers [23].

In the testing of the first 2.74 m deflector [24] it required 8 hours to process through the multipacting levels, but the authors remark that they "were not able to decide whether the breakdown [that eventually limited the field level reached] was influenced by multipacting electrons or due to a thermo-magnetic effect". However, summary remarks concerning the relation of multipacting to cavity performance make the point [14] that neither parasitic mode excitation nor frequency pulling is observed near the breakdown field level and that multipacting is not believed to limit performance.

Crab Cavity Development for CESR-B

We believe that in addition to the CERN separator, the only high-power deflecting-mode cavities that have been operated are the single-cell crab cavity development models [27, 28]. All of these tests reached high field, peak electric fields of 25 - 30 MV/m and peak magnetic fields of 75 - 100 mT at the iris and Q_0 in excess of 1e+09. In some of the tests weak multipacting was observed, but it was attributed to

particular construction features of the heavily-loaded crabbing cells. In tests of accelerator cavities operating in the deflection mode, high fields were reached without any multipacting.

The Tesla Test Facility Accelerator Development

The two major applications of RF superconductivity of recent times are the two electron linacs of the TJNAF (formerly CEBAF) and the storage ring accelerators at LEP, HERA and TRISTAN. Together these installations contain about 500 m of superconducting guide operating at accelerating gradients of 5 - 10 MV/m. There is a summary of the state of the art as represented in these machines in reference [1], and much detailed technical information in the several Proceedings of the Workshops on RF Superconductivity.

More recently this state of the art has been advanced by a large development effort at DESY [32, 33] with the goal of producing high-gradient cost-effective linac for the TESLA linear collider. This development program has constructed a test linac, the TESLA Test Facility, which is soon to be expanded to provide an electron beam for FEL use. Nine structures have been installed in the first tanks of the TTF which operate in the TESLA pulsed mode (see Table 3.5) at an accelerating gradient of 17 MV/m [33]. This very successful program continues to produce important progress.

With TESLA there is a large body of practice to consider, and we will again make a choice of topics to discuss. The materials and processing issues are described elsewhere in this document, and here we will talk about structure design.

Table 3.5: Some Design Parameters of the TESLA Collider Cavity [33]

Type of Accelerating Structure	Standing Wave	
Accelerating Mode	TM0 -π	
Operating Frequency	1300	MHz
Design Gradient	25	MV/m
Quality Factor Q_0	> 5e+09	
Active Length	1.038	m
Number of Cells	9	
Cell-to-Cell Coupling, k	.0187	
Iris Diameter	70	mm
Cavity Equator Diameter	206.6	mm
Geometry Factor, G1	270	Ω
R/Q	1036	Ω
E_{peak}/E_{acc}	2.0	
B_{peak}/E_{acc}	4.26	mT/(MV/m)
Tuning Range	$\pm$300	kHz
$\Delta f/\Delta L$	315	kHz/mm
Lorentz Force Detuning at 25 MV/m	$\approx$600	Hz
Q_{ext} of Input Coupler	3e+06	
Bandwidth at Q_{ext} = 3e+06	430	Hz
RF Pulse Duration	1330	μs
Repetition Rate	5	Hz
Fill Time	530	μs
Beam Acceleration Time	800	μs
RF Power Peak/Average	208/1.4	kW

Structure Design

The TESLA structure consists of 9 cells coupled together and operated in the π-mode. This type of structure is also used in the TJNAF, LEP, HERA, and TRISTAN systems and represents an optimized response to a particular set of design goals. What these cell design goals are is stated clearly in reference [33]: "that the contour should strongly suppress multipacting; that the electric and magnetic fields at the cavity walls should be minimized to reduce field emission and Ohmic heating; and a sufficiently large iris diameter is desirable to reduce wake field effects."

The control of multipacting is properly put at the head of this list as a particularly insidious and intractable problem Control is based on a combination of computer simulation and experimental verification by thermal mapping, a method that has been practical only in the simplest geometries. For a discussion of this topic see reference [1], Chapter 10. This required simplification sweeps away the side couplers, plunger tuners, and weakly excited cells, as in the π/2 mode separator, and leaves only a chain of π-mode cells of spherical or elliptical shape in which multipacting can be reduced to a low-risk problem. The goal of peak field reduction too is best dealt with in a π-mode cell.

Multipacting remains a serious problem in auxiliary devices, particularly input coupler systems and windows. This is a project manager's nightmare. Problems of this kind that turn up late in system development present particularly high risk.

With the power feed and the higher-order mode loads relegated to the beam pipe, the chain of cells must be short enough to get good power flow and to avoid trapped modes. This eases field-flatness tuning as well. Another important limit to the practical length of a structure is the chemical processing ultra-clean rinsing, and draining that is required for high performance of niobium surfaces.

The design of the TESLA structure is seen to be constrained by many requirements that are specific to superconducting RF regime and do not have counterparts in normal-conducting-structures, and the TESLA system has its inner logic.

3.3 A Prototype 3.9 GHz Deflecting Structure

As we begin to write goals for the design of a deflecting structure, certainly high on the list will be the first two set for the design of the TESLA structure. These are to design to suppress multipacting, and recognizing that the gradient is a deflector will be limited by magnetic field, to design to minimize peak magnetic field. In a relatively small application such as is being considered here, it is necessary to play it safe with regard to the big technical issues, and the reasonable thing to do with regard to multipacting is to design a cell that is as much as possible like those proved to operate successfully in previous applications. This means taking the TESLA design as a model in a coherent way, and adopting the design logic that was mentioned in the preceding section.

The structure design must, of course, satisfy the requirements of the separator system. The separator design study that forms the starting point for the present work proposes an RF frequency of 5.7 GHz to keep the beam line as short as possible, and has an aperture at the deflectors with a diameter of 2.6 cm. We have chosen a 3 cm waveguide iris diameter for the trial design.

Thus the goal here is to study a deflector structure that is scaled with the minimum changes from the TESLA accelerator structure. This is not possible at 5.7 GHz, because with a 3 cm iris, such a structure is far removed from the TESLA proportions. Such a guide is possible, but it would be in the regime of forward wave operation mentioned in Section 3.2 above. Accordingly, the lower frequency of 3.9 GHz is taken for the prototype.

The resulting cell shape is shown in Figure 3.4. Since there is a change of mode involved as well as a change in frequency, more than a simple scaling is required. The two radii R are close to the scaled values, but the angle α has been reduced to about 60% of the TESLA value.

Frequency Spectrum

Table 3.6 gives the first 16 frequencies of this cell. The resonances are characterized first by the number of cycles of ϕ variation and second by the nature of the boundary condition imposed on the right and left hand boundaries. In the figure, the heavy line indicates the metal wall and is taken as cylindrically symmetric about the axis indicated. the right and left boundaries can be taken as requiring either normal electric (e) or normal magnetic (m) fields. The electric boundary condition is that of a metal wall and thus produces a mirror reflection in the boundary of a familiar kind. The magnetic mirror also produces a reflection, but one with different symmetries. Thus the right hand boundary condition mirrors the metal wall to form a complete cell with irises, and the mirror in the iris images this cell forming an adjacent cell. An electric condition in the iris gives the condition of 0 phase shift per cell while the magnetic condition gives the effect of a phase shift of π. Thus this is a hall of mirrors, and the frequencies listed in the table are those characteristic of the 0 and π modes of an indefinite chain of identical cells.

In the table modes with zero cycles in ϕ, designated TM0, and one cycle, designated 1, are listed. In the range of the tabulation there will perhaps be modes with 2 cycles in ϕ. This calculation has not been done yet.

In the right hand column some of the modes have been classified according to the corresponding pillbox designations. Thus the modes TM0 - ee - 1 and TM0 - em - 1 are the 0 and π modes of the of the accelerator or TM010 band. The last number in this designation is the ordinal of the list of modes of the particular symmetry defined by first two designators. This designation scheme is exhaustive, and all of the possible modes will be found in this way.

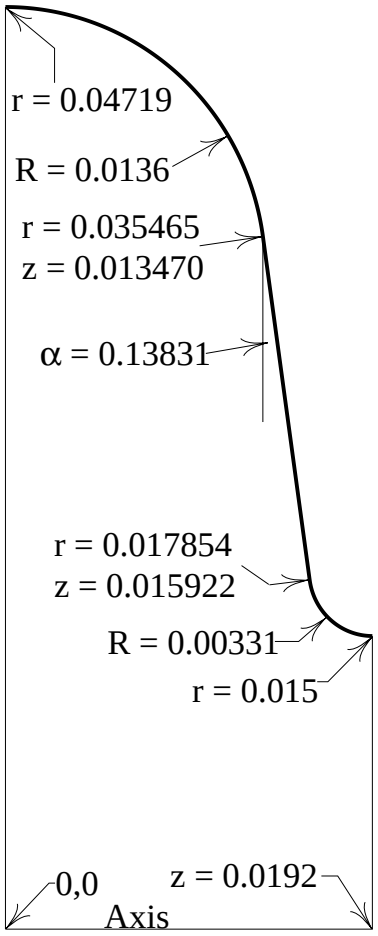

Figure 3.4: Prototype Cavity Dimensions (in meters)

Each 0 and π mode in the table mark the ends of a band of modes found in a real resonator. The 1 - em - 1 and 1 - ee - 1 mark the lowest and the highest modes in the band of deflection modes. This band is also called the TM110 band because the pillbox prototype of the 0-mode in this band is the TM110. The number of modes in this band is equal to the number of cells in the real resonator. The multiplicity of each mode in the band is n + 1 where n is the number of ϕ cycles, and the modes of the deflection band, have two polarizations.

Table 3.6: Structure Resonant Frequency Spectrum from URMEL

URMEL Designation	Frequency, GHz	Assignment
TM0 - ee - 1	2.74803	0 TM010 band
TM0 - em - 1	2.82070	π
1 - em - 1	3.89888	π TM110 band
1 - ee - 1	4.10224	0
1 - mm - 1	4.14381	0 TE111 band
1 - me - 1	5.07919	π
beam pipe cutoff	5.85659	TE11 mode
TM0 - ee - 2	5.90669	
1 - em - 2	6.18651	
TM0 - em - 2	6.20752	
TM0 - me - 1	6.27275	π TM011 band
TM0 - mm - 1	6.49011	0
1 - mm - 2	6.60793	
1 - me - 2	7.07466	
1 - ee - 2	7.37999	
beam pipe cutoff	7.64949	TM01 mode
TM0 - me - 2	8.20991	
TM0 - mm - 2	8.95823	

The Deflection Band

The deflection modes can be modeled by the same circuit model that has been employed for the acceleration band [1, Chapter 7][12]. This model characterizes the individual cells as lumped resonators coupled together by nearest-neighbor, next-nearest-neighbor, etc. interactions, and is often associated with the name of L. Brillouin. The TESLA Structure can be characterized in the model with next-nearest neighbor coupling only. Assuming that a single coupling constant will describe the deflection band as well, the dispersion curve is given by:

$$\omega_n = \frac{\omega_0}{\sqrt{1 - k\cos\beta_n}} \tag{3.9}$$

Here k is the cell to cell coupling constant, taken as positive, ω_n is the resonant frequency of the unperturbed cell, and β_n is the cell to cell phase shift given in two relevant cases by:

$$\beta_n = \frac{n\pi}{N-1}; \quad n = 0...N-1 \qquad \text{(Half-cell terminated)}$$

$$\beta_n = \frac{n\pi}{N}; \quad n = 1...N \qquad \text{(flat } \pi\text{-mode)}$$

Here N is the number of cells in the structure. The first of these relations refers to a structure with half-cells at the ends, and it is the model of the case that is calculated above by URMEL; that is, the chain of indefinite length.

The second dispersion relation refers to the so-called flat π mode structure. This is a structure terminated by whole cells tuned so that in the π mode (n=N), the amplitude of excitation of all cells is the same. This requires the adjustment of the frequency of the end cells by an amount $\Delta\omega/\omega \approx -k/2$. For a 13-cell resonator tuned in this way there will be 13 resonances of each polarization. The two polarizations can be separated in frequency by slightly flattening each cell in the structure on the circumference. This is discussed elsewhere in this document.

The n = 13 mode for which $\beta = \pi$ has the lowest frequency which is listed in Table 3.6 as 1 - em - 1 This is what has been referred to throughout this document as the π-mode and is the deflector operating mode. It is important to recognize that what has been referred to as $\pi/2$-mode operation requires a chain of cells that are $\lambda/4$ in length and so is not one of the modes in the passband of the π-mode deflector. The highest mode of a flat-tuned deflector is not the 0-mode, but one for which $\beta = \pi/13$. The frequency of this mode is not computed by URMEL but can be estimated from equation (3.9).

Equation (3.9) can be arranged to give the parameters k and ω_0 in terms of the URMEL output:

$$k = \frac{\omega_{\beta=0}^2 - \omega_{\beta=\pi}^2}{\omega_{\beta=0}^2 + \omega_{\beta=\pi}^2} \quad and \quad \omega_0 = \omega_{\beta=\pi}\sqrt{1+k} \tag{3.10}$$

Using the frequencies in Table 3.6 we get the following:

TM010 band:	k = 0.0261	ω_0 = 2.78365 GHz
TM110 band:	k = 0.0508	ω_0 = 3.99669 GHz

The π-mode of the Deflection Band

Table 3.7 lists a number of parameters of the prototype resonator under discussion here. At the middle of the cell where the metallic boundary condition is applied, the fields have the same general configuration as in the TM110 pillbox. The electric field is longitudinal and is zero on the z-axis, rising to maxima at two points along the x-axis. As shown in Figure 3.1, the magnetic field is transverse around the electric lines, constant across the cavity center and falling to zero at the electric maxima. There is a secondary magnetic field maximum at the outer cavity radius at $\phi = 0$ and π.

In the plane of the iris where the magnetic boundary condition is applied, the electric field is transverse, and the magnetic field is longitudinal. The field configuration is that of the TE11 waveguide mode. The electric field is normal the y-axis at x = 0, concentrated near the axis, and the magnetic field is in the z-direction, zero at the axis and concentrated around $\pm y = r_0$. It is interesting to note that the deflection is due both to the magnetic field near the cavity center and the electric field across the iris.

The peak fields calculated by URMEL are listed in the Table. The peak electric field is at $\phi = 0$, π, somewhat inside the cavity from the iris diameter very close to the location indicated in Figure 3.2. The peak magnetic field lies at the plane of the iris, at $\phi = \pm\pi/2$.

Table 3.7: Some Parameters of Prototype Deflecting Structure Calculated Quantities from URMEL

Type of Accelerating Structure	Standing Wave, π mode	
Operating Frequency	3.9	GHz
Number of Cells/Deflector	13	
Cell Length	38.4	mm
Deflector Length	499.2	mm
Iris Opening	30	mm
Cell Diameter, Unsquashed	94.38	mm
Cavity Coupling, k	0.0508	
Transit-time factor	0.667	
G_2	247.1	Ω
G_1	236.3	Ω
(r/Q)'	1429.8	Ω/m
E_{peak}/E_{def} at $\phi = 0, \pi$	3.38	
B_{peak}/E_{def} at $r = r_0., \phi = \pm\pi/2, z = L/2$	17.3	mT/(MV/m)
B_{peak}/E_{def} at r = 47.19 mm, $\phi = 0, \pi$, z = 0	5.74	mT/(MV/m)

To get a feeling for the magnitudes of these peaks we can compare the TESLA structure operating at E_{acc} = 15 MV/m accelerating field with the deflecting structure. The peak fields of the TESLA structure are given in Table 3.5.

TESLA Structure:
E_{acc} = 15 MV/m
E_{peak} = 30 MV/m
B_{peak} = 63.9 mT

Deflecting Structure
E_{def} = 3.69 MV/m
E_{peak} = 12.5 MV/m
B_{peak} = 63.9 mT (iris, $\phi = \pm\pi/2$)
B_{peak} = 21.2 mT (at r = 47.19 mm, $\phi = 0, \pi$)

This speaks for itself. It is clear that in this deflecting structure the peak magnetic field reaches limiting levels well before the electric field becomes a concern.

To get a feeling for the shunt impedance given in Table 3.7, it is necessary to have some representative values for surface resistance. This is a complicated issue, but for these purposes we will use the simplest model of dividing the surface resistance into a temperature and frequency dependent BCS part and a residual part that is nearly constant. Again taking the TESLA performance as representative we can get a realizable BCS component by the measurements presented in Figure 3.2.1 of Reference [33]. These can be represented by the expression

$$R_{BCS} = (1.7e-05)\frac{T_c}{T}e^{-1.86\frac{T_c}{T}} \tag{3.11}$$

Taking Tc = 9.25 K, this is not significantly different from the semi-empirical expression generally used [1, equation 4.43]. Table 3.8 gives values calculated from equation (3.10) using an f^2 frequency scaling from 1.3 GHz.

Table 3.8: BCS Component of the Niobium Surface Resistance, nOhms.

From Reference [33] Figure 3.2.1

Frequency,GHz	1.30	2.00	3.00	3.90	5.00	5.70
Temp, K						
1.30	0.2	0.5	1.2	1.9	3.2	4.2
1.35	0.3	0.8	1.8	3.1	5.0	6.5
1.40	0.5	1.2	2.7	4.6	7.6	9.9
1.45	0.8	1.8	4.1	6.9	11.3	14.6
1.50	1.1	2.6	5.8	9.8	16.2	21.0
1.55	1.5	3.6	8.2	13.8	22.7	29.4
1.60	2.1	5.0	11.2	18.9	31.0	40.3
1.65	2.8	6.7	15.0	25.4	41.7	54.2
1.70	3.7	8.8	19.8	33.5	55.0	71.5
1.75	4.8	11.4	25.7	43.4	71.3	92.7
1.80	6.2	14.6	32.8	55.5	91.1	118.5
1.85	7.8	18.4	41.3	69.9	114.8	149.2
1.90	9.7	22.8	51.4	86.9	142.8	185.6
1.95	11.9	28.1	63.2	106.8	175.5	228.1
2.00	14.4	34.1	76.8	129.8	213.3	277.3

The residual part of the surface resistance is discussed in Reference [1] Chapter 9 where data is showed for tests on single-cell 1.5 GHz cells. This distribution centers on about 20 nΩ. Figure 3.2.7 of Reference 33 shows the performance of selected TESLA structures, and for fields out to E_{acc} = 15 MV/m, this value also seems representative. Thus is seems reasonable to take for a deflecting structure at 3.9 GHz $R\neq$ = 70 nΩ at 1.8 K and R_s = 150 nΩ at 2.0 K. This leads for E_{def} = 4 MV/m

$$Power/unit\ length = \frac{E_{def}^2 R_s}{(\frac{r}{Q})' G_1}$$ = 3.315 W/m at 1.85 K

= 7.103 W/m at 2.0 K

It is clear that at 3.9 GHz superconducting cells operate in a regime in which the surface resistance is dominated by the BCS rather than the residual component. It is necessary to be alert, therefore for some different optimization results in this case. The most obvious of these is that the required refrigeration horsepower will be reduced at temperatures below 2 K. This has not in general been the case with lower frequency SRF systems. Further, at this frequency the higher BCS surface resistance limits magnetic field through heating of the inner surface of the cavity. The strong temperature dependence of the surface resistance and the limited thermal conductivity of the niobium wall and the Kapitza resistance at the outside wall of the cavity produces a thermal runaway limit to the field that can be sustained. At 3.9 GHz this limit lies between 0.11 and 0.15 T [34] See Reference [1], Section 11.10. There is further discussion of this elsewhere in this document.

Discussion

The parameter values listed in Table 3.7 fit clearly into the picture provided by the pillbox calculations and the measurements for the π-mode in Figure 3.2. We can see where we are with this prototype deflector with respect to the optimization of the peak magnetic field, and it is clear that some reduction can be expected. The shunt impedance of the prototype is good, and some reduction could be

tolerated. Such cavity shape optimization aside, it is seems likely that the deflector described here provides a good starting point from which to launch development work.

In the immediate future a program of development for the deflector structures includes computer studies, a model program, superconducting cavity and structure construction processing and measurement, and a program of system optimization. The computer studies include: the improvement of the performance and the verification of the accuracy of URMEL; identification of another useful cavity code (SUPERLANS?); verification of the lumped-circuit model and development of this model to support structure flatness tuning activity; and the cell-shape optimization already mentioned.

A model program must support the development of a flatness tuning procedure and operational tuners for the superconducting deflectors, the design of couplers and other auxiliary devices.

The superconducting cavity test program has as its initial problem the verification of the suppression of multipacting in the cell shape chosen. We do not have a project until it is demonstrated that the deflectors will not multipact. The second task of the cavity testing activity is to identify magnetic breakdown in superconducting cells and verify that it is taking place at the locations of peak magnetic field. At this point we are in contact with the process that is expected to limit the performance of the deflector.

Finally, of course, there must to be a system-wide optimized parameter list. Deflector parameters that depend on the system design as a whole include the operating gradient and the frequency, and the overall length and aperture. We expect that the prototype deflector described here is not very many steps away from what if finally required.

3.4 References

[1] H. Padamsee, J. Knobloch, and T. Hays, *RF Superconductivity for Accelerators*, John Wiley & Sons, New York (1998)

[2] M. Tinkham, *Introduction to Superconductivity*, McGraw- Hill, Inc., New York (1996)

[3] P. Wilson, AIP Conference Proceedings 87, American Institute of Physics, New York (1982) p. 450

[4] W. Panofsky and W. Wenzel, Rev. Sci. Instr., **27**, 967 (1956)

[5] W. Panofsky, "Experience with a Microwave Separator",Proc. Int. Conf. on High Energy Accelerators and Instrumentation, L. Kowarski, editor, CERN (1959) p. 428-431

[6] P. Phillips, Rev. Sci. Instr., **32**, 13 (1961)

[7] H. Hahn, Rev. Sci. Instr., **34**, 1094 (1963)

[8] B. Zotter and K. Bane, PEP-Note 308, SLAC, Sept. 1979

[9] H. Hahn and H. Halama, Rev. Sci. Instr., **36**, 1094 (1965)

[10] M. Bell, P. Bramham, R. Fortune, E. Keil, and B. Montague, "RF Particle Separators", Proc. Int. Conf. High Energy Accelerators, Dubna 1963, USAEC CONF-114

[11] P. Wilson, IEEE Trans. Nuc. Sci **NS-16** 1092 (1969)

[12] D. Nagle, E. Knapp, and B. Knapp, Rev. Sci. Instr., **38**, 1583 (1967)

[13] A. Carne, B. Brady, and M. Newman, Proceedings of the 1968 Summer Study on Superconducting Devices and Accelerators, BNL June 1968, BNL Report 50155 (C-55) 1969

[14] A. Citron, G. Dammertz, M. Grundner, L. Husson, R. Lehm, and H. Lengeler, "The Karlsruhe - CERN RF Separator", Kernforschungszentrum Karlsruhe, Institut für Kernphysik Primary Report IK-Nr. 316/78 (unpublished) 1978

[15] P. Bernard, H. Lengeler, and V. Vaghin, J. App. Phy., **40**, 4989 (1969)

[16] P. Bernard, H. Lengeler, V. Vaghin, and P. Wilson, "On the Choice of Deflecting Structures for Superconducting RF Separators" Proc. 7th Int. Conf. on High Energy Accelerators, Yerevan (1969) p. 649

[17] W. Bauer, G. Dammertz, H. Eschelbacher, H. Hahn,W. Jungst, E. Rathgeber, and J. Votruba, "A Superconducting Particle Separator", Proc. Int. Conf. on High Energy Physics Instrumentation, Dubna (1970) p. 173

[18] W. Bauer, A. Citron, G. Dammertz, H. Eschelbacher, H. Hahn,W. Jungst, H. Miller, E. Rathgeber, and H. Diepers, "Experimental Investigation of Superconducting Nb Deflecting Cavities", Proc. 8th Int. Conf. on High Energy Accelerators, CERN (1971) p. 253

[19] W. Bauer, G. Dammertz, H. Eschelbacher, H. Hahn,W. Jungst, E. Rathgeber, J. Votruba and H. Diepers, IEEE Trans. Nuc. Sci **NS-18** 181 (1971)

[20] W. Bauer, A. Citron, G. Dammertz, H. Eschelbacher, H. Lengeler, H. Miller, E. Rathgeber, and H. Diepers, IEEE Trans. Nuc. Sci **NS-20** 59 (1973)

[21] W. Bauer, A. Citron, G. Dammertz, M. Grundner, H. Lengeler, and E. Rathgeber, "Status Report on the Superconducting RF Separator Work at Karlsruhe" Proc. Int. Conf. on High Energy Physics Instrumentation, Frascati (1973) p. 716

[22] W. Bauer, A. Citron, G. Dammertz, M. Grundner, L. Husson, H. Lengeler, and E. Rathgeber, "Measurements on the First 20-Cell Deflector Sections for a Superconducting RF Separator" Proc. IXth Int. Conf. on High Energy Accelerators, Stanford (1974) p. 133

[23] W. Bauer, A. Citron, G. Dammertz, M. Grundner, L. Husson, H. Lengeler, and E. Rathgeber, "Status of the CERN-Karlsruhe Superconducting Particle Separator", IEEE Trans. Nuc. Sci **NS-22** 1144 (1975)

[24] A. Citron, G. Dammertz, M. Grundner, L. Husson, P. Kneisel, H. Lengeler, and E. Rathgeber, "Progress on the Superconducting RF Particle Separator for CERN", IEEE Trans. on Magnetics **MAG-13** 508 (1977)

[25] A. Citron, G. Dammertz, M. Grundner, L. Husson, R. Lehm, and H. Lengeler, Nuc. Inst. and Methods **155** 93 (1978)

[26] H. Padamsee, P. Barnes, C. Chen, J. Kirchgessner, D. Moffat, D. Rubin, Y.Samed, J. Sears, and Q. Shu, Proc. IEEE Particle Accelerator Conference, San Francisco, May 1991, p.2423

[27] K. Akai, J. Kirchgessner, D. Moffat, H. Padamsee, J. Sears, and M. Tigner, Proc. IEEE Particle Accelerator Conference, Washington D.C., May 1993, p.769

[28] J. Kirchgessner, P. Barnes, H. Miller, D. Moffat, H. Padamsee, D. Rubin, D. Saraniti, J. Sears, Q. Shu, and W. Hartung, Proc. IEEE Particle Accelerator Conference, San Francisco, May 1991, p.2426

[29] T. Weiland, Nuc. Inst. and Methods **216** 329 (1983)

[30] U. Lauströer, U. van Rienen, and T. Wieland "URMEL and URMEL-T User Guide", DESY Report M-87-03, Feb. 1987

[31] D. Proch, "The TESLA Cavity: Design Considerations and RF Properties", Proceedings of the 6th Workshop on RF Superconductivity, CEBAF,October 1993

[32] Tesla Collaboration, "Tesla Test Facilily Linac - Design Report", D. Edwards, editor. DESY Tesla 95-01 (March, 1995)

[33] *Conceptual Design of a 500 GeV e^+e^- Linear Collider with Integrated X-ray Laser Facility*, R. Brinkman, G. Materlik, J. Rossbach and A. Wagner, editors, DESY 1997-048 (1997)

[34] H. Padamsee, Proceedings of the 5th Workshop om RF Superconductivity, DESY, August 1991, DESY Report M-92-01, April 1992: See the section "On the Choice of the RF Frequency for TESLA", p. 899

4 R&D Program

This section will cover the proposed R&D activity which will be necessary prior to fabrication of the final separator system components to be installed in the beamline. A scenerio of fabrication and test of cavity prototypes is outlined. The required infrastructure to carry out the cavity program is given. The potential for sharing resources among collaborators and a fabrication model leading to the final cavity production are discussed.

4.1 Provisional Cavity Parameters

Here we present the parameters and specifications chosen for the purposes of a point design. These parameters are listed in Tab. 4.1.

Table 4.1: Provisional cavity parameters for initiation of the R&D program and for the point design outlined in this report

frequency	3.9 GHz
mode	…, TM110
equator diameter	94 mm
iris diameter	30 mm
cell length	38.4 mm
cells per meter	26
cells per cavity	13
(R/Q)′	55 ohm/cell
(r/Q)′	1430 ohm/m
V_{trans} @ 0.1 T	5.7 MV/m
E_{peak}	22 MV/m
B_{peak}	0.100 T
U (stored energy)	0.92 J/m
coupling factor	0.051
$G_1 = Q \times R_{sur}$	236 ohms
R_{sur} @ 2K, T_c/T=4.6	$1.04 \times 10^{-7}\Omega$
Q @ R_{sur}	2.2×10^9
Power dissipated @ 5.7MV/m, 2K	10 watts/m
System Requirements for 60 MV/m total kick	
Total cryogenic power[a]	95 watts @ 1.8K 230 watts @ 2K
Q_L (loaded Q)	6×10^7
RF power @ 5.7 MV/m	380 watts/m
RF power including factor of 2 for regulation	760 watts/m
Total RF power	8 kilowatts

[a]Total cryogenic power = instantaneous power × contingency factor/duty factor. Here, the ratio of contingency factor to duty factor has been taken to be unity.

A 3.9 GHz structure operating in …-mode and scaled from the TESLA shape has been adopted in order to initiate the R&D program. The cavity shape is shown in Fig. 4.1. Fig. 4.2 shows a five-cell assembly and Fig. 4.3 illustrates a 13 cell cavity in a helium vessel.

The 13 cell cavity has 1/2 meter active length, and an overall length of 0.7 m. The length has been selected in order to limit the number of cells per structure to what is expected to be a

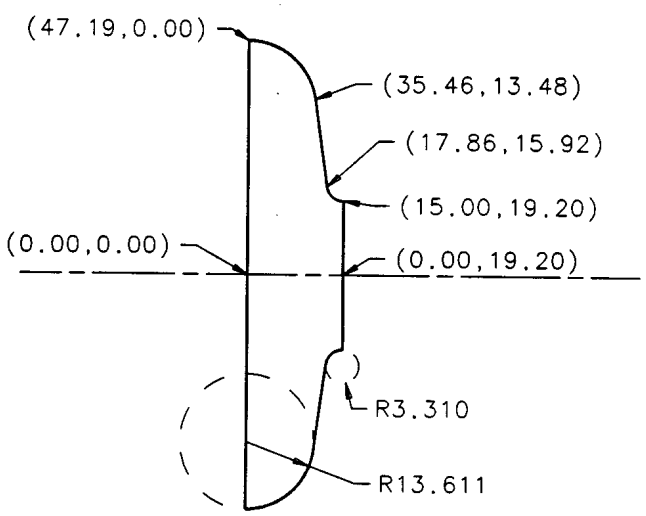

Figure 4.1: Half-cell

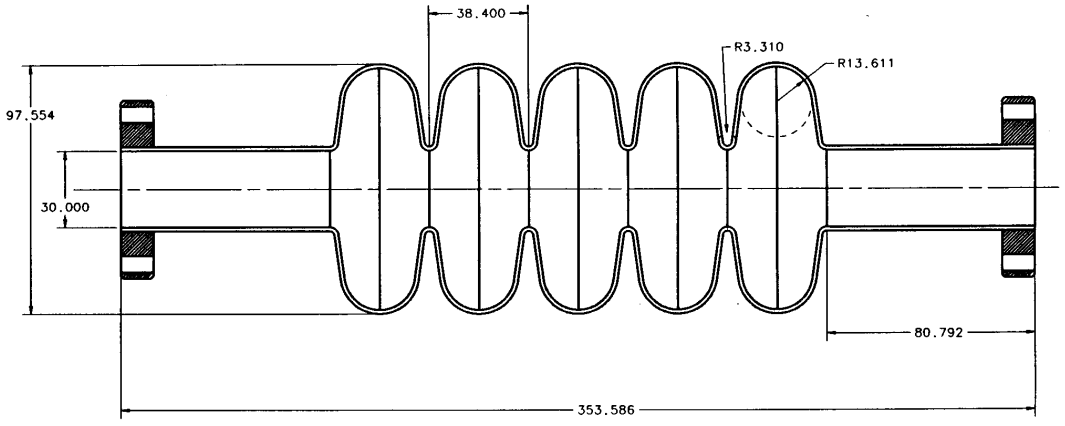

Figure 4.2: Five-cell assembly.

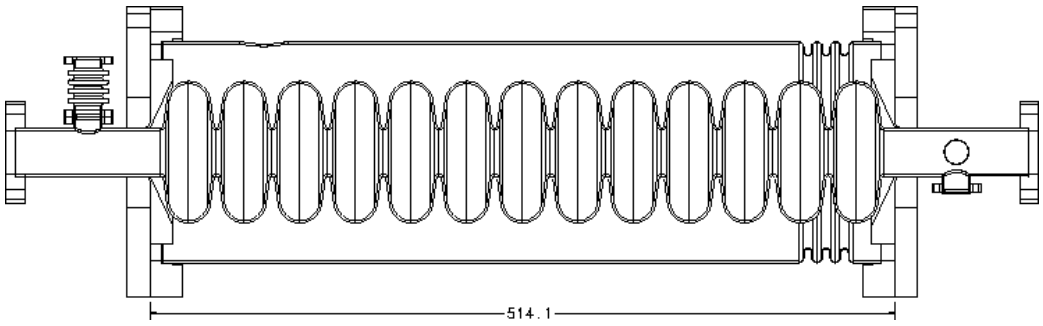

Figure 4.3: Conceptual drawing of cavity in demountable helium vessel.

manageable number for tuning, field flatness, and mode frequency separation. The equator and iris diameters are 94.4 mm and 30 mm respectively. The cavity would be polarized either by deforming a finished azimuthally symmetric cavity, or by using slightly elliptical dies.

There are two beam pipe flanges and four coupler flanges which must seal the cavity vacuum. One of the coupler flanges would be for the input RF power. The others are for monitor and (fundamental or HOM) power extraction. Beam pipe and coupler flanges are of a size comparable with CF35 and mini-conflat respectively.

It is proposed to use NbTi flange material and an Al o-ring design under development at DESY. This design allows for a reliable vacuum tight interface to stainless flanges while still using a solid o-ring with low particle production (as compared with helico-flex).

The flange arrangement shown in Fig. 4.3 would allow for a demountable helium vessel. End flanges of NbTi would be welded on the cavity end pipes. The rest of the vessel would consist of end caps and a cylindrical spool of titanium preferably (or of 316L, 316LN stainless). As shown this arrangement would allow for easy testing of different length cavities and a bellows section would accommodate tuning adjustment and thermal contraction. The vacuum seals here could be helico–flex as they are not associated with the cavity surface. (Further investigation is needed on the relative merits of stainless or titanium for the vessel construction.) The outer diameter of the vessel is $6''$ and consequently does not fall under pressure vessel code requirements (chapter 5031 of the FESHM). It is premature to say if such a helium vessel design would be appropriate for the final production cavities, but for the purposes of this report we have assumed so.

4.1.1 Mode and Shape

The …-mode has been selected, at least for the initial study. Other cavity modes such as …=2 or 2…=3 have been suggested because of their more favorable location on the dispersion curve and consequently their lower sensitivity to tuning and frequency errors, and the possibility of longer structures with more cells which clearly would be an advantage. Further work will need to be done to justify the choice of cavity mode. However the greatest experience lies with the …-mode and it minimizes the number of cells per meter and consequently the number of welds.

Some investigation of cavity shape has been made (Sec. 4.2.1). Perhaps more investigation is necessary; however multipacting is probably the key criterion and actual test results are needed.

Another key criterion is cell-to-cell coupling which needs to be kept large in order to minimize the effort needed for field flatness tuning. The potential difficulties in cavity tuning can and will be investigated with Cu models. These issues include achieving and maintaining field flatness and resonant tune.

Thus there remain a significant number of R&D paper studies, measurements, and bench tests to be carried out in parallel with moving ahead with construction of prototype cavities.

4.1.2 Frequency and Temperature Selection

The 3.9 GHz frequency is a frequency near where there is experience in building superconducting cavities. It is about as low as can be accommodated in the proposed beamlines; the 5.8 GHz choice outlined in Sec. 2.2 would be shorter in total length. The lower frequency leads to a larger iris and thus to larger beam size acceptance. It also reduces the required number of welds per meter, allows for longer structures (with cells/cavity fixed), and lessens the surface resistance losses (watts/m) which scale linearly with frequency for a fixed length of cavity structure and gradient.

Qualitative statements such as those in the preceding paragraph can be quantified by suitable analysis. Consider, for example, the impact of the rise of surface resistivity with frequency on heat transfer to the helium bath. The power per unit area developed on the inner cavity surface due to the RF is

$$\frac{dP}{dA} = \frac{1}{2} R_{sur} H^2; \tag{4.1}$$

where the surface resistivity, R_{sur} is the sum of the BCS resistivity

$$R_{BCS}[\Omega] = 2 \times 10^{-4} \frac{1}{T} \left(\frac{f[GHZ]}{1.5} \right)^2 \exp\left(-\frac{17.67}{T} \right) \tag{4.2}$$

and

$$R_{res}[n\Omega] = 0.3 H_{ext}[mOe] \sqrt{(} f[GHZ]) \tag{4.3}$$

Here it is assumed that R_{res} comes primarily from residual fields not shielded by the cavity magnetic shield. Typically, TESLA has been able to shield to about 10 mOe.

There are two factors contributing to the temperature difference between the inner surface of the cavity and that of the helium: the thermal conductivity of niobium, •, and the Kapitza conductance, H_k, which characterizes the temperature increment at the niobium-helium interface.

The thermal conductivity is very dependent on the purity of the Nb and is related to the RRR. It will be important for us to have material with as high a RRR as practical as heating from H_{peak} is likely to be the limiting factor in the achievable gradient.

For the purpose of this discussion, we have chosen • expressions that fit RRR=380[4.1]. However, it should be stressed that • values vary wildly.

$$\bullet = 0.27 T^{3.93} = 4.1 \ \frac{W}{m\ K} \ \text{ at } \ 2\text{K} \tag{4.4}$$

The Kapitza conductance[4.2] can be fit by

$$H_k = 0.02 \exp(2T) = 1.1 \ \frac{W}{cm^2\ K} \ \text{ at } \ 2\text{K} \tag{4.5}$$

Using the relationships above, plots of RF surface temperature versus helium coolant temperature can be made for various conditions. In Fig. 4.4, a number of contours are shown for various frequencies at the same surface field of 1000 gauss. Note that at 5.8 GHz and a material thickness, a thermal runaway situation at an inner surface temperature of approximately 2.1 K. In Fig. 4.5, the frequency is 3.9 Ghz throughout, and the variable parameter is peak field. The last two figures on this topic use cryogenic power as the ordinate. Fig. 4.6 maintains a constant gradient of 5.7 MV/m while varying the frequency, while Fig. 4.7 keeps the frequency constant at 3.9 GHz at different gradients.

In principle, the picture painted by this analysis could be changed by considering a thinner material or an alternative cavity fabrication technique, for example, sputtering niobium onto a copper substrate. But this leads to further R&D. In balance, we have selected a lower frequency

[4.1] TESLA LC Draft CDR, page 301

[4.2] H. Padamsee, J. Knoblauch, and T. Hays, *RF Superconductivity for Accelerators*, John Wiley and Sons, New York (1998), page 211

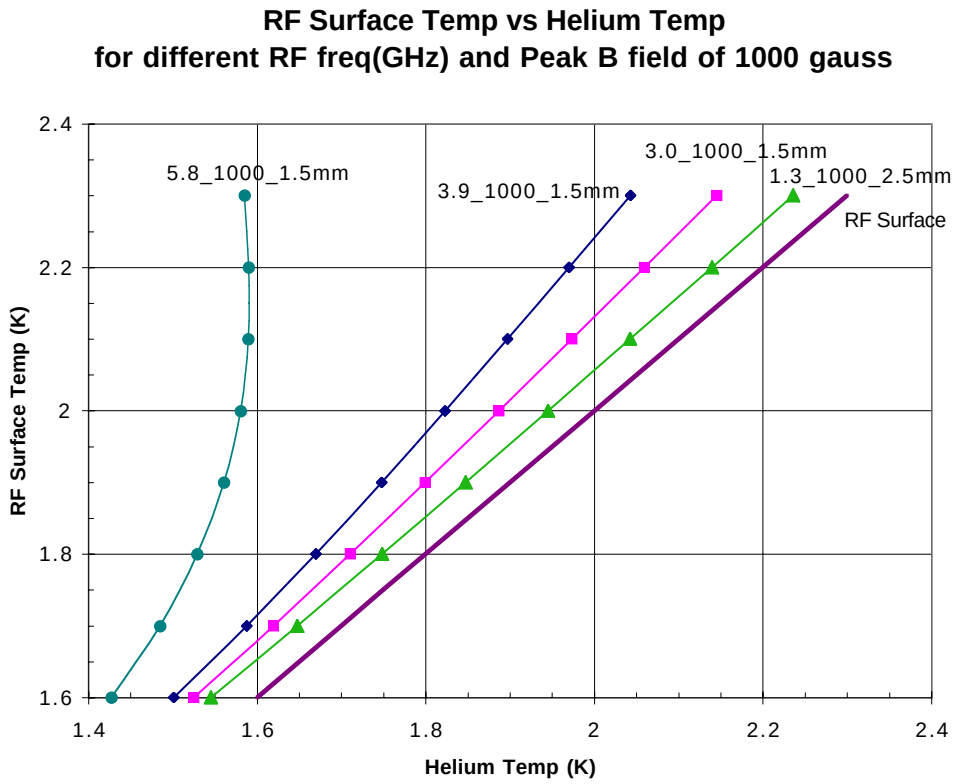

Figure 4.4: Inner surface temperature versus helium bath temperature for various frequencies at a peak field of 1000 gauss. Material thickness is 1.5 mm except for 1.3 GHz.

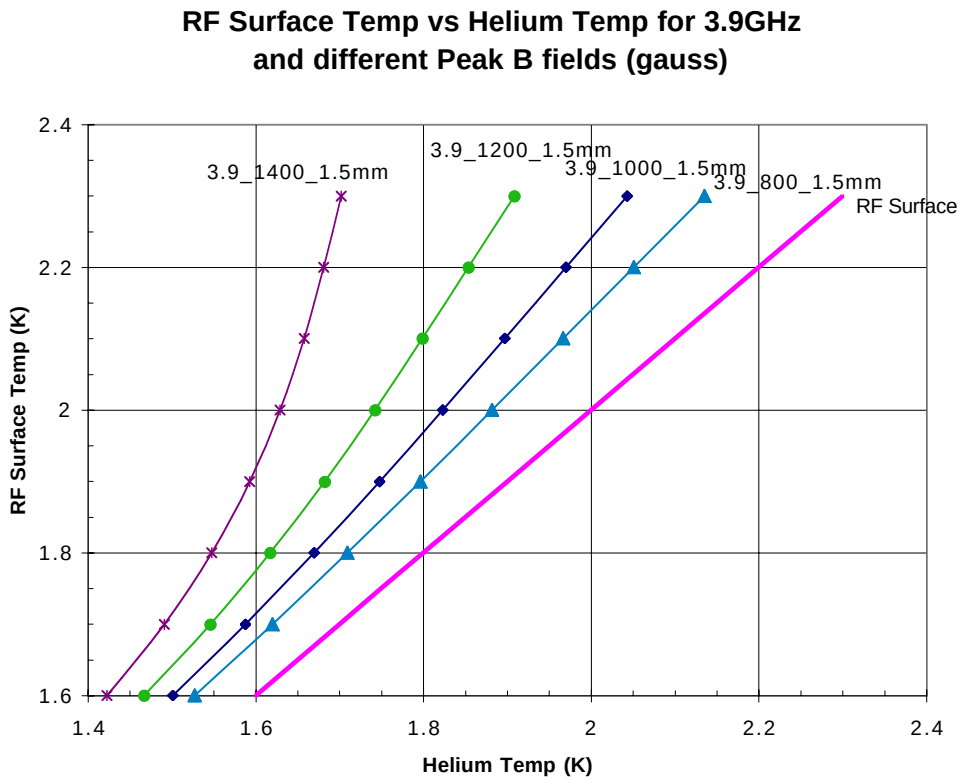

Figure 4.5: Inner surface temperature versus helium bath temperature for various peak fields at a frequency of 3.9 GHz. Material thickness is 1.5 mm except for 1.3 GHz.

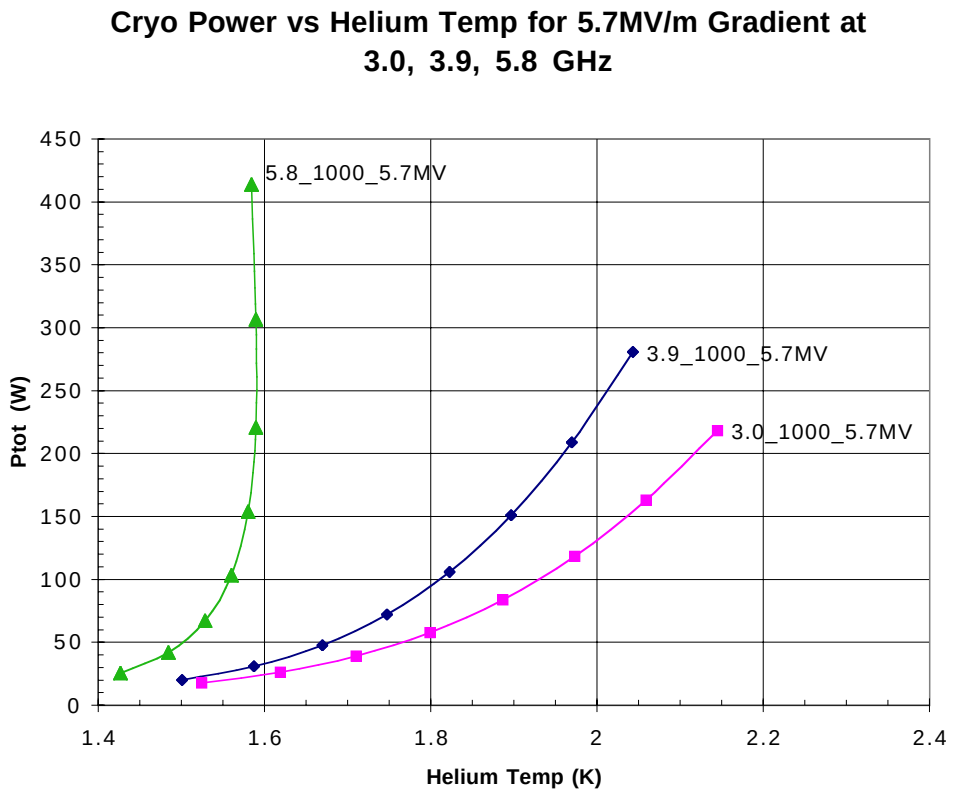

Figure 4.6: Cryogenic power requirement versus helium bath temperature for various frequencies at a deflection gradient of 5.7MV/m.

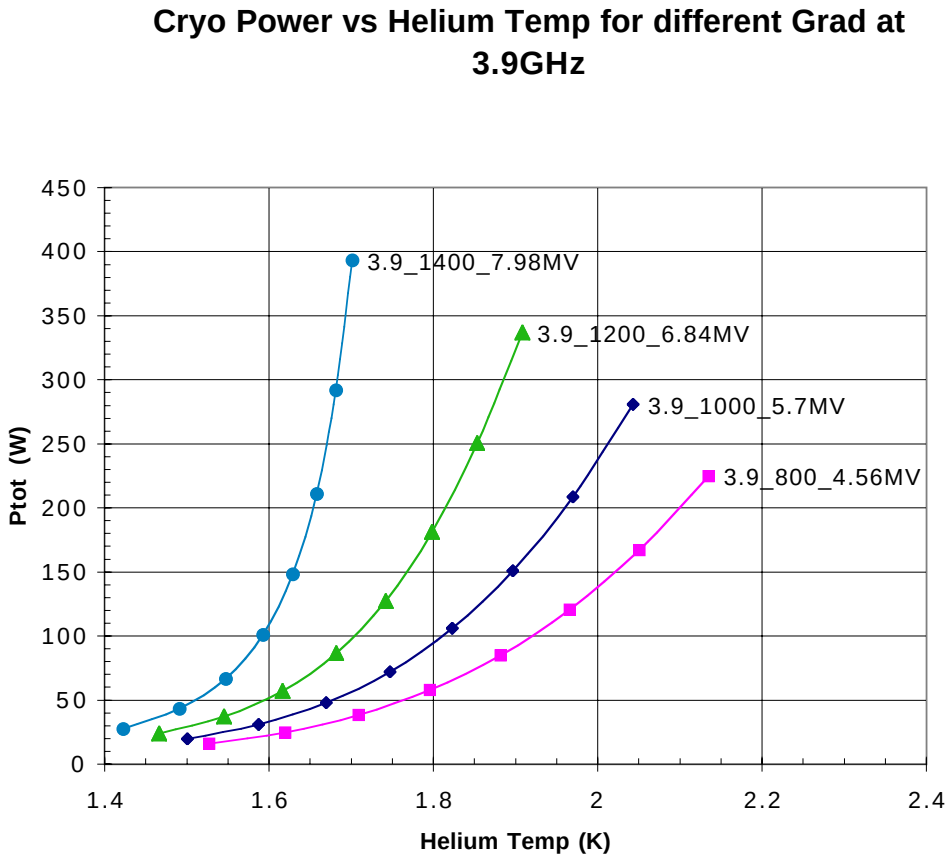

Figure 4.7: Cryogenic power requirement versus helium bath temperature for various deflection gradients at 3.9 GHz.

in the range of possibilities. The particular figure of 3.9 GHz was selected because, as a multiple of 1.3 GHz, there is the possibility of testing in the A0 beamline. A second look at 3 GHz will be worthwhile once the beamline is better understood.

4.1.3 Operating Parameters

Deflecting Gradient

The choice of operating gradient or transverse kick of 5.7 MV/m per meter has been made by requiring that the maximum surface B field on the cavity (near the iris) not exceed 0.1 Tesla. This can be compared with a peak of 0.105 Tesla at 25 MV/m for the TESLA 1.3 GHz accelerating mode cavities. (The theoretical limit is $\approx 0.2 - 0.24$ T.) It is interesting to note that TESLA cavity gradients are not only limited by B field quenches but also by field emission. In the transverse mode it may be possible to reach higher peak B because of the reduced ratio of peak electric to peak magnetic field. It will be interesting to compare maximum gradient limitations in transverse and accelerating modes (see Tab. 4.2). At this stage, the figure of 5.7 perhaps is better characterized as a goal rather than a choice.

Cavity Q and Dissipated Power

The achievable cavity Q will greatly affect the needed cryogenic power and system cost. Therefore a reasonable estimate of the expected Q is of considerable importance. As discussed in Sec. 4.1.2, the surface resistance scales like f^2. From measured Q's of existing cavities and their geometry factors, typical surface resistance, $R_s(f;T)$, numbers can be obtained and scaled to our frequency, geometry, and temperature.

The design Q specification for the TESLA cavities is 3×10^9 for TTF and 5×10^9 for TESLA LC. Actual measurements give typical Q's in the range 1–5$\times 10^{10}$ for lower field gradients before field emission and Q drop begins, but the Q then decreases into the 10^9 range at higher gradients. Thus we can see that even here there is a very wide range of just what Q should be chosen for a design specification.

We have chosen to use Fig. 3.2.1 of the DESY Draft Linear Collider Design Report to obtain a "typical" R_{BCS} using the scaling

$$R_{BCS} \propto \frac{f^2}{T} \exp\left(-\frac{1.76 T_c}{T}\right) \tag{4.6}$$

This paramaterization gives

$$R_{BCS}(3.9 GHz; 2K) = 1.1 \times 10^{-7}\ \ \Omega; \quad Q_0 = 2 \times 10^9;$$

and at a deflecting kick of 6 MV/m, the cw power dissipation is

$$P_{sc} = 12\ \text{ watts=m}.$$

A word of caution, however. The R_{BCS} curve of the TESLA cavity would lead to a Q of 1.9×10^{10} in a TESLA cavity. Though this sort of Q is realized, it is almost 7 times better than the specification for TESLA LC.

Cryogenic Power

In order to size the cryosystem which might be needed for the separators we have assumed a budget of about 20 watts/m and 10 meters of RF. Also we have assumed an operating duty factor

of one second in three (DF=1/3) and an overall contingency of a factor of 3, so that these two terms cancel resulting in a cryo system size requirement of 200 watt. We realize that this requirement has a somewhat arbitrary justification. Also we note that if higher gradients can be achieved the RF losses will increase.

RF Power

The RF power requirement depends on the loaded Q; our present choice of Q_L is 6×10^7 – a factor of 20–40 less than Q_0. This would lead to an RF power requirement of 400 watts/m, or total power of 4 kW. 200-400 watts is well within the range of TWT's though other sources may be more economical. The bandwidth (f=Q) at this Q_L is only 50 Hz, which may present a problem in terms of microphonics and rf phase/amplitude control. Lower Q_L's will need more RF power on resonance but may actually use less if microphonics and resonance frequency control lead to an f_0 spread larger than the bandwidth. We note that Darmstadt operates with a Q_L of 3×10^7 at 3 GHz.

In any case the final RF system must have a power margin for regulation, control and possible higher gradient operation, so an overall system size of 8-10 kW is probably reasonable to consider at this point.

Two types of systems should be considered: a) a system with few sources (one per RF station) able to drive many cavities, and b) a system with many sources each driving only a few cavities (one to two). These two choices might be represented by a) a klystron system, b) a TWT system.

The low level RF system will need to reflect the choice of high power system chosen. We note however that the TESLA vector modulator low level system is probably directly applicable to a system of type "a". Also the work at DESY on cavity "superstructures" where one coupler can drive a number of cavities through weak cavity to cavity coupling may make the …-mode structures more effective.

Cavity amplitude and phase (A&P) regulation requirements are not expected to be stringent compared with what would be required in an accelerator. Cancellation of the RF kick delivered to the beam probably need not be as good as 3%. Given the possibility of 4 separate stations, each with A&P control (or I&Q – see Fig. 5.36 leads to $\approx 1\%$ requirement for each amplitude component at each station. (Or about 1 degree for phase.)

4.1.4 Beam Tube Length

The Nb beam tube must be long enough to avoid excessive power dissipation in the flange joint and the adjacent normal conducting beam tube or endcap. The electromagnetic field of the $TM_{110\cdots}$ mode can be expected to decrease exponentially in the beam tube, since the resonant frequency is below the cutoff frequency for the lowest mode of waveguide propagation through the beam tube (the TE_{11} mode of a circular waveguide). For the parameters of choice (resonant frequency = 3.9 GHz, beam tube diameter = 30 mm) the decay distance ‡ is 10.9 mm, with the field varying in the axial direction as $e^{-z/\zeta}$.

A simple and conservative method for choosing the beam tube length is to specify that the field must decrease by a factor of 10^4 over the length of the beam tube. The electromagnetic energy density then decreases by a factor of 10^8, which is amply sufficient to compensate for the difference in surface resistance between the superconductor and the normal conductor. This method gives a beam tube length of 100 mm.

For a slightly more quantitative answer, the results of a numerical calculation with URMEL can be used. URMEL allows us to estimate the Q_{ext} due to power dissipation in stainless steel endcaps at the ends of beam tubes of length Δz. (We can expect the Q_{ext} to be somewhat higher in the case of a transition to a stainless steel beam tube, as opposed to stainless steel endcaps.) URMEL was used to calculate the stored energy U in a single-cell cavity with beam tubes of length $\Delta z_0 = 20$ mm, as well as the power dissipation $P_d(\mathrm{Cu}; \Delta z_0)$ in Cu endcaps. Using the surface resistances R_s(SS)

and R_s(Cu) of stainless steel and Cu, respectively, and the analytically known dependence of the field on axial position in the beam tube, one can estimate the Q_{ext} for stainless steel endcaps at the end of beam tubes of length Δz in an N-cell cavity. Solving for Δz as a function of Q_{ext}, we obtain

$$\Delta z = \Delta z_0 + \frac{\ddagger}{2} \ln \left[\frac{Q_{ext}}{N} \frac{R_s(\mathrm{SS})}{R_s(\mathrm{Cu})} \frac{P_d(\mathrm{Cu}; \Delta z_0)}{!\, U} \right] \; : \tag{4.7}$$

We will use the resistivity of stainless steel at room temperature to calculate R_s(SS); although there is some decrease in the resistivity with temperature, it is less than a factor of two. We also neglect the anomalous skin effect, which is not very significant for stainless steel. Taking a typical resistivity value for 304 stainless steel, we get $R_s(\mathrm{SS})/R_s(\mathrm{Cu}) = 6.51$. Using the values from URMEL, we get

$$\Delta z = 20 \text{ mm} + (5.45 \text{ mm}) \cdot \ln \left[8.7 \cdot 10^{-7} \frac{Q_{ext}}{N} \right] \; : \tag{4.8}$$

Thus, if we require $Q_{ext} = 10^{12}$ with $N = 1$, we need beam tubes of length $\Delta z = 94.5$ mm. However, if we require only $Q_{ext} = 10^{10}$ with $N = 13$, the beam tube length can be as short as 55.4 mm. Thus the choice of $\Delta z = 100$ mm is indeed conservative; we could make the beam tube shorter, if it is advantageous to do so.

4.2 Models and Measurements to Date

4.2.1 URMEL Calculations

Shape Selected for Modeling

URMEL has been used to adjust the cavity shape for frequency and to determine the expected Q, R_s (shunt resistance), transverse kick, associated peak electric and magnetic surface fields, and stored energy. The transverse kick and peak fields scale in proporation to one another, so an assumption of the maximum allowable peak field (either E or B) determines the maximum transverse kick that can be expected. The Q and R_s are based as well on an estimate of the superconductor surface resistance at the chosen frequency and temperature.

Fig. 4.1 illustrates the geometry chosen for the half cell in the body of the cavity. This shape was based on the TESLA shape with modifications for frequency and proportionately shorter half-cell length of the transverse mode due to beam transit time. URMEL output for this shape is presented in Appendix A.2.

Tab. 4.2 summarizes the URMEL results for copper and gives the scaling to the superconducting case.Included are the accelerating (fundamental mode TM010) and the two dipole modes. Both 0 and … members of the pass band are given. We are interested primarly in the TM110 … mode. Calculations with beam end tubes have also been run, but adjustment of the end cell shape to the body frequency is not complete. The fundamental mode (TM010) of the deflecting cavities is 2.7819 GHz, which is much lower in frequency than the desired 3.9 GHz operating frequency. Care must be taken as not to excite this fundamental mode and other dipole modes. The measured frequency spectrum of the cavity is shown in Fig. 4.8.

Variation of Cavity Shape

Our current design shape was taken from the TESLA accelerating cavities whose design has been optimized to reduce the various limiting effects of multipacting, field emission, etc. However, to ensure that this cavity design is still an optimum geometry for our application and to investigate the dependence of E_{trans}/B_{peak}, 25 variations, holding only the iris and the equator diameters constant, were examined. This exercise yielded no significant increase in deflecting voltage ($\pm 10\%$

Table 4.2: URMEL results for copper.

	1.3TESLA acc,pi	3.9cav acc,0	3.9cav acc,pi	3.9cav tranM,0	3.9cav tranM,pi	3.9cav tranE,pi	3.9cav tranE,0
Assignment	TM010	TM010	TM010	TM110	TM110	TE111	TE111
Urmel bound. [l,r,rot]	120	110	120	111	121	211	221
Urmel term	tm0em1	tm0ee1	tm0em1	1-ee-1	1-em-1	1-me-1	1-mm-1
freq [mhz]	1297.2	2748	2820.7	4102.2	3898.9	5079.2	4143.8
q (copper)	27103	14740	14665	19472	14508	27109	13076
r/q @r0 [ohm per cell]	115.5	176.4	76.5				
$(r/q)'$ [ohm per cell]				42.0	55.0	2.8	16.8
Ep/Eeff	2.13	1.52	2.68	3.14	3.84	9.12	8.10
Hp/Eeff [a/m/(v/m)]	0.0033	0.0033	0.0049	0.0066	0.0139	0.0322	0.0469
Bp/Eeff [gauss/MV/m]	41.5	41.5	61.7	83.2	175.2	404.3	589.6
r/q per m [ohm/m]	999.2	3233.2	1440.0				
$(r/q)'$ per m [ohm/m]				1150.2	1428.2	94.5	463.7
G1=R_{sur}×q [ohm]	254.7	201.7	203.2	325.4	236.4	504.1	219.6

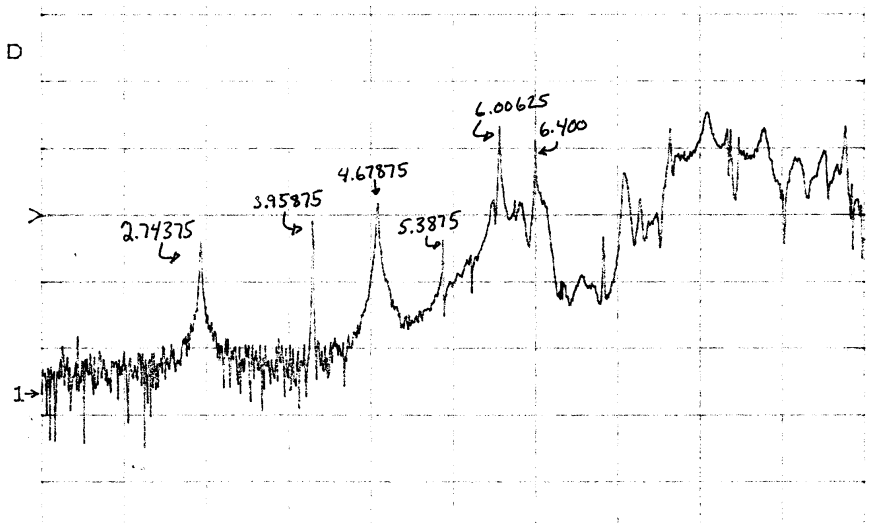

Figure 4.8: Measured frequency spectrum of copper cavity.

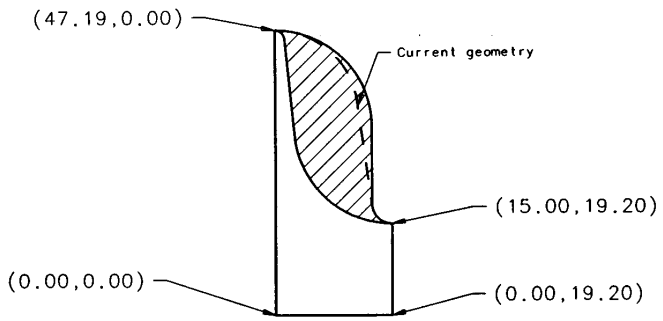

Figure 4.9: Region (shaded) of cell shape variations.

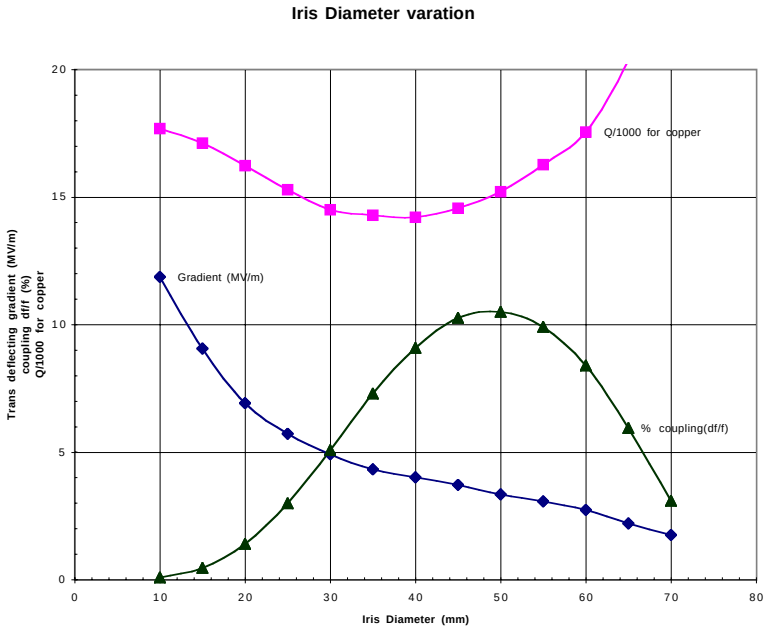

Figure 4.10: Sensitivity of deflecting gradient to iris size.

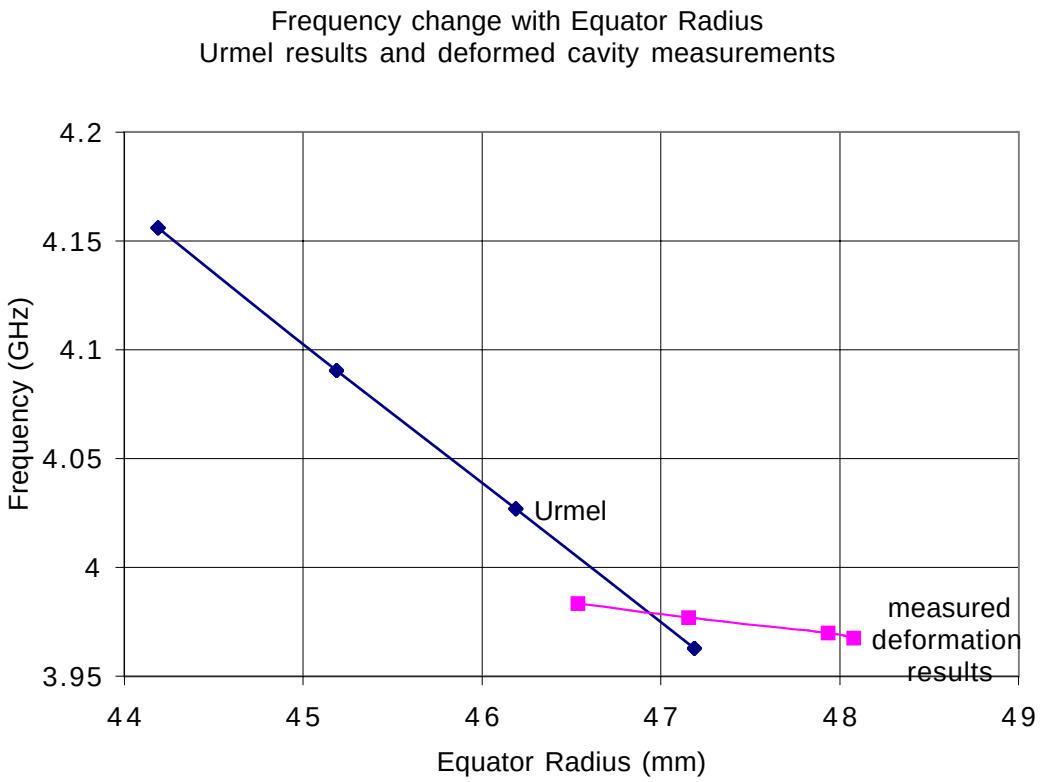

Figure 4.11: Sensitivity of deflecting gradient to equator diameter.

about 5MV/m), though a diverse collection of geometries were tried. The envelope of shapes that were tried is shown in Fig. 4.9.

Next, changes in the iris diameter were explored. Preliminary results are given in Fig. 4.10. Making a smaller diameter does lead to a higher but at the expense of cell-to-cell coupling and aperture. The result of changing the equator diameter is shown in Fig. 4.11. Here, one would not expect agreement between calculation and measurement; the deformation due to the C-clamp is scarcely axi-symmetric.

4.2.2 Single Cell Copper Model

Since the resonant frequency is dependant on the physical geometry of the resonator and not of the material used, a copper structure physically modeling the geometry of the proposed superconducting niobium structure was made for several reasons. First, the copper model provided the step-by-step knowledge required in the manufacturing of the actual niobium cavities without the expense of using niobium. Secondly, the copper cavity provided an excellent device to test the RF properties, verifying the URMEL predictions, and allowing us to proceed with confidence in niobium construction of the cavities.

Coupling and Q Measurements

RF coupler test fixtures were machined to allow the input and transmission coupling to be varied from over-coupled, to unity-coupled, and beyond to under-coupled. With very small input coupling,

Table 4.3: Data for tuning rate.

Distance (mils)	Freq. Change (MHz)	Rate (kHz/mil)
10	4.13	413
20	12.0	600
30	19.0	633
40	25.0	633

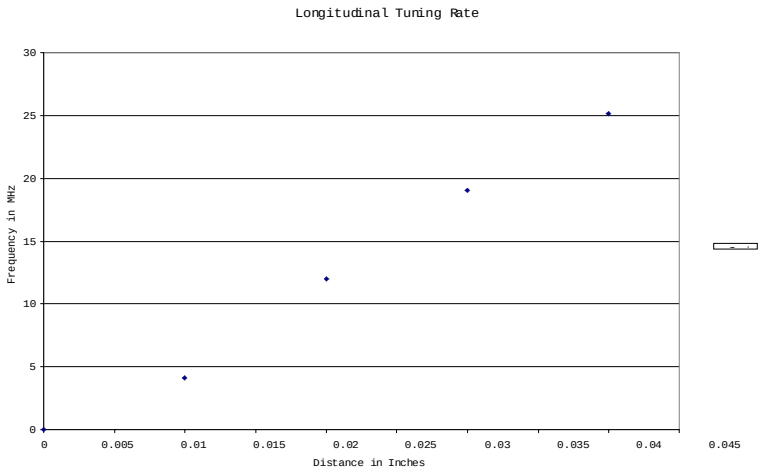

Figure 4.12: Tuning rate under longitudinal compression.

on the order of 1%, the effect of the Q_{ext} becomes minimal, and a transmission measurement on the cavity provides a good measurement of Q_0. Care must be taken to identify the polarization that one is interested in.

Longitudinal Tuning and Tuning Rate

Once the cavity is in place in its cryostat its frequency will need to be fine tuned. This tuning is generally done by adjusting the length of the cavity. The longitudinal tuning rate of the single cell copper model has been measured. A clamping fixture, that snugly and uniformly applied pressure directly to the cavity walls near the Iris, (to mock pressing on the beam pipe), was placed around the single cell to measure the tuning rate. Four uniform compressions that did not exceed the yield tolerances of the copper were performed. The results are given in Tab. 4.3 and Fig. 4.12, and yielded a value of about 24MHz/mm (600 kHz/mil). For a 13 cell cavity this would become about 2MHz/mm.

Polarization of Deflecting Mode

Deflecting mode resonators will have two polarization vectors which must be controlled to provide the desired transverse kick direction. Deflection in the desired direction can be obtained by constructing the cavity so as to have different frequencies for the two polarizations, and exciting only the one which gives the appropiate kick. Typically this is achieved by choosing a different equator diameter on the horizontal and vertical axis of the cavity. If the diameters are equal (symmetrical

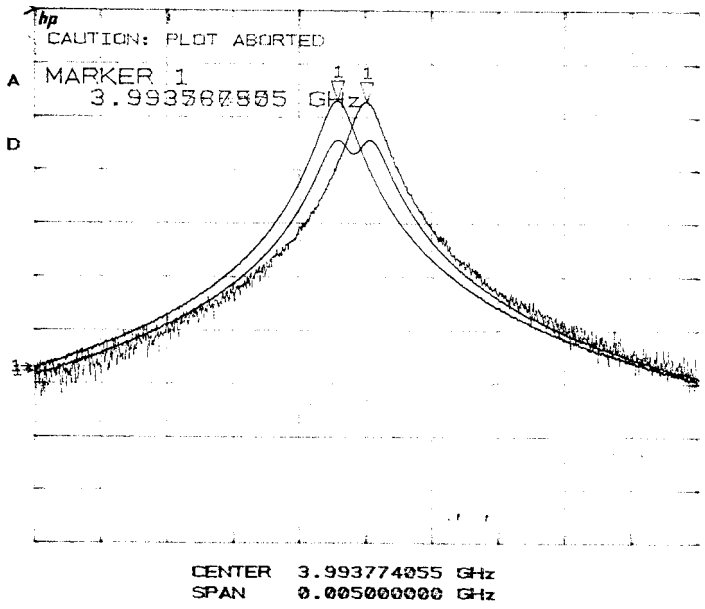

Figure 4.13: Initial separation of polarizations.

cavity)then the frequency split is very small and determined by dimensional tolarances.

In order to experiment with frequency separation of the two polarizations, the single cell copper cavity was setup in a test fixture. Each polarization could be individually excited as well as both partially excited simultaneously. This was done by fixing the position of two input couplers whose RF antennas were asymmetrically located in the beam pipes, while the cavity was free to rotate about the longitudinal axis.

The two polarizations were located and marked on the cavity. The initial separation of the polarizations was 360 kHz, relating to a machining tolerance of about 0.001 inches. An attempt was made to see this difference by measuring the outside equator diameter at the two locations corresponding to the two polarizations. This physical difference was not seen, and it is assumed that the difference lies in the variation of the bead from the electron beam welded seam that joins the two half-cells at the equator.

We proceeded to separate the polarizations further by squeezing the cavity radially on its equator. The diameter that was chosen was the one relating to the higher frequency. A large C-clamp was positioned around the cavity applying force to the two locations defining the higher frequency polarization. Three systematic compressions were performed. A spectrum plot was made before compressions began and then after each one had stabilized. Fig. 4.13 is a compilation chart that shows each polarization being individually excited, as well as them both being equally excited. The separation here is approximately 360 kHz. After the longitudinal tuning experiment the separation became 964 kHz. This value of 964 kHz is assumed to be the initial separation for this experiment. Fig. 4.14 shows a typical plot of frequency separation as the cavity was compressed further.

The results are tabulated in Tab. 4.4 and in Fig. 4.15. After each compression, the physical dimensions of both polarizations were re-measured ensuring that only the dimension we were interested in changing changed while the other held tight. Indeed this was found to be true. It should also be noted that the cavity was checked to see if the orientation of the polarization rotated in the cavity as a result of the squeezing, but they were found to remain fixed. The Q and frequencies

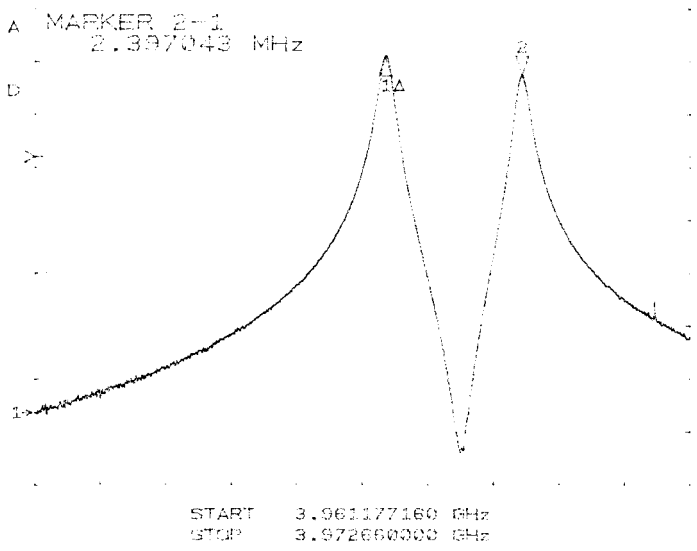

Figure 4.14: Separation after first compression.

Table 4.4: Study of transverse polarization modes, as the single-cell cavity is compressed along the axis associated with the upper frequency mode.

Measurement	Initial value	Comp. 1	Comp. 2	Comp. 3
Freq. Sep. (Mhz)	0.964	2.937	7.083	11.658
LFP Comp. (mm)	0.00	0.00	0.00	0.00
LFP Freq. (MHz)	3.9964	3.9673	3.9697	3.9713
LFP Q	15255	14169	14177	15274
UFP Comp. mm	0.00	0.29	1.85	3.09
UFP Freq. (MHz)	3.9673	3.9672	3.9768	3.9831
UFP Q	15258	14178	16570	15319

of both polarizations were meaured each time. As was to be expected, the Lower Frequency Polarization (LFP) frequency moved slowly while the Upper Frequency Polarization (UFP) frequency changed much faster. The change in the split of the polarization frequencies is about 3MHz/mm cell diameter distortion.

4.3 Cavity Fabrication

In principle superconducting cavities can be made by a variety of manufacturing process. The processes include: machining, deep drawing and electron beam welding, hydroforming, spining, sputtering on copper. We have chosen deep drawing and ebeam welding as this is the most common method employed. Sputtering might also be interesting as copper forming of multicell structures might be possible, though sputtering in such a small cavity might be difficult and the high surface magnetic fields might lead to low Q's.

A number of cavities with various numbers of cells will be built. At this writing, the effort will concentrate on 3.9 GHz , …-mode cavities. Cavities of Cu, reactor grade Nb, and high quality Nb

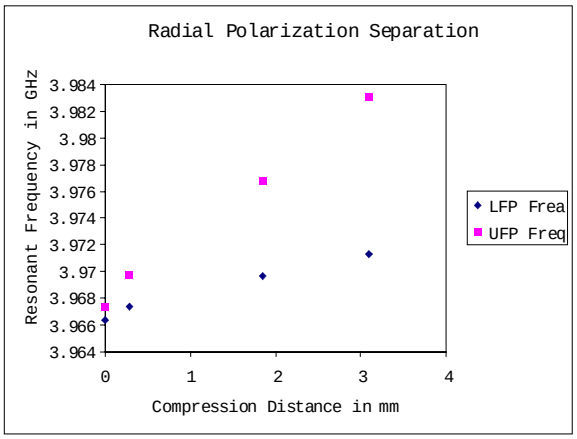

Figure 4.15: Summary of polarization separation results.

Table 4.5: Planned cavity prototypes.

Cu models	
1 cell	1 (done)
2 cell	2 (done)
5 cell	2 with coupler ports, end flanges
13 cell	2 with coupler ports, end flanges
Nb reactor grade	
1 cell	2 with end flanges
3 cell	2 with end flanges
5 cell	4 as above and with helium vessel flanges
13 cell	4 as above
Nb high RRR	
13 cell	4 as above

are planned. The Cu cavities allow for bench testing and measurements; the reactor grade Nb allows for the development of the fabrication process while using less expensive material; final cavities will be built with high RRR material after some expertise with fabrication has been gained. Tab. 4.5 indicates the sorts and number of prototypes which might be expected.

Following fabrication, the cavities will be subjected to processing and test procedures. These steps are described in Sec. 4.4 and Sec. 4.5 respectively.

4.3.1 Fabrication Overview

This subsection will outline the process for fabricating a multi-cell, superconducting, deflecting cavity[4.3]. The geometry of the 3.9 GHz half cell is shown in Fig. 4.1. The niobium material to be used has a thickness of $0.062''$.

1. Discs of the proper diameter are cut from $0.062''$ niobium plate of prescribed grade. A small hole is punched in the center of each disc.

2. Half-cells are deep drawn from the niobium discs using a die. The die consists of three parts: a male die, a female die, and a material retention ring (see Fig. 4.16.

[4.3]This discussion draws freely upon the TESLA cavity fabrication specification and on conversations with Axel Matheisen

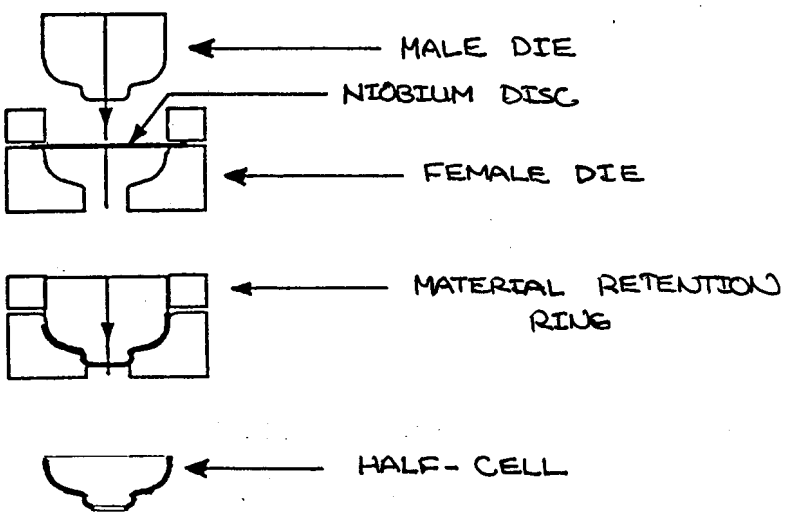

Figure 4.16: Die for deep drawing.

3. The iris and the equator of each half cell are machined to the specified tolerances to prepare them for welding.

4. Half cells are cleaned, etched, rinsed, dried and packaged prior to welding.

5. Pairs of half-cells are ebeam welded together at the iris to form a dumbbell structure.

6. Dumbbells are cleaned, etched, rinsed, dried, and packaged prior to welding.

7. Dumbbells are ebeam welded together at the equator to form a multi- cell cavity structure.

8. Beampipes and flanges are ebeam welded to the ends of the structure to form a complete cavity.

9. The cavity is leak checked, cleaned, and packaged preparatory to processing.

The superconducting RF properties of a niobium cavity are extremely sensitive to surface imperfections, discontinuities or inclusions of foreign material. These may be introduced by: (i) Improperly processed or formed niobium plate, (ii) Machining of the interior (RF) surface of the cells, (iii) The welding process used for joining the half-cells and dumbbells, or (iv) Unintended contact with the RF surface of sufficient force to gouge, dent or otherwise mar the surface. The preparation and fabrication procedure outlined above and detailed in the following subsection is designed to minimize the probability of such an occurrence.

Specified cell profile and length are important factors necessary to achieving desired resonant frequency. Dimensions in drawings prepared for the fabrication of half cells must allow for shrinkage due to ebeam welding and loss of material due to etching, so that after final assembly the tolerances specified for cell profile and length are met. Sample welding will determine typical shrinkage.

4.3.2 Details of the Fabriciation Process

Specifications for the chemical, mechanical and metallurgical properties of niobium plate for both reactor grade and high RRR material are listed in Appendix A.3. Reactor grade material will be used initially until the fabriciation process has matured.

Half-cells

Circular blanks 125 mm in diameter are saw cut from the niobium plate. A small hole 3 mm in diameter is punched in the center of each blank. Using a die each blank is deep drawn into a half-cell. The surface profile of the male and female dies is machined to match the design profile for the interior (RF) surface of each half-cell, with the exception that the female die profile incorporates a 0.062″ allowance for material clearance. The dies are machined from 7075-T6 aluminum. Clean 10W-30 motor oil is used as a die lubricant for each deep drawing operation. Parts are then cleaned with acetone.

The iris and equator of each half-cell are machined in preparation for welding. Experience[4.4] has shown that square butt joints at both locations are the most desirable. The material adjacent to each weld location must be machined to be of consistant uniform thickness, and any gap existing between two mating surfaces to be welded must not exceed 0.004″.

The half-cells are cleaned etched, rinsed, dried and packaged as described under Chemical Etching below. To prevent oxidation of weld preparations, the welding operation must commence within eight hours of the time the prepared parts have been packaged for transfer to the welding site.

Dumbbells Welding half-cells together at the iris to produce a dumbbell is an operation especially critical to the achievement of maximum accelerating gradient. Welds must be full penetration with smooth underbead and wide uniform width on the RF surface of the cavity. Protrusion or drop-through of the underbead relative to the surrounding unwelded surface is required not to exceed 0.004". No defects, cracks, pores, or inclusions of foreign material are allowed. Eddy current and other measurements can be performed to check the welds. Distortion of the half-cells must be minimized. The thermal conductivity of the material at the finished weld must not decrease by more than 10%. These requirements effectively eliminate any process other than ebeam welding.

Half-cells are butted at the iris and secured in a welding fixture. The welding fixture must hold the equator planes of both half-cells parallel, while allowing them the freedom to draw together axially to accommodate shrinkage. The welding fixture must not contact the interior surface of either half-cell. Any initial out-of-roundness at the joint is corrected by securing a stainless steel belt around the joint and spot welding through small holes in the belt. The belt is then removed for the final circumferential weld.

Electron Beam Welding

Successful ebeam welds require proper adjustment of several welding machine parameters. Among these are beam power (accelerating voltage and beam current) and material feed rate. These parameters are best determined by performing a sequence of preliminary sample welds using the same machine that will be utilized for the production welds.

To achieve the required uniform, smooth underbead previous research[4.5] has found it is desirable to distribute the beam power as the weld progresses by deflecting the beam into a continuously repeating pattern. The effect is to reduce the deposited energy density at the point of the weld while heating the whole weld area. (see Fig. 4.17).

The most appropriate pattern is another factor best confirmed by preliminary sample welds.

Due to the high attraction of oxygen for niobium, a vacuum of less than 5×10^{-5} torr is required during welding. When the welds are completed the welder vacuum chamber is vented with clean nitrogen after the temperature of the parts has dropped below 100C at the hottest point.

The welds (or weld samples) must be tested to determine if electrical conductivity (RRR) at the weld has degraded by more than 10% relative to that of the unwelded niobium. RF frequency tests

[4.4] Kirchgessner, J., *Forming and Welding of Niobium for Superconducting Cavities*, Proceedings of the Third Workshop on RF Superconductivity, Report No. ANL-P-88-1, Vol. II, p. 533, Argonne National Laboratory, Argonne, IL

[4.5] Kirchgessner *op. cit.* and P. Kneisel, *Statement of Work – Cavity Procurement*, 1988, CEBAF, Newpoer News, VA.

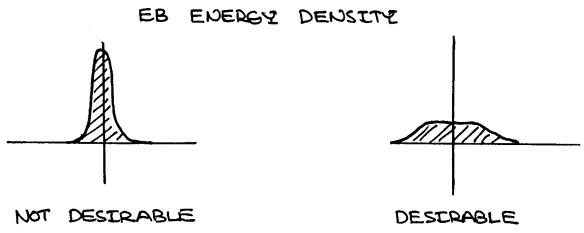

Figure 4.17: Energy density distribution in ebeam weld.

and possible machining of the equator weld prep areas can take place at this time. The dumbbells are etched and inspected for surface imperfections. Grinding if necessary takes place at this time and the dumbbell is re-etched.

Multicell Assemblies

The dumbells can now be welded into multicell assemblies by joining at the equator. The same weld specifications listed above apply.

The dumbbells are cleaned, etched, rinsed, dried, and packaged. As above, there is an eight hour window for welding. The etching at this step can be just in the region of the weld (e. g., from the edge to be welded back $1/2''$.)

The dumbbells are butted together at the equator and secured in a welding fixture that maintains the equator planes parallel and perpendicular to the beam axis, and the iris bore diameters coincident. The welding fixture must not contact the interior surface of the dumbbells. As before a stainless steel belt is used to force the equator joints round, and each joint is spot welded through holes in the belt. The belt is then removed for the circumferential equator weld(s). The same welding procedure is followed as that described above. During welding all other prepared joints must be shielded to prevent contamination due to deposition of niobium vapor.

End Cell and Beam Pipe

The end half cell and beam pipe assembly represents significiant detailed welding. The beam pipe consists of: the pipe itself which (most likely) must be rolled and welded from flat material, the end flange (Nb, Ti), two coupler side port pipes and flanges (NbTi), and the cavity helium vessel end flange (NbTi). This assembly must be joined to the end half cell, which is of slightly different shape than the body half cell (in order to have the same resonant frequency). (It would be desirable for this half cell to have a long enough neck in order to make the welding of the helium vessel end flange easier.) Details of the welding steps must be developed. The process follows a procedure similar to that above for the central cells. A special welding fixture that forces coincidence of the beam pipe and iris apertures is required.

The finished cavity components are leak checked (leak rate less than 10^{-10} Torr l/s on 10^{-9} scale or less) cleaned and packaged.

Welding Complete Cavity

The complete cavity consists of 12 body cells and 2 end half cell beam pipe assemblies. The proposed welding cycles are:

- 12 dumbells are welded from half cells (4 at a time, 4 welds each)
- 3 4 cell cavity sections are assembled from 4 dumbells (3 welds each)
- 2 end half cells and beam tube assemblies are fabricated ($\approx$ 8 welds each end, about 5 weld cycles total)
- 2 end assemblies and 3 body assemblies welded (4 welds)

From this the total number of weld cycles per cavity would be about 13. If one estimates 5 hours per weld cycle at 200$/hr this would result in $13,000 in welding costs per cavity.

The ebeam welding is done in two pumpdowns of the weld chamber which involve a total ot three welding steps:

- First pumpdown – mount tack weld fixturing, pump down, tack weld, cool down, vent, remove tack weld fixturing.
- Second pumpdown – mount final weld fixturing, pumpdown, weld 1st pass (half penetration–half current), weld 2nd pass (full penetration–full current), cool down, vent.

This 2 stage final weld process employing a wiggled beam is considered very important for achieving flat, wide, and complete penetration welds. Welding from the outside surface has been found to be fine, so one need not consider inside welding.

Welding parameters, weld chamber preparation, material handling procedures, plastics, and grinding information are covered in Appendix A.4.

4.3.3 Approaches to Cavity Fabrication

Several approaches to cavity fabrication are possible:

1. We could fabricate and weld the cavities ourselves
2. We could fabricate parts (or have them fabricated) and have welding done outside
3. The whole cavity could be fabricated by an outside vendor

Different approachs may be appropriate during prototype R&D and final production. Certainly the number of cavities needed for final production will influence just how it is best carried out. Fabrication of 28 or more cavities to specific drawing specifications probably could be best carried out by a vendor. However the ability to do one-of-a-kind fabrication for R&D and initial prototype structures is key to a laboratory program.

The proposed approach for the initial R&D is "2". Complete fabrication of cavities by an outside vendor can be considered later in the program. Gaining experience with the design and fabrication details on first prototype cavities, as well as flexibility in just what is built and feedback from the testing program make this choice desirable. The infrastructure needed is the same as for the testing program.

The choice of working with an outside welding company is strongly influenced by the near location (Chicago) of one of the leading ebeam welding companies and the availability of their state-of-the-art welding machines and welding expertize. This alternative appears much more attractive than using welders at Fermilab or Argonne. Both welding machines are old and at Fermilab little expertize has

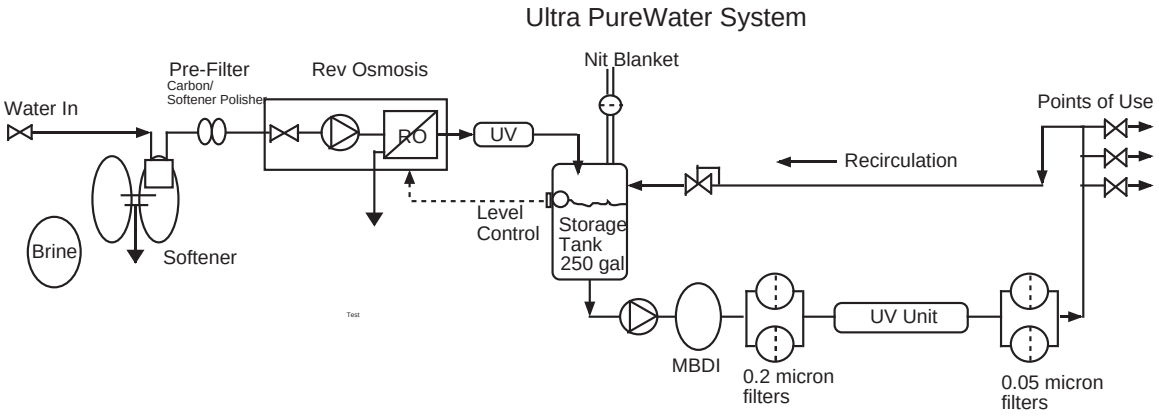

Figure 4.18: Ultrapure water system at A0.

been built up. Acid etching prior to welding would need to be done at Fermilab or Argonne as it would be difficult for the company to set up chemistry for a limited job.

The deep drawing and machining of parts could be done either at Fermilab or at a local fabricator. At least one fabricator in the area has experience with niobium.

Were the initial prototype cavities to be completely fabricated in industry, a flexible (development) contract would need to be initiated. Even so it would seem difficult to get the initial program of one cell to few cell to the first 1/2m test cavities underway. The most qualified vendors are in Europe and a close connection to the company (perhaps through a European collaborator) would need to be set up.

4.4 Cavity Processing

4.4.1 Infrastructure

Ultrasonic Cleaning

Immersion in an ultrasound bath is the basic initial (and sometimes final) cleaning process for almost all but the most fragile of components. Till now, units adequate for small parts have sufficed at A0, supplemented by an old and larger unit no longer needed by the Linac group. The latter has now aged beyond repair, and needs to be replaced. At Argonne, there are very large tanks that were used for cleaning the vacuum chambers of the APS, and these can be used for the occasional outsize item.

Ultrapure Water

An ultrapure water system has been set up at A0. This system is rented from CWC Fluids–Culligan Industrial and is shown in Fig. 4.18 The system follows the standard 2 part layout. Inlet water feeds a pretreatment softener– reverse osmosis unit that delivers its output to a storage tank; the storage tank is part of a polishing loop that includes the points-of-use (POU's). The softener–reverse osmosis system includes a standard water softener, a carbon prefilter, a particulate filter, a booster pump, and the 200 gallon per day reverse osmosis unit feeding the 250 gal polypropylene storage tank. The tank has a nitrogen gas blanket fed by a pure nitrogen source. The secondary loop contains a recirculating pump, a mixed bed deionizer (MBDI), 0.2 micron filters, followed by a

UPWater System						
		CU	LANL	Grade E1	ASTM Type1	Milli-QPlus
	units					
Resistivity	MOHM-cm	>18	"	*	16.7	18.2
Silica	ppb w	5	"	*	<1 ppm	10
Particulates	>0.5mic/lit	<5	2@1mic/ml??	*	<500/lit@>0.2mic	
	>0.1mic/lit	<100	<25			
Micro Organisms	per mlit	<1	1	*		
TOC	ppb	50	50	*		5
Bacteria	CFU/100mlit	<1	<1			<1cfu/mlit
Total Residue	ppm	<0.1	<.1		0.1	
Cu	ppb w	1	1	*		
Chloride	ppb w	2	2	*		
Potassium	ppb w	2	2	*		
Sodium	ppb w	1	1	*		10
Residual solids	ppb w	10	10	*		
Zinc	ppb w	5	5	*		
Dissolved SiO2	ppb w	<5	<5			
Iron	ppb w	<2	<2			
Heavy metals	ppb w					10
Note ppb w=micro-g/lit						
LANL lists ASME Elect Grade E-1						
CFU colony .... unit?						

Figure 4.19: Typical specifications for ultrapure water systems.

UV unit and 0.05 micron final filters. The resin used in the beds is semiconductor grade precleaned and validated. Piping on the water skid is PVC. Tubing into the cleanroom area is polyethylene.

The system is specified to provide Type 1 water similar to Millipore Milli Q-Super: 18 MegOhm-cm, 0.05 micron filtered, low total organic carbon (TOC) water. POU flow is 5 GPM, daily usage 150 GPD.

This system is not as exacting as that specified by other labs. For instance PVC pipe is used instead of PVDF. Even so $\approx$ 200 ppb TOC is expected after initial run–in whereas the requirements of other labs call for 50 ppb TOC.

Typical specifications provided by other labs with superconducting cavity programs are listed in Fig. 4.19. As it is not completely clear to us just exactly which of these are most critical we will need to not only see just what our quality is but also estimate whether improved quality is indeed necessary. Even so some "bad" practices such as tubes without continuous flow at use valves should be corrected. The system has been used extensively over the past year in the cleaning of components for the A0 photo injector. However a water sample analysis has not been made and would need to be carried out and gross deficiencies rectified prior to work on cavities.

The TESLA cavities require of the order of 300-400 liters ($\approx$ 100 gal) of water after chemistry to reach 18 Mohm-cm water conductivity. Typically during high-pressure rinsing 20 l/min is used for up to 2 hours (total of $\approx$ 650 gal). As the area of the separator cavities is considerably smaller the 250 gal storage tank is probably sufficient but could easily be increased in size if necessary.

Additionally a separate system which recirculates and refilters used water could be implemented.

Not only will the present water system be needed at A0 but a similar one will be needed in the village in association with the chemical etching process where rinsing with UP water follows the etch

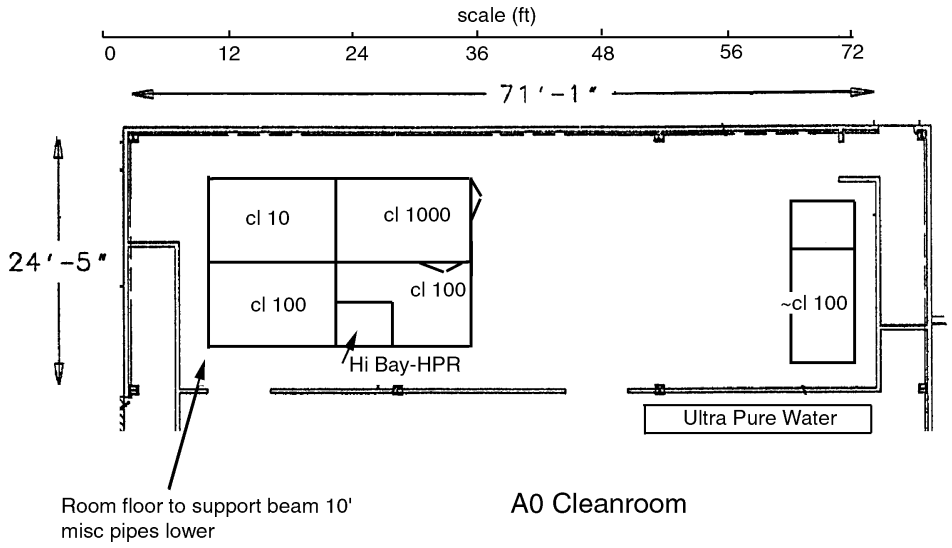

Figure 4.20: Cleanroom area at A0.

process.

Cleanrooms

A cleanroom area has been set up at A0. Fig. 4.20 illustrates the layout. Including movable units, cleanrooms available include:

- some home built portable units $4' \times 2'$ and $2' \times 2'$. These are used wherever a temporary clean environment is required.
- a $4' \times 6'$ movable unit
- a home built/surplus unit of about $5.5' \times 12'$ with a $5.5' \times 4'$ entry/anteroom area. This area is located against the north wall of the room.
- a $16' \times 25'$ commercial unit which includes an $8' \times 12'$ entry/anteroom area (class 1000), a $4.5' \times 5.5'$ hi bay area for high pressure rinsing, and an $8' \times 12'$ class 10 region. The rest of the area is class 100.

All of the units are soft wall. The north wall unit presently has ultrapure water and filtered $N_2 2$ available and is typically better than class 100.

It is expected that these clean rooms when outfitted with water, air and the high pressure rinsing system will be sufficient for the planned cavity preparation. The $4' \times 6'$ unit will probably be moved to the village chemistry area.

High Pressure Rinsing

High pressure rinsing with ultrapure water has become a standard stage in the superconducting resonator manufacturing process. After rinsing with the use of ultrapure water, the number of

particles that contaminate the resonators inner surface can be significantly reduced. It helps to achieve high quality and reproducibility of cavity performance –see for example, Kneisel and Lewis[4.6].

The system which has been designed for Fermilab will accommodate resonators as large as the 9-cell TESLA style, which is about 53 inches (135 cm) in length. Vertical space available is limited by the height of the room (133 inches or 3.35 m) where the system is to be installed. The approach with fixed water pipe and movable resonator was chosen because it did not require a filter installed in series with a moving pipe; that helped to save some vertical space. As usual, the way to clean the resonator surface is to scan water jets from nozzle orifices located at the end of the delivery pipe, along the resonator surface. The surface must be cleaned systematically; the resonator rotation and vertical movement rates must be coordinated so that no part of the resonator surface is left untreated.

The system consists of a pump assembly and process tower. The pump assembly includes the pump itself, filters, pressure gauges, relief valve, and a pipe with nozzle. It takes water from the ultrapure water system available at A0. The amount of water needed for treatment was chosen based on the analysis of the available data from DESY, CEBAF, Cornell University, and KEK. This number varies from 50 cm^3 to about 120 cm^3 of water for each 1 cm^2 of the surface depending on size of a resonator to clean. If we choose 100 cm^3 as a target number, the total amount of water required for rinsing the 9-cell TESLA resonator (2 m^2 of surface area) is about 2 m^3. The water pressure range usually used for rinsing varies from 80 to 150 Bar. For a pump driven by a 5 kW motor that can provide maximum water flow of 4.0 GPM (15 l/min) at 1800 PSI (125 Bar), it will take more than 2 hours to process all the resonator surface.

Two filters are used to reduce the amount and size of contaminating particles in the water. The first has a 1.2 „m cartridge; the polishing filter uses a 0.2 „m cartridge. The filter housing is made from stainless steel and rated to 1500 PSI (100 Bar) pressure. In order to protect the system, a pressure regulator (relief valve) is installed in the system that keeps the pressure below 100 Bar. The total water flow can be adjusted by changing the number and size of the orifices in the nozzle. The nozzle has a stainless steel body with twelve 0:02″ (0.5 mm) diameter orifices located in two rows. This will limit water flow to about 2.5 GPM (10 l/min). The inclination of jets in each row is about 30 degrees to the midplane of the nozzle.

Process tower provides the movement needed to scan the surface of the cavity. Taking into the account the diameter of the water jets, which can (theoretically) be slightly less than the diameter of the nozzle orifice, and the number of orifices, it is possible to find the required vertical movement rate based on the chosen rotation rate. To make the vertical movement rate reasonably large, the rotation rate was chosen to be about 30 RPM; it gives a vertical movement rate of about 0.08 in/sec (2 mm/sec). With this movement rate, it will take about ten strokes to complete the rinsing.

The layout of the process tower is shown in Fig. 4.21. The cavity structure to be cleaned is installed onto a rotating table and clamped in position with the use of an adjustable support structure. The table is rotated by a gearmotor; the needed rotation rate is insured by the proper choice of timing pulleys and motor type. The vertical movement of the table is provided by the set of three ball screws and three ball nuts that are attached to the carriage plate that bear the rotating table. Rotation of the screws causes the plate to move up and down. This rotation is synchronized with the use of a timing belt and pulleys. A gearmotor is used as a driver, and a couple of timing pulleys adjust vertical movement rate. The tower frame is a welded triangular prism with top and bottom plates that house end bearings for the driving ball screws and end clamps for three alignment rods. The top plate has a circular opening for the resonator to go through while it is moving vertically. To adjust the system stroke, two Reed switches can be installed to give a feedback signal to a movement control circuit.

The water delivery pipe must be located along the axis of the resonator. An alignment fixture is installed on the bottom plate of the tower frame that provides the opportunity to change the pipe

[4.6]P. Kneisel and B. Lewis, *Advanced Surface Cleaning Methods*, Seventh Workshop on RF Superconductivity, Saclay, Oct. 1995; Proceedings, pp. 311-327

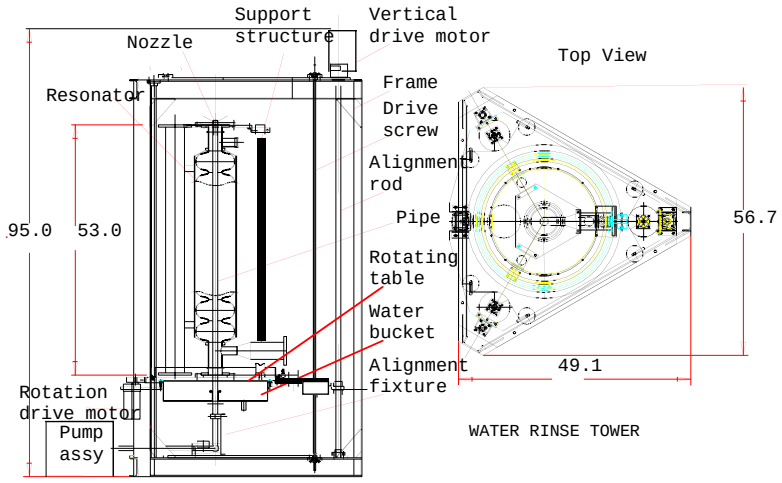

Figure 4.21: Tower for the high pressure rinsing system.

position and pitch and roll angles. After initial alignment, it is possible to remove and to install the nozzle pipe without additional adjustment. To collect water after rinsing, a bucket is attached to the carriage plate. Water goes out the bucket through the hole in its bottom into a flexible collector hose.

The system is made as simple as seemed reasonable to allow easy adjustment for different kinds of cavities to be cleaned. The strongest limitation is that the size of the cavity must not significantly exceed the size of the TESLA 9-cell cavity.

Chemical Etching

The Nb cavity material and assembled cavities must be surface etched a number of times during fabrication and preparation for testing and operation. The etching removes oxidation, surface contamination, surface crystal structure damage, and after titanium oven treatment, the titanium which has diffused into the surface during the gettering process.

The cavity and sub components are etched at the following times:

- After deep drawing and machining of half cells, 8 hours or less prior to welding dumbbells. 3 microns each side.
- Prior to welding any of parts to make end half cell and beam tube assembly. 3 microns each side.
- After dumbbells or other subassemblies welded and inspected for weld and dimensional quality. 20 microns each side.
- After any machining or grinding step prior to final welding. 20 microns each side.
- Prior (<8 hr) to welding dumbbells and half end cells together to make cavity. 3 microns each side. (This could be just in the area of the weld, within 1=2″ of the end.)
- After final cavity welding, inspection, leakcheck, and tuning. Followed by ultrapure water rinse, high pressure rinse prior to preparation for cavity test. 20 microns each side?
- After oven titanization treatment. 20 microns outside, 70 microns inside.

- Prior to any cavity retest. 5-20 microns inside?

A total of about 100 microns must be removed in order to remove the "damaged" surface layer. Full cavity etching of each cavity inside and outside can be expected to take place at least 3 times and probably more.

It is important that the chemical etching of half cells and cavity sub assemblies be closely coordinated with the ebeam welding as etching must proceed welding by no more than 8 hours. The etching of the complete cavity is not time critical but must be located in conjunction with ultrapure water and cleanroom facilities. The volume of acid needed for internal or external surface etching of a complete cavity is about 3 or 7 liters respectively. A dumbbell could be etched inside and out with about 3/4 liter of acid.

The standard buffered chemical polishing (BCP) mixture is 1 part by volume of 48% concentration hydroflouric acid, 1 part by volume of 65% nitric acid, and 2 parts by volume of 85% phosphoric acid. The phosphoric acid buffers the reaction. The removal rate 1 micron/min at 15C, but the temperature must be well controlled to below 20C as there is a fast exponential increase in etch rate with temperature and higher temperature increases the risk of Q disease through hydrogen absorption.

The acid mix is replaced when niobium content reaches 16g/lit. The freshest acid is used for final cavity preparation.

The etched parts are rinsed immediately (within 15 sec) in ultrapure water until 10 Mohm-cm conductivity is reached.

An Etching System

Fig. 4.22 shows an arrangement for both inside and outside etching. The cavity fits into a tank so that to etch the cavity inside, acid is poured inside, and water is put around the outside to control temperature. To etch the outside, acid is put into the tank and water into the cavity. The volume which is not undergoing etching is filled with water which is used to control the temperature of the reaction. The assembly is located within a chemical hood which acts as a secondary containment vessel and has its own catchment basin. Fig. 4.23 illustrates the way in which the acid is transfered in and out of the etching assembly. A limited volume of acid is stored in a supply tank below the assembly. The acid can be transferred to a tank above the cavity either by pumping to an additional tank or by using an elevator to raise and lower the supply tank. Acid is fed to the cavity container (either inner or outer) by gravity feed. The acid is removed from the cavity container, again by gravity feed, to the recovery tank, from which it can be filtered and returned to the supply tank which is now at its lowest position. The piping and containers (for short term storage) are made out of PVDF (Kynar?) or PTFE (Teflon); Viton can be used for o-ring seals at the flanges. Water is brought into the cavity container internal or external volume from the top and drains into the waste tank. The water is used to control the acid temperature and to rinse the cavity after etch.

The final fabrication ebeam welding assembly step would involve the welding of the two end half cell-beam tube assemblies and for instance three 4 cell sections. The end equator areas would be etched (in about 1/2 inch) prior to making the 4 final welds, not the total surface of the sub assemblies. Similarly prior to the 3 welds needed for the 4 cell sections, those equator ends of the dumbbells would be etched.

A simpler system for small sub assemblies would be to have acid tanks into which the assembly is lowered. After etching it is raised up again, (sprayed with water?) and then rinsed in a separate tank. Though this arrangement is conceptually simpler, especially for half cells and small assemblies, it would seem to be less controlled and might need a larger controlled space overall if used for full cavity assemblies.

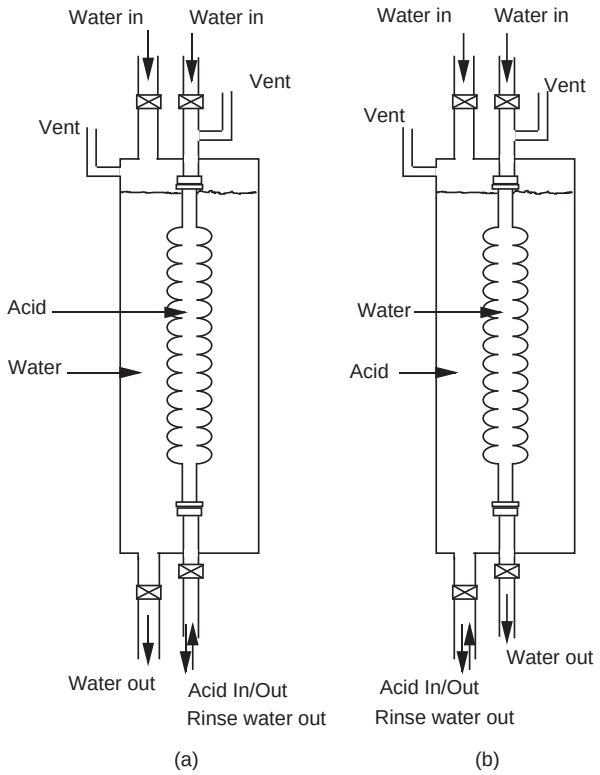

Figure 4.22: Etching assembly.

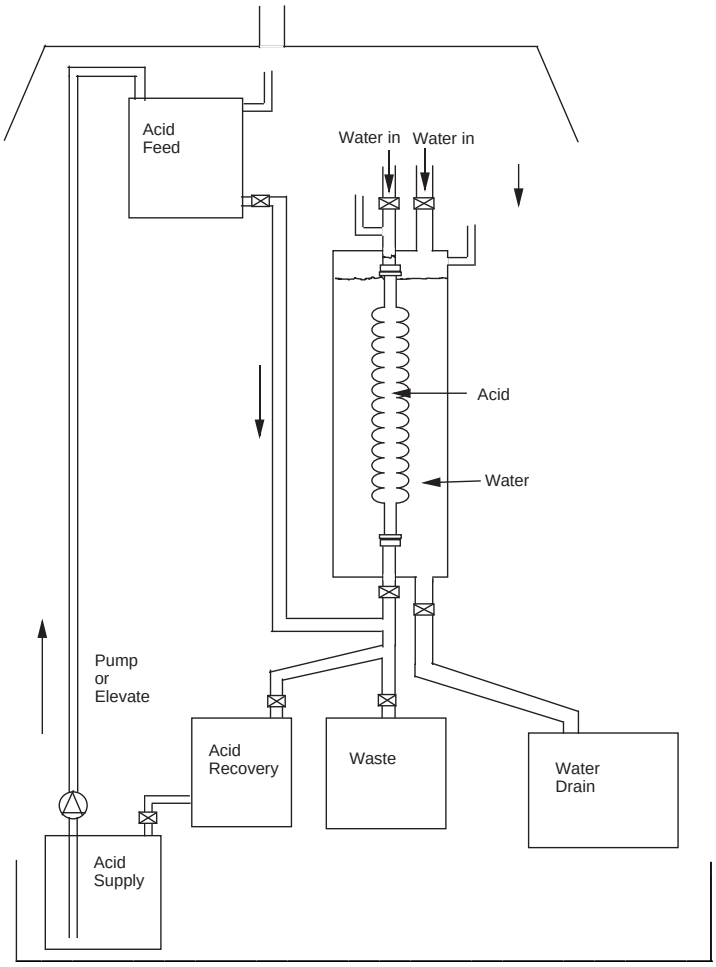

Figure 4.23: Arrangement for acid transfer.

Alternative Locations for the Etching System

We have been working on a model where the etching is set up in the village Lab 5, where expertise with handling acids already exists as well as some infrastructure.

Certainly it is key that the etching of components prior to e beam welding be done at a readably accessable location where the time coordination between etch and weld is all important. We believe that this lab could also be set up to etch complete cavities without tremendous effort. However possible alternatives are listed below.

1. The etching set up could be placed at A0. Water and cleanroom facilities already exist and would not need to be replicated at least in part as they would in the village. However key supervisory personel for this process are located at Lab 5.

2. We certainly would like to encourage Argonne-APS to put together an acid treatment facility on a scale larger than anything we might be able to provide in the near future. We would be very happy to try to make use of such a setup.

3. For etching of cavities after fabrication we may be able to use the facilities at either Cornell or Jefferson Lab. This certainly would not be as convenient as an on site location and would not be feasible for etching during fabrication, but it would allow for the final cavity etching.

Other Considerations

A number of subjects related to an etching facility have not been fully addressed as yet in the Fermilab context. These include safety (both personnel and equipment), containment and storage, spill response, procedures, and protective clothing.

Oven, Vacuum Degassing, and Titanization

Vacuum degassing removes both hydrogen and oxygen from the niobium surface. Oxygen removal is accomplished through titanium getter reaction at 1400C. Hydrogen is removed at a lower temperature (900C). The two actions increase the RRR of the material and consequently the thermal conductivity by about a factor of two, and reduce the potential for Q disease.

A special high temperature vacuum oven is needed to carry out the process. Titanium plates are suspended in the oven to allow for titanium coating of the cavity surface as the higest temperatures are reached. The vacuum is kept to less than 10^{-6} torr by limiting the rate of temperature rise. After initial outgassing the temperature is finally increased to 1400C for about 1/2 hour in order to evaporate the titanium onto the cavity surface. The temperature is then lowered to 1300 C for 1.5-2 hours in order to slow the difusion into the niobium while still maintaining gettering action.

The oven process and improvement of RRR is very important for these cavities because of the high peak magnetic fields in the transverse mode. Processing of completed cavities is standard, however oven processing of individual half cells has been shown to be equally successful and in our case it would be attractive to consider treating the dumbbell units. (The magnetic field maximum occurs near the iris.)

As a high temperature vacuum oven is expensive, we would propose using an existing oven. The Cornell oven is the obvious possibility. If Argonne gets their oven converted to higher temperature then that would be a more convenient possibility. Use of the Cornell oven would fit well with use of their chemical setup for the heavy etch that is required after oven treatment, but it would not eliminate the necessity for small piece and full cavity chemistry at Fermilab or Argonne.

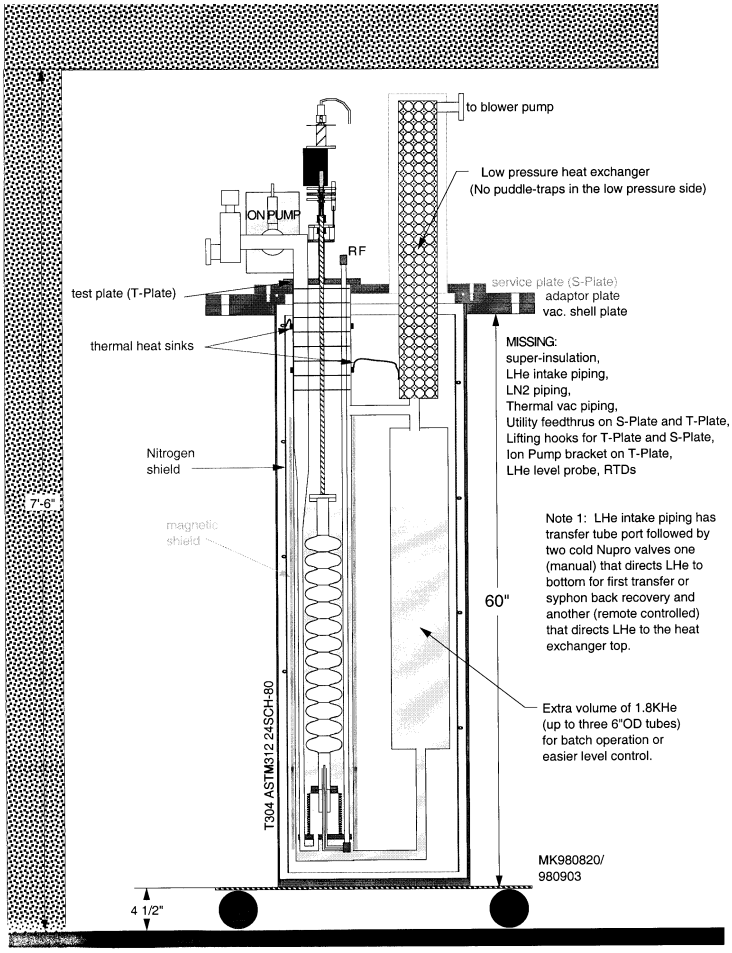

Figure 4.24: Vertical test dewar.

4.5 Cavity Testing

Vertical Dewar

The RF cavities will initially be tested in a vertical dewar. The advantages of a dewar relative to a cryostat are: it can be mechanically simpler; it does not require a refrigerator; and the mounting of a cavity, cooldown and rf testing can generally be done faster than in a cryostat.

An existing dewar will be modified to the geometry shown in Fig. 4.24. The dewar consists of a vacuum vessel, a liquid nitrogen shield and a liquid helium vessel. The LHe vessel is composed of one or more 6 in diameter tubes to eliminate the need for pressure vessel certification. The first tube contains the test cavity. The remaining tubes add LHe inventory to allow He operation in batch mode. The blowers used to cool the A0 superconducting capture cavity will also be used to pump the He vessel to a He vapor pressure equivalent to 1.8 K. LHe and LN will be supplied to the test dewar via transfer lines from a 500 L LHe dewar and a small LN dewar. The He transfer efficiency during continuous transfer operation is enhanced by precooling the incoming 4.2 K LHe with the He boil-off from the test dewar.

The test cavity and all cavity attachments are suspended from the dewar test plate. The RF

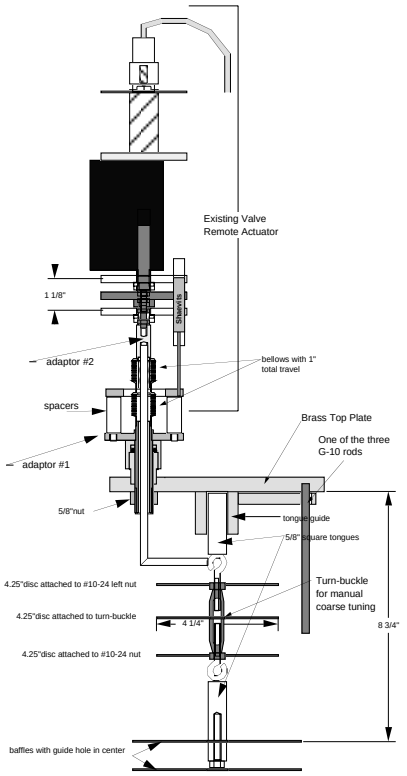

Figure 4.25: Mechanism to provide vertical cavity adjustment within dewar in order to vary RF coupling.

input coupler and cavity vacuum connections are made at the bottom of the cavity to minimize particulate contamination within the cavity. The RF input coupler remains stationary relative to the test plate. The RF coupling is adjusted by moving the test cavity; the mechanism on the top of the dewar is shown in an expanded view in Fig. 4.25. It is mounted with bellows at both ends. Baffles between the test plate and the 1.8K LHe level will intercept the thermal radiation from the test plate and will moderate He vapor convection. All connections to the test plate will have heat sinks. The total static heat load into the 1.8 K LHe is expected to be less than 1W.

The test cavity insert is assembled on the test plate and then lowered into the dewar. The dewar is then rolled into the existing concrete shielded enclosure and connected to the pumping and cryogen transfer tubes. The RF drive inside the dewar is via rigid coax.

Magnetic Shield

The Q of the cavity is inversely proportional to the surface resistance of the cavity. The surface resistance is composed of two terms, the BCS resistance which varies as the frequency squared, and a residual term. The residual term, when composed primarily of trapped magnetic flux, varies as the square root of the frequency. At 3.9 GHz, the separator cavities operate at a frequency 3 times higher than TESLA and scaling yields a BCS surface resistance estimate of 150 nΩ at 2K for niobium having a RRR of 300. The residual surface resistance at 3.9 GHz for a trapped field of 10 mG is 5 nΩ. If we are willing to accept a 10% degradation of cavity Q due to trapped magnetic fields, then the remanent surface resistance must be limited to less than 15 nΩ and the magnetic shielding must

reduce the magnetic field during cool-down to less than 30 mG.

The earth's magnetic field in the Chicago area has a vertical component of 540 mG and a horizontal component of 186 mG. The mechanically simplest means of reducing this field is to surround the He vessel that contains the cavity with a cylinder made out of high permeability material. This suggests an outside diameter for the shielding of 6 in (15.24 cm). Its length must be equal to the cell length of the cavity plus additional length to keep the field enhancement at the shield ends from the cavity end cells. This adds an additional length equal to twice the shielding diameter if annular end caps are used. The total length of the shield is therefore 80 cm. The permeability of Cryoperm at 4 K is approximately 12000. A 1 mm thick cylinder with above dimensions and composed of Cryoperm will reduce the field perpendicular to the cylinder bore by a factor of 80, the fields parallel to the bore by a factor of approximately 18. A 2 mm thick Cryoperm shield is proposed for some shielding margin.

5 A Point Design for the Separator Facility

In this section we take a look at what the overall RF separator system might be like, based on what we know of the beam separation system requirements and our present point design of 3.9GHz for the RF cavities. It is obvious that further work on the beam line and frequency choice needs to proceed. At this point, there are a number of uncertainties which are associated with: just how much RF is really needed and where, what RF gradient can reasonably be expected, and just what contingency factor allocations should be given to the cavity, cryogenic and RF power systems. In outlining these systems we have chosen to be conservative in the sense that we have drawn an envelope which we believe should encompass most of the perceived requirements. It is of course possible that final requirements may be less. Alternatively there may develope justification for an increase in total gradient capability. However it seems very unlikely that this increase could be greater than of order 15% and would need strong justification in terms of kaon ecomomy or background contamination..

5.1 Layout in the Meson Area

The Meson area is shown in Fig. 5.26. Meson East (ME) and Meson Test (MT) beam lines are the

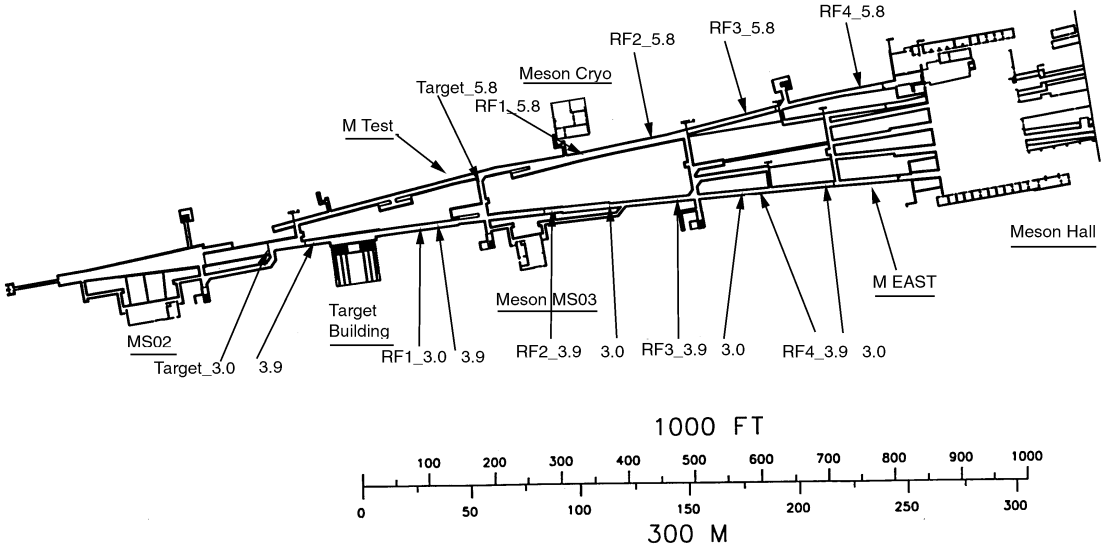

Figure 5.26: Various alternatives for location of separated beam in Meson Area

two alternatives under consideration. Meson East has the longest tunnel length and therefore is best suited for the lower RF frequencies (3.9, 3.0 GHz). Approximate locations of the four RF stations are indicated for the different frequencies.

The end point at the detectors is fixed in the Meson Hall. Also the beam length from station 4 (recombination station) to the detectors is fixed. The distance from station 4 upstream to station 1 and the production target is inversely dependent on RF frequency. Also of note in Fig. **??** are the two service buildings: MS03 and Meson Cryo. MS03 could house RF and refrigator system components. Meson Cryo already houses some of the refrigator components which could be used

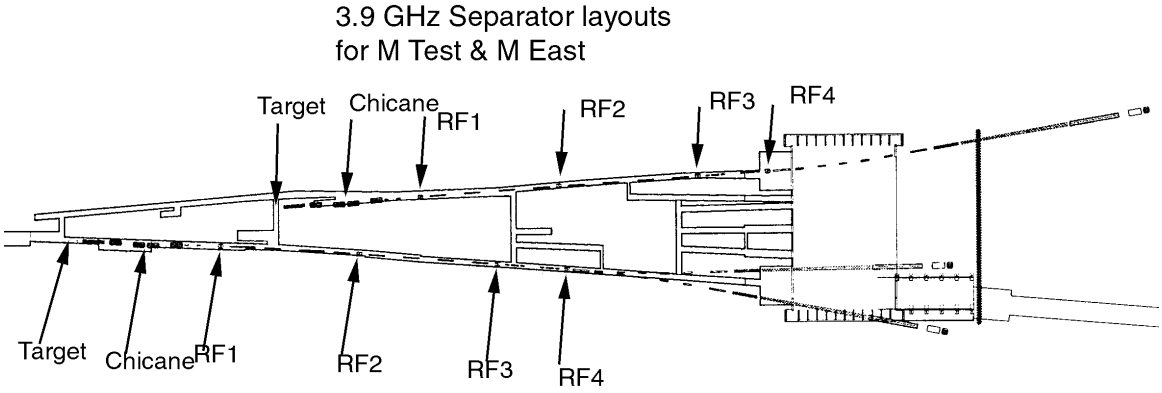

Figure 5.27: Beam layout in Meson Area at 3.9 GHz.

and could house more. It is not clear if additional building space will be needed for cryo vacuum pumps.

Fig. 5.27 shows a 3.9GHz layout for either ME or MT. It can be seen that for the ME line, construction would be needed upstream of the detector hall in order to accomodate the two 6 degree bends to the experiments. In the MT area, the experiments would lay considerably downstream of the Meson Hall.

Tab. 5.6 lists the general system requirements and specifies the total cryogenic power and RF power which must be available for the cavities. Tab. 5.7 gives a more detailed listing of various separator RF station combinations which have been investigated and the needed distribution of cavities, cryogenic power, and RF power at the RF Stations.

The requirements of CKM and CP/T are different as shown in Tab. 5.8. Some of the data related to this tabulation are given in Tab. 5.9.

The primary RF stations are RF1 and RF3, The difference in momentum between the two experiments requires the addition of a third station RF2. The desired intensity differs by a factor of 10. This means that the momentum acceptance for CP/T must be considerably larger than for CKM. The recombination cavity RF4 leads to an increase in flux of almost a factor of 2 above that achieved without it. The experiment which needs the higher flux (CP/T) also needs the higher purity beam. CKM may desire parallel beam which means it benefits from the recombination (RF4) as well. (This parallel beam requirement is under evaluation.)

The various separator optics arrangements[5.7] can be characterized as follows:

- CKM1- RF1,2,3 at 10MV each, No recombination, intensity 1.8×10^7.
- CKM2- Same with full recombination, intensity 3.6×10^7, i.e. double intensity.
- CP/T1- RF1,3,4 at 20MV each, partial recombination [full recombination would need $0.70 \times (RF1 + RF2)$], intensity 3.1×10^8
- CP/T2- Same but with no recombination, intensity 1.8×10^8
- CP/T3- RF1,3 at 10MV each, RF4 at 20 MV, full recombination, intensity 2.2×10^8.

[5.7] J. Doornbos, *Optics design of 25 GeV/c RF separated K^+ beam*, unpublished note.

Table 5.6: System parameters.

Main Injector cycle time	3 sec
Extracted beam duration per cycle	1 sec
Main Injector intensity used	5×10^{12} protons
Secondary beam intensity	$\approx 1.4 \times 10^{10}$
Secondary beam current	$\approx 2.2 \times 10^{-9}$ ampere
Potential beam loss on cavities	$\approx 2\%$
Power in lost beam	11 watts
RF	
Frequency (a)	5.8 GHz
Frequency (b)	3.9 GHz
Frequency (b)	3.0 GHz
Distance, stations 1 to 3[a]	
@ 5.8 GHz	72 m
@ 3.9 GHz	107 m
@ 3.0 GHz	139 m
Station Configurations	
Station deflection angle (typ)	0.4-0.8 mrad
Deflection per station	10-20 MeV
Total deflection required	30-60 MeV
Deflection gradient (typ)	5 MV/m
Total effective RF length @ 5 MV/m	6-12 m
Overall distance of station region	100-150 m
Number of stations	2-4
Station effective RF length @ 5 MV/m	2-4
System requirements (5.7 MV/m, 60 MV)	
Total cryogenic power[b]	95 watts @ 1.8K
	230 watts @ 2K
Q_L (loaded Q)	6×10^7
RF power @ 5.7 MV/m	380 watts/m
RF power including factor	760 watts/m
of 2 for regulation	
Total RF power	8 kilowatts

[a] For 90 degree phase difference at 25 GeV

[b] Total cryogenic power = instantaneous power × contingency factor/duty factor. Here, the ratio of contingency factor to duty factor has been taken to be unity.

Table 5.7: Separator station layout combinations and transverse kick (MV) required.

RF station		1	2	3	4	total
Case - Intensity						
CKM1 1.8 $\times 10^7$	MV	10	10	10	0	30
CKM2 3.2 $\times 10^7$	MV	10	10	10	20	50
C/PT1 3.1 $\times 10^8$	MV	20	0	20	20	60
C/PT2 1.8 $\times 10^8$	MV	20	0	20	0	40
C/PT3 2.2 $\times 10^8$	MV	10	0	10	20	40
total RF kick needed	MV	10 to 20	0 to 10	10 to 20	0 to 20	30-60
Maximum Requirements						tot installed
Kick required @ 5 MV/m	MV	20	10	20	20	
design kick maximum	MV	23	11.5	23	23	80
effect length of cavity	m	4	2	4	4	14
# of cavities		8	4	8	8	28
Maximum RF power	kW	3.2	1.6	3.2	3.2	11.2
Max cryo power@2K	watts	88	44	88	88	308
Max cryo power@1.8	watts	36	18	36	36	126
Assumed parameters						
gradient	MV/m	5.7				
cavities/m		2				
cavities/ module		2				
RF power/m	watts	800[a]				
cryo power/m@2K	watts	22[b]				
cryo power/m@1.8K	watts	9[c]				

[a]This assumes a loaded Q 6×10^7 and a factor of 2 for regulation.
[b]This assumes a helium temp of 2K, Q_0 1.0×10^9, a duty factor of 1/3, and a contingency factor of 3.
[c]This assumes a helium temp of 1.8K, Q_0 2.5×10^9, a duty factor of 1/3, and contingency factor of 3.

Table 5.8: Beam requirements for the proposed kaon experiments.

	CKM	CP/T
momentum	22 GeV	25 GeV
kaons per cycle	3×10^7	2×10^8
purity– kaons/other hadrons	2/1	10/1
ΔP/P	1%	
spot at decay volm	80/80 mm^2	5mm (FWQM)
beam angle sigma	0.1-0.5 mrad	

Table 5.9: Ancillary data to tables in this section.

Item	Unit	Value
particle ratio	pion/proton/kaon	10/3.3/1
kaon lifetime	second	1.24×10^{-8}
$^\circ_K$		≈ 48
decay length	m	≈ 178
typ beamline length	m	210–225
typ decay factor		0.29, 1/3.4

We see that the best of both solutions can be covered with a total of 70 MV. The highest voltage needed for any one option is 60 MV. CKM2 and CP/T3 can both be outfitted with 50 MV, however CPT would have 2/3 its maximum rate. A phased approach to building up the quantity of installed RF is certainly a possibility.

We have chosen to focus on the 70MV option (RF1,3,4 at 20MVeach, RF2 at 10MV) . However the power needed at any one time need not exceed that for 60MV.

It is assumed that 4 meters of active cavity length is needed to supply 20 MV, i.e. 5 MV/m gradient. This is about 12% lower than the 5.7 MV/m gradient associated with 1000 gauss peak field. The total number of 1/2m cavities needed is 28. In Tab. 5.7 maximum kicks obtainable with 5.7 MV/m are listed along with the associated RF and cryo power needs. These are of course slightly larger than what would be needed to meet either the 70MV installed requirement or the 60MV maximum used at one time.

5.2 Cryogenic Cavity System and Refrigation

5.2.1 Cavity System

The cavity system with cryostat is depicted in Fig. 5.28. We have chosen a cryo module with two cavities. The active RF length is 1 meter and the overall module length is about 1.75 m. Up to four modules might be required at a station location (Tab. 5.7). Total beamline length used by this layout (4 m active) at a station would be about 8 m including vessel to vessel distance. An isometric view of the same appears in Fig. 5.29.

Helium Vessel

The helium vessel of titanium or stainless steel has a 6″ diameter. Flanged ends provide the transition from Nb to Ti or SS (via a NbTi plate) and allow for removal of the cavity without grinding. Bellows are provided in the vessel shell for tuning and thermal contraction.

Cryostat

It is proposed to make the vacuum vessel from 316L SS for magnetic reasons. An 18″ diameter schedule 10 pipe should be big enough. End caps would be demountable. Alternatively a vacuum vessel of mild steel could be used. With proper *in situ* degaussing (as done at TESLA) it could aid in the magnetic field shielding. It is premature at this point to consider the pros and cons of more than 2 cavities per cryo–module.

Tuner

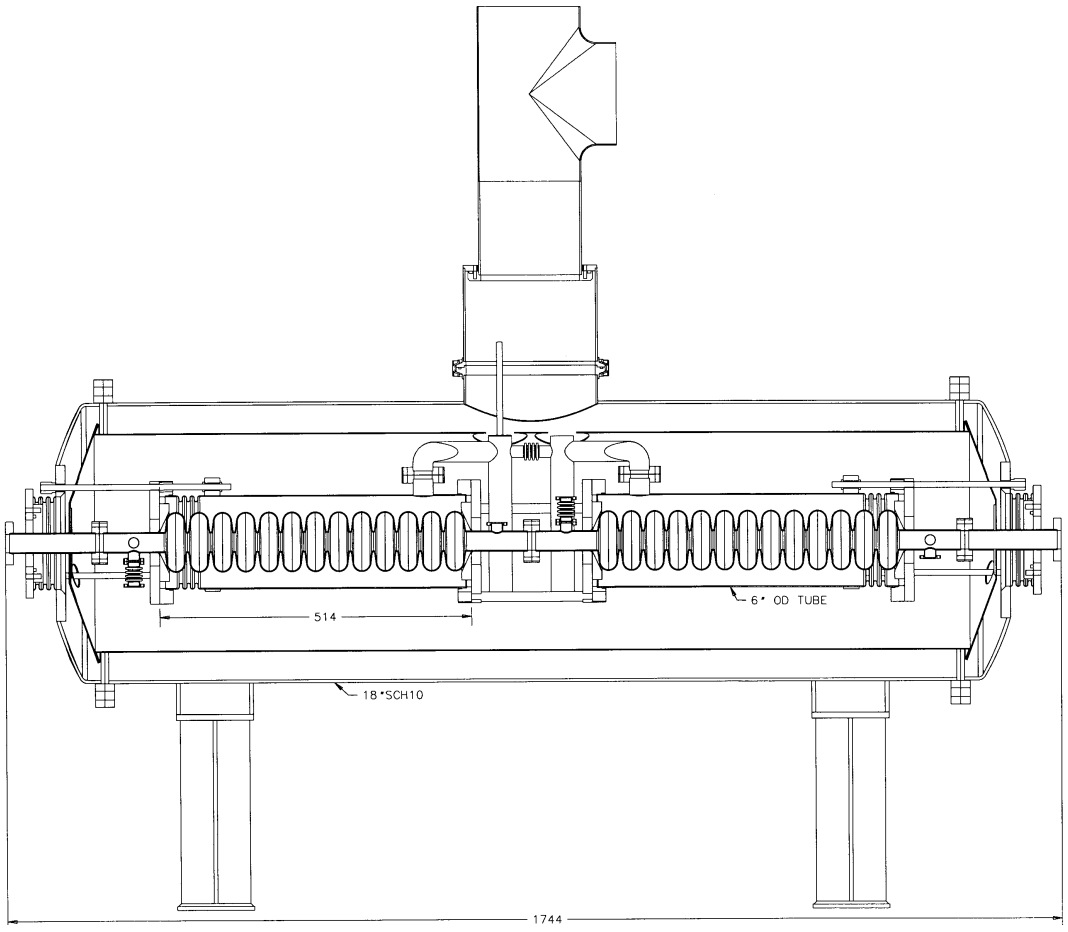

Figure 5.28: Cryostat module with two cavities.

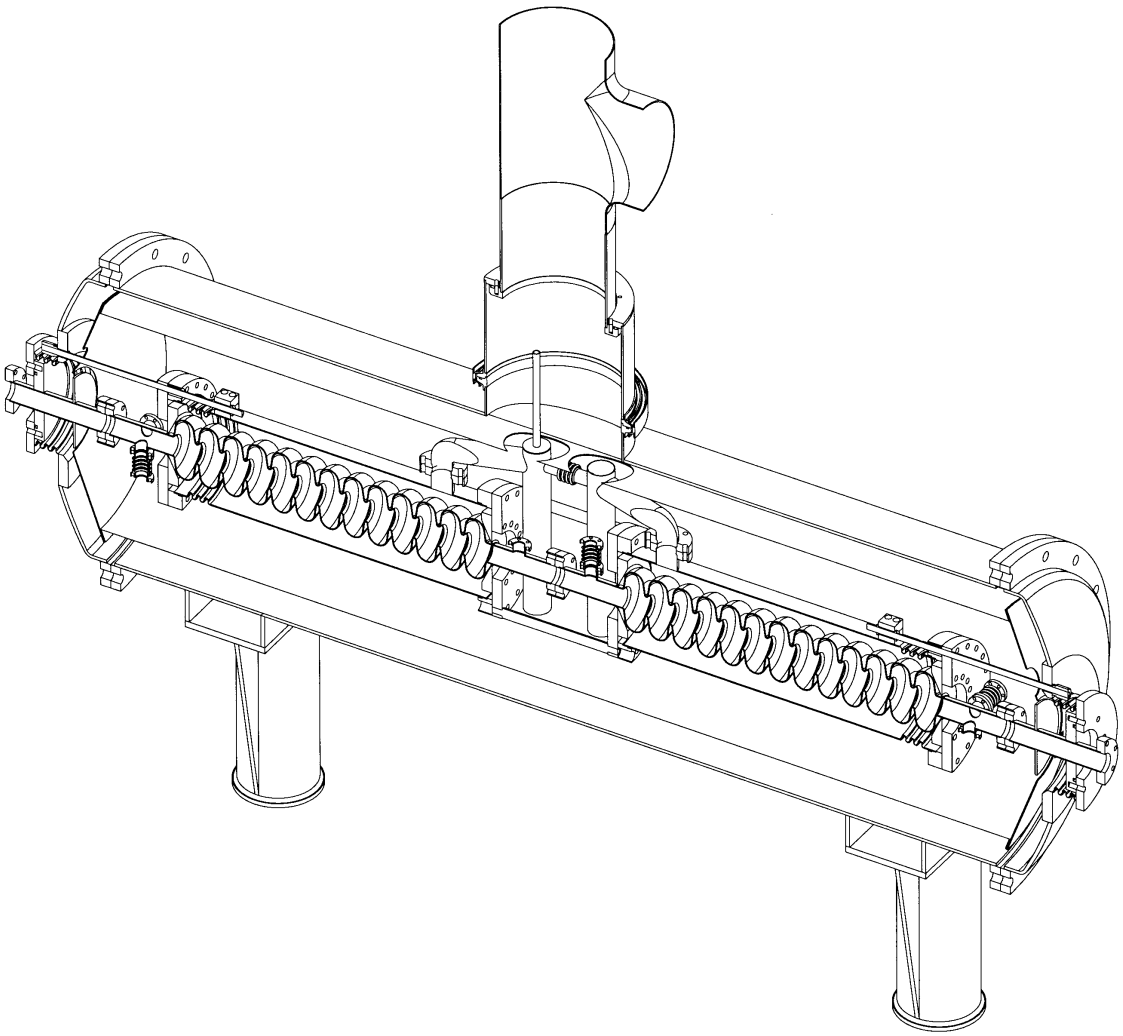

Figure 5.29: Isometric of cryostat.

As one (of many) tuning scenarios, imagine two 13-cell cavities in each vacuum vessel, arranged per Fig. 5.28. Manual tuning for each cavity could be accomplished by pushing or pulling on the rigid beam tube at either end of the vacuum vessel. The beam tube can feed through a welded bellows at the vacuum vessel end plate where it is acted on by the tuming mechanism. Horizontal rods guide the movable part of the helium vessel and help to anchor the assembly in the vacuum tank. This approach has the advantage of removing the tuner from the insulating vacuum space, but may be prone to microphonics through structural vibrations. Another possibility would be to mount the mechanism inside as done with TESLA. Evaluation should be made of the new magnetistrictive material being worked on in conjunction with TJNAF.

Coupler

Cavities should have an input coupler and monitor probes. A cold type N feed-through fed with semi-rigid coax may be adequate for power input. Fixed coupling may be adequate although variable coupling provided by bellows section is shown in the figure. (Possible operation with circular polarization would mean two sets of input and monitor probes oriented at 90 degress with respect to each other along the longitudinal axis.)

Magnetic Shielding

Cryoperm would be wraped around the helium vessel as in the TTF cavities. Additional correction could be provided by a coil on the outside of the vacuum vessel.

Cavity Support

A number of support arrangements are possible: spoke rods as in the TTF capture cavity, posts as in the TTF modules, etc. Here minimization of microphonics, ease of assembly, heat leak, and cost will all enter in the design. In Fig. 5.28 the tuner rods play a double role. One might tension up the tuner guide rods to suspend the cavity axially and transversely, with some additional support rods or posts perpendicular to the beam line.

Cavity Mechanical Considerations

Structural analysis of the cavity has only just begun. Finite element analysis of the current cell ($1/16''$ wall) design shows elastic behavior under external pressure up to 6 atmospheres. At that point deflections of about 0.0008 inch appear in the cell wall.

A force of 50 lb is needed to extend or contract such a cavity by 1.2 mm for tuning purposes. This motion induces a maximum stress of about 50 MPa, which approaches the elastic limit. Helium distribution in cryostat

Fig. 5.28 shows the proposed scheme. The TTF capture cavity has been used as a guide. A cylindrical phase separator with removable heater and level probe is mounted vertically between the cavities at the center of the vessel. One must insure that the HeII has sufficient free surface to transport the heat. About 2 cm^2 of free helium surface area is necessary per watt of dissipated power. The bottoms of the cavities and the separator are tied together with small tubing to keep levels equal and for warmup/cooldown flows.

Heat Leak Budget

The 10 watts of RF loss per meter of cavity length is relatively large. This means that the static heat load does not need to be managed as carefully as in the TTF, for example. Even so one would

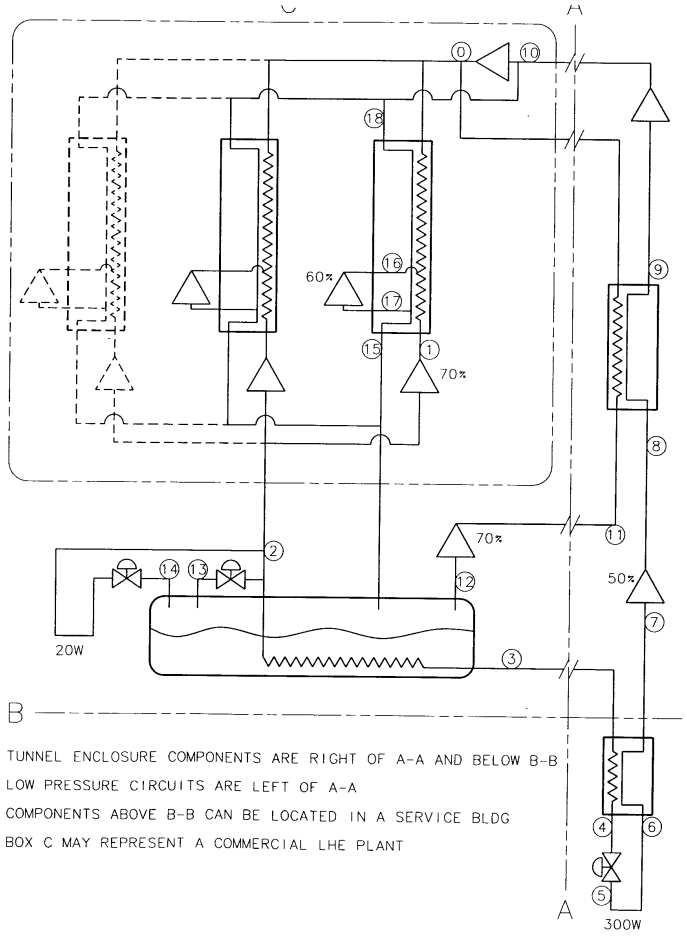

Figure 5.30: Possible refrigeration system for the RF separator.

like small load when the RF is not being used. The static heat load budget probably should be set to ≤ 3 watt/m, reflecting a static loss equal to the 10 watts of RF loss times the 1/3 beam/RF duty factor. It may be possible that the beam tubes can be rigid and various helium vessel supports can be metallic. The TTF injector capture cavity which contains one TESLA cavity has been measured by Orsay to have about a 3 watt heat leak at 1.8K.

5.2.2 Refrigeration System

System Outline

Fig. 5.30 shows a schematic of one possible refrigeration system for the RF separator beam line. The system is divided into 3 regions: the helium plant region which provides liquid and 4.5K cooling, the 2K heat exchanger-cold compressor area followed by a warm up heat exchanger and vacuum pump, and the cavity stations which use the 200- 300W at 2K.

The system could use two of the three refrigerators at Meson Central Cryo (MCC) which together are capable of about 400 W at 4.5K along with 2 g/s liquefaction. Two of the four Mycom compressors at MCC could provide 80 g/s of compressor flow. There exists transfer line as well as a

purification system, which could be scavenged from MCC. Alternately if the MCC equiptment were not available one would purchase: a commercial helium plant captable of 400W at 4.5K and 2g/s liquidifaction, warm compressors for the 80g/s flow, transfer line and a purification system.

The cold compressor and warmup heat exchanger need not be located close to the cavities. For example a 3″ insulated pipe flowing 16g/s of 1.8K saturated vapor has a pressure drop of 0.07 torr/10m of length. Runs of 100 meters should be possible for this line. (The saturated vapor pressures of 1.8K and 2.1K helium are 12 torr and 30 torr, respectively.) The line would probably need to be shielded at 5K and 80K to minimize the heat leak.

By the same token, gas entering the vacuum pump after the warmup heat exchanger could be handled by a 6″ pipe. At 280K, 40 torr and 16g/s, the pressure drop is about 0.62 torr/10m length.

Taking these pressure drop numbers into account it seems possible to locate the cold compressor, warm up heat exchanger, and vacuum pumps at the Meson Cryo Building Area.

The state point and heat balance calculations given in Fig. 5.31 assume a total heat load at 1.8K of 300 watts. The pressure, temperature, flow, etc are given for each numbered point.

Distribution and Feed

4.5K refrigeration at 2.5 atm (point 3) would be produced and delivered to the RF cavity cryostats at the remote station locations. There the flow is cooled to slightly above lambda by heat exchanging with the boil-off gas (point 4). At each cryostat the flow is throttled through a control valve to 12 torr (80% liquid), keeping the phase separator at the desired liquid level (point 5).

Saturated vapor from the cavity cryostats flows to the cold compressor station where it is compressed to 40 or 50 torr (point 8), then sent into the low pressure heat exchanger at about 6.7K. Refrigeration is recovered via heat exchange with a high pressure stream (point 11) which is returned for expansion and injection into the refrigerator plant. The low pressure exchanger exhaust (point 9) is routed to a vacuum system which discharges (point 10) into compressor suction at slightly positive pressure. Such a vacuum system could be obtained surplus from TJNAF (or purchased).

Effect of Operating Temperature

The dissipated heat from the RF losses is very dependent on temperature of the cavity surface. Further investigation of the tradeoffs of different temperatures will need to be carried out. A preliminary look indicates that below 1.7K multiple stages of cold compression would probably be needed alone with vacuum pumps. In the range of 1.8-1.9 K a single stage of cold compression with vacuum pumps can be used. In the range of 2.0-2.1 K one stage of cold compression and vacuum pump or double pump capacity (two TJNAF skid units) without cold compression would be possible. Given the existence of the Meson refigerators which are capable of 300 watts, the benefits of lower power demand at lower temperature may not be as great as one would expect. Again, further investigation is necessary.

Cost Estimate

We assume the MCC refrigerators/compressor systems are available and that buildings MCC and MS03 can be used to some extent. The refrigerators represent $1M per plant but could be used here with essentially no modification. However, the control system is gutted and would need to be replaced at a cost of maybe several $100K.

A dewar and low pressure heat exchanger need to be built, maybe around $50K.

The vacuum pump must be several $100K but may be available for shipping costs from TJNAF.

The cold compressors could be several $100K and need to be bought. The Tore Supra refrigerator provides some experience with cold compressors in this performance range.

PT	T (K)	P (ATM)	h (J/g)	s (J/gK)	%liq	F (g/s)
0	300.	20.0	1573.	25.3		78.7
1	7.91	18.0	32.4	5.07		20.0
2	5.35	2.50	22.8	5.85		40.0
3	4.43	2.50	11.3	3.60		16.0
4	2.20	2.50	4.72	1.62		16.0
5	1.80	.016	4.72	2.69	83	16.0
6	1.80	.016	24.2	13.5		16.0
7	3.01	.016	30.8	16.3		16.0
8	6.72	.053	50.0	18.0		16.0
9	280.	.053	1469	37.3		16.0
10	300.	1.00	1573	31.4		16.0
11	10.0	18.0	45.1	6.49		14.7
12	4.42	1.20	29.7	7.99	5	14.7
13	4.42	1.20	22.8	6.42	40	14.0
14	4.42	1.20	24.8	6.87	30	10.0
15	4.42	1.20	30.6	8.20		19.4
16	31.0	18.0	174.	13.6		12.0
17	18.8	1.20	112.	16.8		12.0
18	277.	1.00	1456	31.2		31.4

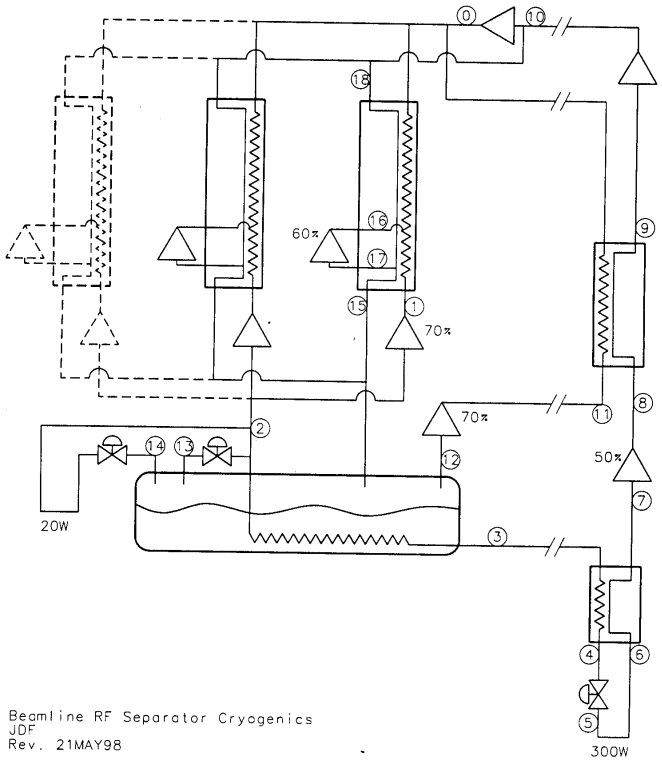

Figure 5.31: Process calculations for the refrigeration system.

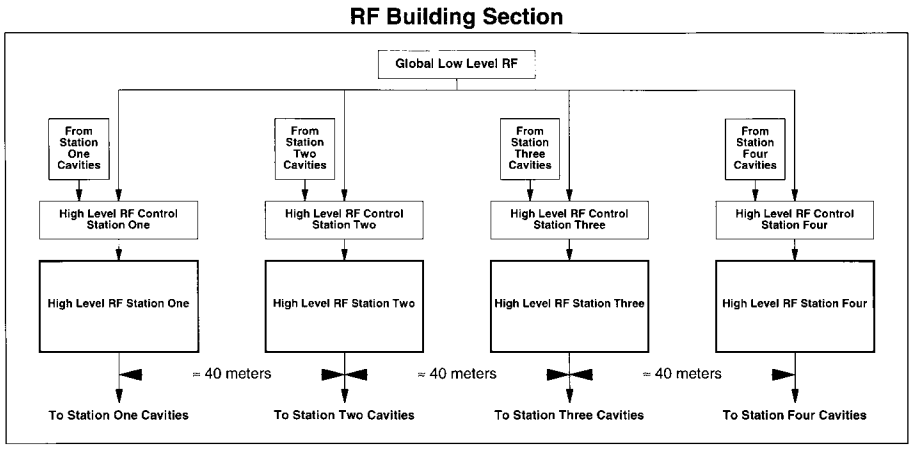

Figure 5.32: RF system components in service building.

If a building has to be built near the cavity installations to house the vacuum pump, cold compressor, and low pressure exchanger, we estimate it at \$120K ($20' \times 20'$ at \$300/sqft based on what FESS charged for DA compressor building).

Summarizing these estimates and choosing the most optimistic:

- refrig/comp controls \$200-300K
- dewar and low p H Ex \$50K
- vac pump- TJNAF \$0
- cold compressors $\approx$ \$300K
- building \$120K

Adding it up yields about \$750,000 and might approach \$1M.

For comparison, the paper "An Update on Estimating the Cost of Cryogenic Refrigeration" by Byrns and Green (CEC 1997) says that a refrigeration system capable of 300 W at 1.8K costs \$1.5M, exclusive of controls, infrastructure, etc. These items could add another \$0.5M to \$1M. This would put the cost of a new system at 2.0 - 2.5M\$.

5.3 RF System

The present design specifications call for four deflection stations with a total RF power requirement of 8 to 10 kW at 3.9 GHz. The four cavity regions are to be separated by approximately 40 meters. Fig. 5.32 illustrates the service building components, and Fig. 5.33 the components in the tunnel. Each station comprises four parts: the High Level RF Station, Station Cavities, High Level RF Control, and Global Low Level RF. This subdivision is depicted in Fig. 5.34.

5.3.1 Station Cavities

The power distribution to four cavities will require three magic tees and an amount of rectangular waveguide to be determined by the location and dimensions of the cavities. The magic tee is a

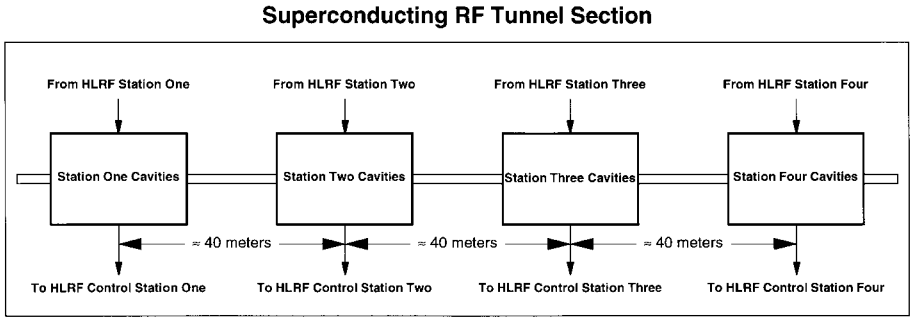

Figure 5.33: RF system components in Meson Area tunnel.

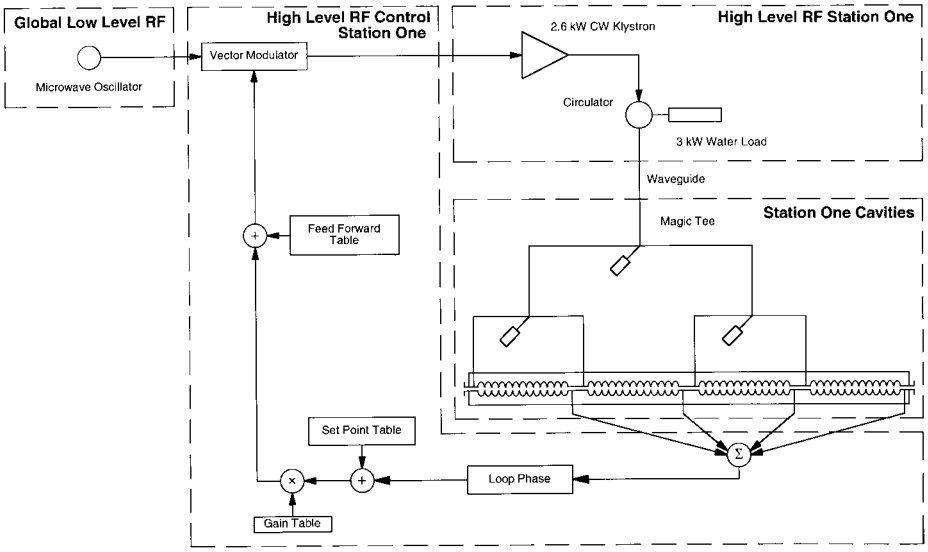

Figure 5.34: Functional division of RF components for a station.

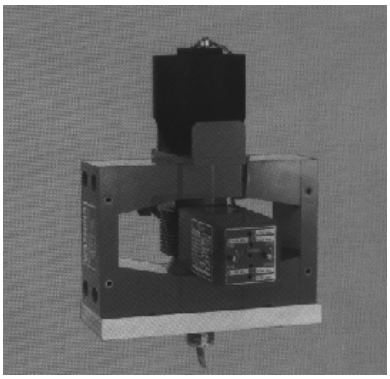

Figure 5.35: CPI Varian 2.6 kW klystron, model VKC-7810M6.

known 4-port device that provides a well–balanced power split and good isolation, but there is a possibility that rectangular wavegude directional couplers could be used to distribute the power to the cavites also. Only the magic tee design will be discussed here. An estimate from Andrew for 10 m of waveguide with flanges is $6,300 per four cavity station and for six 90 degree waveguide bends is $3,660. The price of a circulator, three magic tees and 3 kWatt load for a four cavity station still need to be determined.

5.3.2 High Level RF

The power requirements for one–half of the cavities associated with a station as shown in Fig. 5.34 is 400 Watts/cavity given a coupler β of 20-40. There are four 1/2m cavities shown and will require 1600 Watts of total power to be delivered to the cavities for this system. For now we will assume the power source will be put in the tunnel. This would give approximate losses of 0.429 dB for 10 m of WR-229 Al waveguide and 1.4 dB for the three magic tees and one circulator. This raises the power required from the HLRF source to 2.43 kW.

One could meet the power requirements by either using travelling wave tubes (TWT) or klystrons. TWTs have been considered because we were uncertain of the availability of klystrons at the 3.9 GHz frequency. A typical 1 kW TWT produced by Amplifier Research Model No. 1000T2G8 is in the price range of $255,000. Three TWTs would add up to $765,000 which is very expensive. Smaller power (200 watt) TWTs such as used in the P-Bar Source cost about $30K and could be adjusted to a narrower bandwidth to supply 400 watts each. Even with these the cost would be $180K for 2.4 kW. One 2.6 kW, 3.9 GHz, CPI Varian Model No. VKC-7810M6 Klystron as shown in Fig. 5.35 could be modified to operate at 3.9GHz and would cost around $70,000. This price includes the focusing magnet. The power supplies required for the Klystron are one 8.5 kVDC–1.2 ADC beam power supply, and one 6 V, 1.2 A Heater power supply. These power supplies would need to be purchased at an additional cost.

A typical eight cavity station (two Fig. 5.34 HLRF systems) would require 4860 Watts power supplied before the circulator. The cost at this power level would $140,000 for two 2.6 kW klystrons. With a coupler β of 20, a circulator is shown with a 3 kW water load. The circulator will direct any power reflected by the cavity into the water load and protect the klystron.

5.3.3 RF Control

For amplitude and phase control of a region of cavities a digital RF control sytem using a vector-sum scheme from each of the cavities seems applicable. This is actually what is being used in the

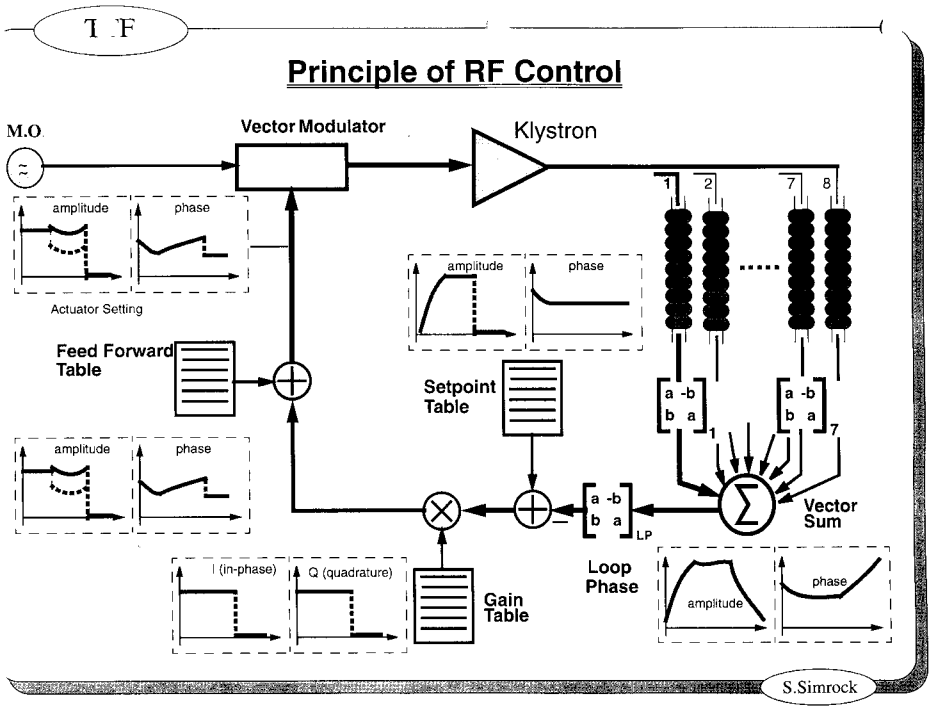

Figure 5.36: Schematic of RF control as implemented at DESY.

TESLA vector modulator low level system (Fig. 5.36). The vector modulator will need to have an upper output of 1/2 Watt to achieve a 2.6 kW output. The sytem hardware required is a digital signal processor, analog to digital converter, and a digital to analog converter. The sytem hardware is controlled by LabVIEW. A 3.9 GHz oscillator fanout is required for keeping the phase between stations correct since the inter-station spacing is about 40 m.

6 Cost, Schedule, and Effort

In this section, we take a look at what the expected M&S expenditures for the R&D phase and the costs for production. A rough schedule is suggested, and manpower needs for the R&D activity outlined. In some cases the cost figures represent established materials and component prices, but in many instances the numbers are guesses, hopefully educated, but nevertheless unsupported by documentation. Some may be considered as only placeholders for needed activities. Neither G&A nor contingency has been included, nor has a profit margin for industrial fabrication.

The project as described in Sec. 5 calls for 28 cavities installed. It may well be that with refinements in beam design and experimental needs this number can be substantially reduced. Also some phasing of cavity installation with particular experimental runs is probably possible.

In Sec. 4, we have outlined an R&D program that calls for the fabrication and test of 16 Nb cavities ranging from single cell to 13 cell Tab. 4.5. It is difficult to imagine how this can be accomplished in less than 3 years. The cost model proposed in Fig. 6.37 has 4 short cavities and one long cavity in year 1, 4 short and 3 long in year 2, and 4 long in year 3. It is anticipated that some of these will end up as scrap. If fabrication is extremely successful perhaps fewer prototypes will be needed.

	Cavity R&D Costs by year									
1	**Cavities R&D**	cost each	num year1	tot year1	cost each	num year2	tot year2	cost each	num year3	tot year3
2	Cavities-short_copper	16	2	32			0			0
3	Cavities-long_copper	22	1	22	22	1	22			0
4	Cavities- short_Nb	24	4	96	21	4	84			0
5	Cavities-long_Nb	35	1	35	30	3	90	30	4	120
6				**185**			**196**			**120**
7	Helium vessel	10	2	20	10	4	40	10	4	40
8	Cryo vessel		see test equipt					30	2	60
9	Cryo tower		see test equipt					30	1	30
10	Couplers			20			20	15	4	60
11	Tuner			20			20	15	4	60
12	Mag Shield			10			10	4	4	16
13	Vacuum			20			20	20	2	40
14				**90**			**110**			**306**
15										

	Summary of cavity costs									
	Summary	RRR long	RG short	long Cu	short Cu		RRRlong	hi RRR 13cell		
	material**	5	2	0	0		RG short	Reactor Grade 1-5cell		
	machining*	15	11	7	5		long Cu	13 cell Cu		
	welding	13	9	13	9		short Cu	1-5 cell Cu		
	tooling/exp	2	2	2	2					
							* The listed machining costs for Nb are expensive			
	ToT	**35**	**24**	**22**	**16**		They should decrease after some experience.			
	**Reactor Grade materi	2-2.7								

Figure 6.37: Prototype cavity costs in thousands by year during 3 year R&D phase.

We believe, again optimistically, that production and installation of 28 cavities could be carried out in 3 years, with some overlap between the last year of R&D and the initiation of preproduction.

The total time scale is ambitious, especially considering the lack of experience at Fermilab. It is a major effort, and would need to be treated as such to be successful. However, it seems unlikely to us that the program can go much faster than the TESLA Test Facilty Linac. There it has taken a large and experienced group 6 years to install 17 of the 25 L-band cavities required for the first

stage of that project.

The estimated costs are given in Fig. 6.37, Fig. 6.39 and Fig. **??**. A detailed estimate of cavity fabrication cost is given in Appendix A.5. This latter estimate has the flavor of a workwheet and is not easy to follow or explain in detail. The resulting summary costs from Appendix A.5 are given at the bottom of Fig. 6.37, and have been broken into material, welding, and machining costs per cavity. The estimates reflect costs for fabrication during the initial learning curve; they are expected to go down as experience is gained and material is procured in larger quantities. This is reflected in the costs of 13 cell cavities dropping from 35K$ to 30K$ in years 2 and 3 even though high RRR material is used in later years.

At the top of Fig. 6.37, the estimates for cavity fabrication and associated components is given by year. In years 1 and 2, an allotment for development of the associated components is given without specific quantities being specified. (The notes in lines 8,9 refer in lines 23, 24,25 in Fig. 6.39.) By year 3, 4 fully "dressed" cavities are proposed. The estimate runs from about 275K$ in year 1 to 425K$ in year 3.

Fig. 6.39 outlines the estimate for the overall R&D activity (lines 1-51. Fig. **??** shows the estimate for the production phase (lines 61-104) as well as the preproduction activity (lines 52-58). The preproduction costs are part of production costs, not additional costs, but are associated with production efforts which could take place early in the program, such as refrigeration improvements (e.g., controls), or production activities which should be initiated early (e.g., cold compressor, RF station prototype, industrial cavity fabrication).

The R&D estimate is broken into Infrastructure, Testing, and Cavities. The cavity estimate comes from Fig. 6.37 information.

Remarks pertaining to some of the items in Infrastructure and Testing are given below, referenced to the line numbers in the spreadsheets.

7. The ultrapure water system installed at A0 is a rental system. If etching is set up another location (village) then another water system will be necessary there. At some point it may be more economical to buy the systems and continue with a maintenance contract.

9. The model for chemistry is that in year 1 the equipment necessary for etching during fabrication will be put in place. this will focus on the fume hoods and secondary confinement. In year 2, the actual vessel and piping for complete cavity etching would be installed. In the meantime any complete cavity etching would need to be done elsewhere – Cornell, for example. We encourage Argonne to set up a chemistry system and we would certainly make use of it when available. We believe that Argonne, as a multidisciplinary laboratory is in a much better position to do this than is Fermilab.

11. This is for oil-free pump carts.

12. A low temperature (350C) oven, though not an absolute necessity for the cavity program, would significantly aid in the bakeout of cleaned vacuum components.

13. We have on loan a very nice dry leak detector cart from Argonne.

14. A high temperature oven will be key to obtaining the necessary RRR. As this is very expensive, we plan to use the oven at Cornell or at Argonne after the latter is upgraded.

23,24. The horizontal test dewars would be similar to the A0 Injector capture cavity. They would allow for interchange of cavity-helium vessel units and could be used with the A0 Injector for beam tests.

1	**R&D M&S Est**					
2		year0-done	year1	year2	year3	
3	**Infrastructure**					
4	Cleanroom(s)	40				
5	Floor	4				
6	A/C		12			
7	UPWater-install/rental	24	32	32	32	
8	Ultra Sound	10	20			
9	Chemistry		50	50	10	
10	HP Rinsing	7	27	5	5	
11	Vacuum, oil free		25			
12	vac oven-low temp		25			
13	Vac Eq	Argonne(80)	25	25	25	
14	HT Oven		CU/Argonne			
15						
16	Misc CR Eq	12	10	10	10	
17	T&M	7	15	10	10	
18	Supplies/other	48	48	72	72	
19		**152**	**289**	**204**	**164**	
20						
21	**Testing EQ**					
22	Vert Dewar w tuner,HX, etc		30			
23	Hor Test Cryo (1 cav)		50			
24	Hor Test Cryo (2 cav)			50		
25	Cryo Feed Tower		20			
26						
27	Helium	20	50			
28	A0 Refrig		50	50	20	
29						
30	R&D Tests/Measure		100	100	100	
31	Instrumentation		70	50	50	
32						
33	RF circulator load etc		20			
34	RF Power-TWT/KLy		TWT borrow	100		
35	Misc RF		20	30	50	
36			**410**	**380**	**220**	
37						
38		year0-done	year1	year2	year3	
39	**Cavity program R&D**					
40	Cavities_CU		54	22		
41	Cavities-Nb		131	174	120	
42	Helium vessel		20	40	40	
43	Cryo vessel			0	60	
44	Cryo tower			0	30	
45	Couplers		20	20	60	
46	Tuner		20	20	60	
47	Mag shield		10	10	16	
48	Vacuum		20	20	40	
49			**275**	**306**	**426**	
50						
51	**Tot 3year R&D**		**974**	**890**	**810**	**2674**

Figure 6.38: Year by year breakdown of R&D costs for materials and supplies.

52	**Pre/Production**		year1	year2	year3	
53	cavities				150	
54	Refrig		50	50	100	
55	RF			50	100	
56	**Tot Pre-Prod**		**50**	**100**	**350**	**500**
57						
58	**Tot R&D+PreProd**		**1024**	**990**	**1160**	**3174**
59						
60						
61	**Production**					
62						
63	**Cavities Production**	cost each	number	tot		
64						
65	Cavities-Nb	25	28	700		
66	Helium vessel	5	28	140		
67	Cryo vessel	20	14	280		
68	Cryo tower	30	4	120		
69	Couplers	10	28	280		
70	Tuner	10	28	280		
71	Mag Shield	2	28	56		
72	Vacuum	15	14	210		
73						
74	**TOT Cavities**			**2066**		
75						
76	**Refrigeration**					
77						
78	Refrig/comp	MCC exists				
79	controls	~200		200		
80	low press dewar/HX	50		50		
81	vacuum pump	TJNAFexists				
82	cold compressor	350		350		
83	transfer line	25/100ft	6	150		
84	building	120		120		
85						
86	**Tot Refrig**			**870**		
87						
88	**RF Power**					
89						
90	Klystrons*	70	7	490		
91	PowerSupplies	15	7	105		
92	Wave guide*	10	7	70		
93	Power spliters	0.7	21	14.7		
94	Circulator/Water load	7.5	7	52.5		
95	Water load	2.5	7	17.5		
96	Direct couplers	0.9	7	6.3		
97	CW Osc	25	1	25		
98	Microwave Fanout	32	1	32		
99	LLRF & dist	150	1	150		
100	Misc	10	7	70		
101	**tot RF Power**			**1033**		
102						
103	**TOT Production**			**3969**		
104		**Without spares/contingency/profit, etc**				

Figure 6.39: Year by year breakdown of preproduction and production costs. No allowance for contingency, G&A, and supplier profit has been made.

25. This tower goes with the horizontal cryostats and contains the heat exchanger, valves, and hookup to the helium supply.

27,28. Helium is presently supplied at A0 through dewars. A typical test run would need about four 500 liter dewars and cost about 5K$ ($1200 per dewar). Once testing becomes routine it probably will be desirable to connect the testing at A0 to the central helium system rather than continue to use dewars. This hookup has been estimated at 100K$.

33,34,35. Initial testing would be done with a TWT power source. By year 2, assembly of a klystron system should begin.

Remarks pertaining to preproduction items:

53. In year 3, preproduction of final cavities is started.

54. The refrigerator at MCC can be refurbished and controls installed starting anytime. Work should be initiated on the cold compressor by year 3 after the specifications and contract have been worked out.

55. The funds here are for production of a complete RF system as shown in Fig. 5.34.

Remarks pertaining to production:

76,88. Features of the refrigeration and RF systems have been discussed in Sec. 5.

What is not listed in the production costs is the operating costs associated with maintaining the infrastructure and testing activities during production. Based on the estimates during R&D, these could be expected to run about 300k$ per year.

Summary of M&S Costs

The R&D and Preproduction run about 1M$/y for 3 years. The order of magnitude of the production costs including operating costs (at 300K$/y) during production is 4.9M$. After subrtraction of preproduction, the production costs are 1.5M$ for 3 years.

R&D Manpower Personnel Effort

The manpower effort needed to carry out the R&D activity is outlined in Tab. 6.10 below. Assuming these people are 2/3 dedicated or can be shared between the above listed catagories gives a FTE count of 8 professional staff and 8 1/2 technical personnel.

The needs will change as the program progresses. Personnel requirements for the production phase probably will be larger in order to cover assembly and installation.

Table 6.10: Estimate of personnel needed to carry out the R&D effort. (p=physicist, e=engineer, p-e=physicists or engineer, t=technician, d=designer, exped=expediter)

	staff	support
Group leader	1p-e	
RF cavity conceptual design/measure	2p-e	
RF cavity mechanical design/fab	1e	1t
RF cavity component design/fab	1p-e	
cavity system procurement		1/3 exped
Infrastructure/testing	2p-e	1 1/2t
Specialized R&D	1p	1/2t
Chemistry	1e	1t
Cryo/Refrig design/fab	1e	3t
Electrical design/fab	1/2e	1t
RF System design/fab	1e	1t
Design/Drafting		2d
Summary		
p-e	6	
p	1	
e	4 1/2	
11 t		9
d		2
exped		1/3
Total	11.5	11.3

A Appendices

A.1 Kaon Separation with Two-Axis Deflection

The RF separated beams that have been constructed have employed deflection in one transverse direction. Almost forty years ago, Panofsky suggested the use of a circularly polarized mode to kick in both transverse degrees-of-freedom, however the idea was not pursued for a variety of reasons.[A.1] The design outlined in Sec. 2 of this report has four deflector stations to meet energy range, high rejection ratio, and exit phase space requirements. It is worthwhile to look again at the two d-o-f scheme.

To illustrate the difference between the two cases, consider a simple one particle model of a two station separator. Look at the single transverse plane version first.

If a particle transits station 1 at RF phase $\grave{}$, suppose it receives a kick $\cos\grave{}$ where the amplitude of the deflection is taken to be unity. At station 2, it will receive a kick $-\cos(\grave{} + 2\pi f t_s)$, where t_s is the transit time between stations for a particle of species s travelling at speed v_s, and f the frequency of the separator cavities. Without loss of generality, it is assumed that the two stations are running in phase, and that the intervening optics represents an integral number of betatron oscillations. The total kick is then

$$\Delta = \cos\grave{} - \cos\left(\grave{} + \frac{2\pi f L}{c}\frac{1}{\beta_s}\right); \tag{A.1}$$

with L the distance between stations and $c\beta_s = v_s$. The unwanted hadrons, characterized here as pions, are to receive no net kick, and so

$$\frac{2\pi f L}{c}\frac{1}{\beta_\pi} = 2\pi n.$$

The net kick received by the kaons then is

$$\Delta = \cos\grave{} - \cos\left[\grave{} + \frac{2\pi f L}{c}\left(\frac{1}{\beta_K} - \frac{1}{\beta_\pi}\right)\right] \tag{A.2}$$

Note that there is always a value of $\grave{}$ for which the net deflection of the kaons is also zero. This makes clear the reason why the unwanted hadrons are sent straight ahead at the exit of station 2. If the kaons were directed straight ahead, there would be an inevitable contamination of undeflected pions. It is the kaons that must receive a net deflection. As already noted in Sec. 1.2, the protons will follow the pions.

The kaons receive a net kick taking on all values between 0 and 2 (in the arbitrary units in use here). The maximum kick is to be found at the value of $\grave{}$ given by

$$\grave{}(fL) = \frac{\pi}{2} - \frac{\pi f L}{c}\left(\frac{1}{\beta_K} - \frac{1}{\beta_\pi}\right); \tag{A.3}$$

and the maximum deflection, using Eq. A.2, becomes

$$\Delta = 2\left|\sin\frac{\pi f L}{c}\left(\frac{1}{\beta_K} - \frac{1}{\beta_\pi}\right)\right|: \tag{A.4}$$

[A.1] M. Bell, P. Bramham, R. D. Fortune, E. Keil, B. W. Montague, *RF Particle Separators*, Proc. Int. Conf. High Energy Accelerators, Dubna 1963, USAEC CONF-114. This paper discusses the Panofsky suggestion, the reasons why it was not pursued at CERN, and the addition of a third deflector station, as proposed by Schnell, to achieve tuning of the beam over a range of energies.

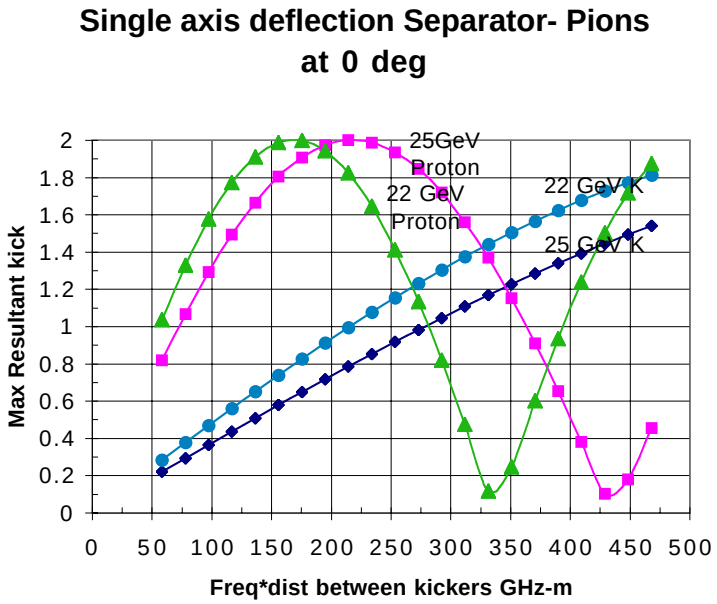

Figure A.1: One degree of freedom deflection.

For the 2 d-o-f case, a station provides equal amplitude kicks at right angles to each other and with …=2 phase difference. Eq. A.1 is now joined by its counterpart in the other transverse direction:

$$\Delta_1 = \cos ` - \cos\left( ` + \frac{2\ldots f L}{c}\frac{1}{fl_s}\right); \tag{A.5}$$

$$\Delta_2 = \sin ` - \sin\left( ` + \frac{2\ldots f L}{c}\frac{1}{fl_s}\right): \tag{A.6}$$

Taking the square root of the sum of the squares of the components of Eq. A.5 yields

$$\Delta \equiv (\Delta_1^2 + \Delta_2^2)^{1/2} = 2\left|\sin\frac{\ldots f L}{cfl_s}\right|: \tag{A.7}$$

This result no longer depends of the phase `. One may direct the kaons straight ahead, by setting

$$\frac{\ldots f L}{cfl_K} = \ldots n \tag{A.8}$$

and then the deflection of another species is

$$\Delta = 2\left|\sin\frac{\ldots f L}{c}\left(\frac{1}{fl_s} - \frac{1}{fl_K}\right)\right|: \tag{A.9}$$

Not surprisingly, the result is essentially the same as Eq. A.4, though the interpretation is different. Fig. A.1 and Fig. A.2 plot Eq. A.2 and Eq. A.9 respectively over a range of the product $f L$. Fig. A.3 and Fig. A.4 are similar plots for the particular frequency of 3.9 GHz.

In the 2 d-o-f case, over the range 22-25 GeV, the resultant kick is above one unit for the unwanted hadrons. The 1 d-o-f case, in contrast, is a monoenergetic beam.

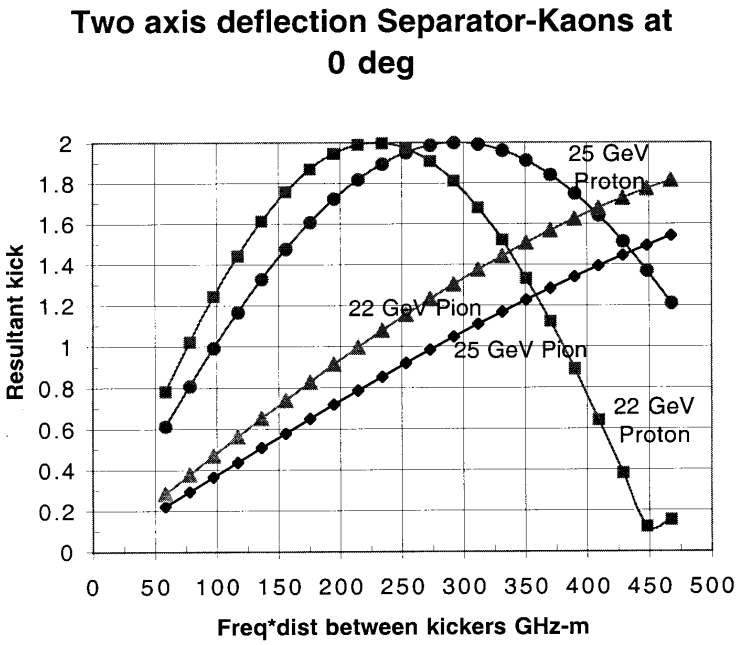

Figure A.2: One degree of freedom deflection.

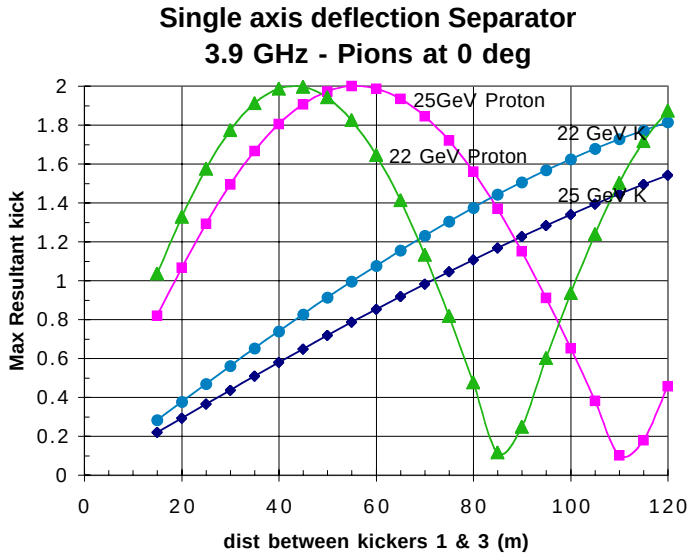

Figure A.3: One degree of freedom deflection, 3.9 GHz.

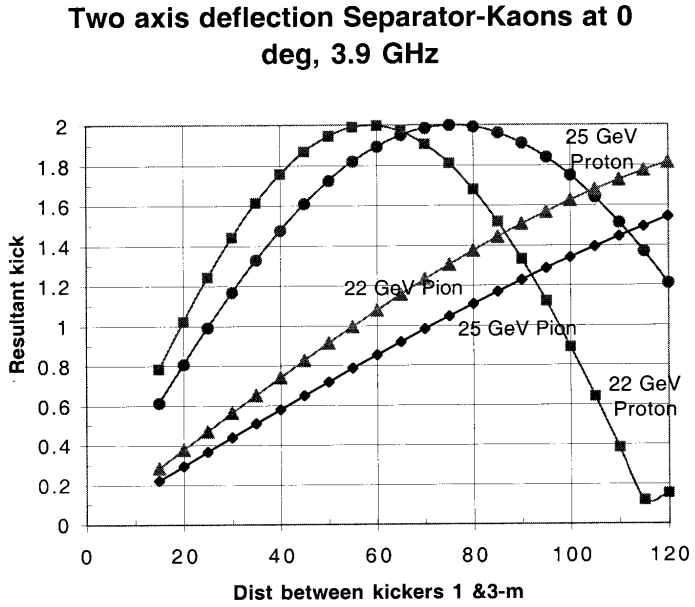

Figure A.4: Two degree of freedom deflection, 3.9 GHz.

One of us (J. D.) has run preliminary simulations that illustrate the behavior with a particle distribution. In Fig. A.5 the angular acceptance at the target has been limited to ± 2 mrad; the upper part of the figure shows kaons straight ahead in an x-y plot; the lower part shows the pions. Fig. A.6 is carried out for the larger angular acceptance of the base design. Other parameters are typical of the base design.

It is felt that further examination of the two-axis approach is worthwhile.

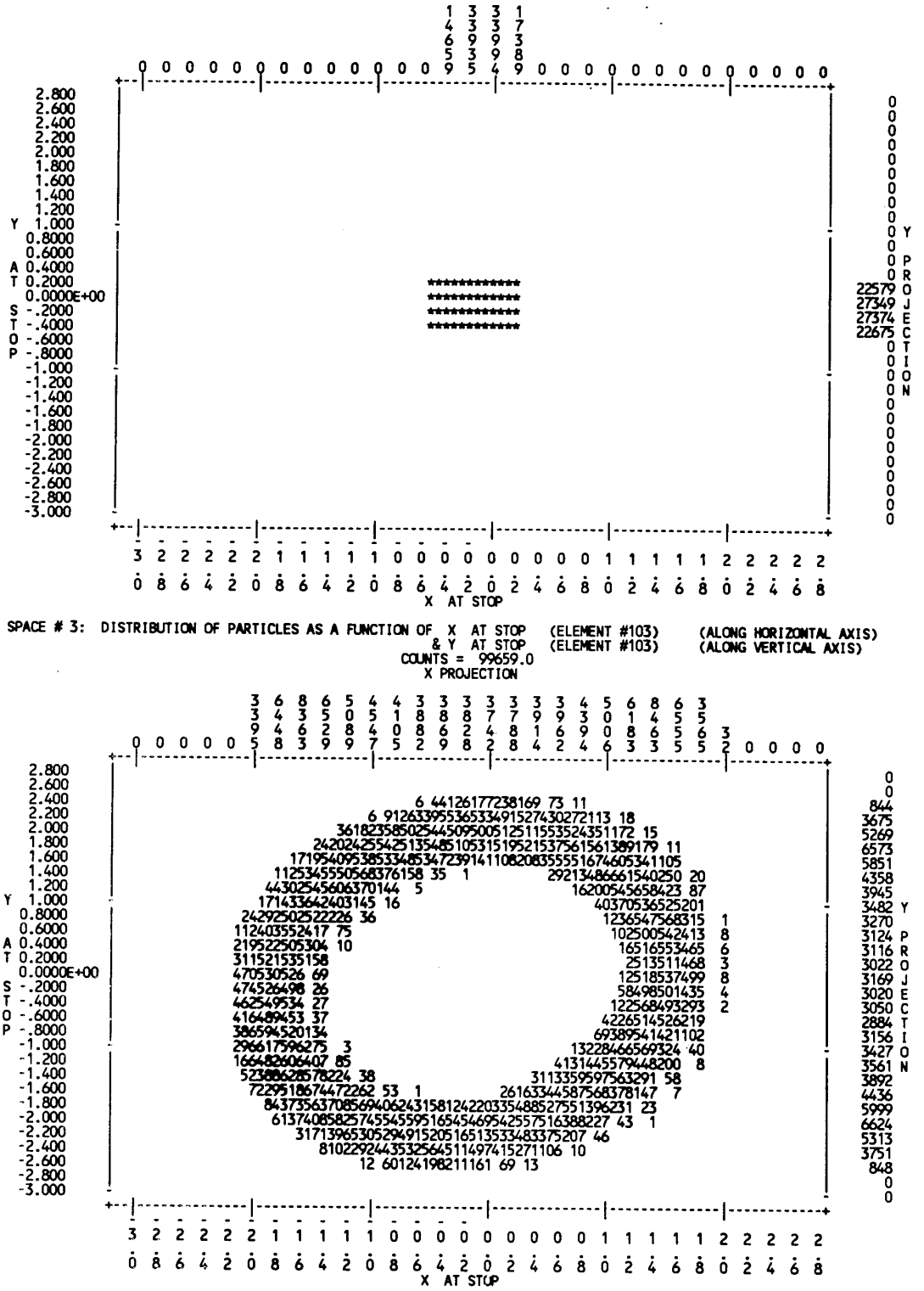

Figure A.5: Transvserse position distributions for kaons (upper) and pions (lower) at stopper position for reduced angular acceptance at target.

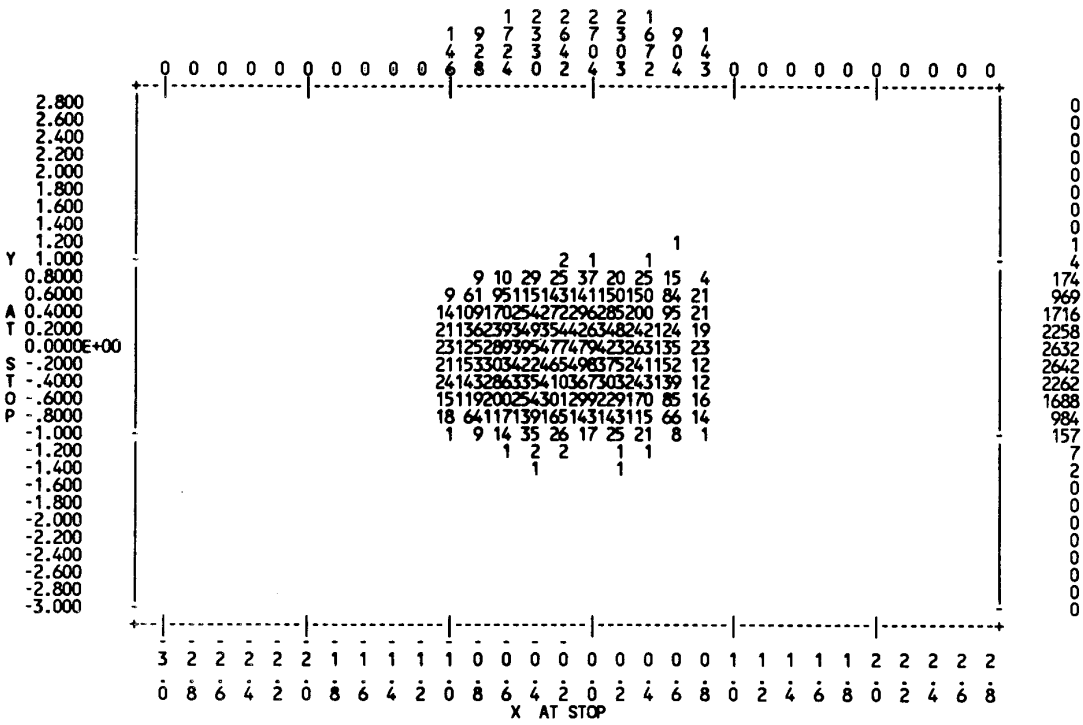

SPACE # 3: DISTRIBUTION OF PARTICLES AS A FUNCTION OF X AT STOP (ELEMENT #103) (ALONG HORIZONTAL AXIS)
& Y AT STOP (ELEMENT #103) (ALONG VERTICAL AXIS)
COUNTS = 15019.0
X PROJECTION

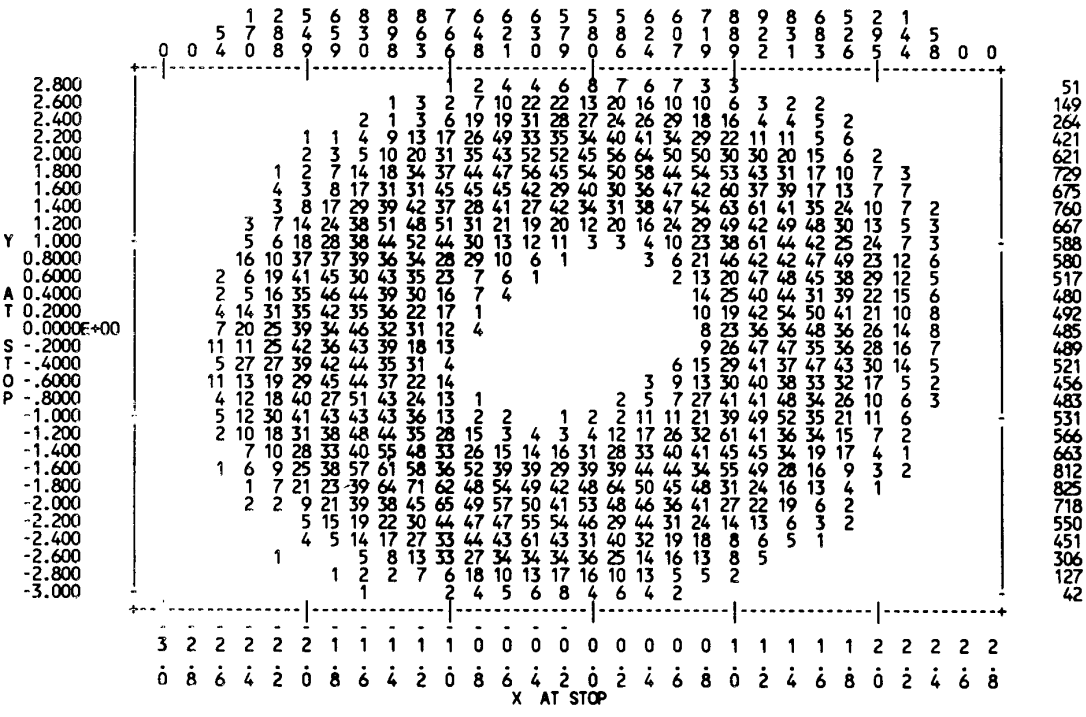

Figure A.6: Transvserse position distributions for kaons (upper) and pions (lower) at stopper position for nominal angular acceptance at target.

A.2 Urmel Output and MathCad Analysis for 3.9 GHz Cavity

Urmel input file 121

```
$file  lsav=.t., itest=0, lrec=.f., lplo=.t.  $end
3.9 GHz 1-cell no beam pipe boun 121
 $boun  izl=1, izr=2  $end
 $mesh  npmax=20000  $end
 #cavityshape
0.00
0.000  0.000
0.04719 0.00
-1, -0.0136
0.035465 0.013470
0.017854 0.015922
-1, 0.00331
0.015 0.0192
0.00 0.0192
0.000 0.000
9999.  9999.
 $mode mrot=1, fup=20000., pfac0=0.01, pfac1=0.1 $end
 $plot lcavus=.t., lfle=.t., lflh=.t., modpl=1, nplot=50 $end
 $prin lhr=.t., lhfi=.t., lhz=.t., lez=.t.,lez2=.t.,ler=.t.,lefi=.
modpr=1 $end
```

```
1,2,1   { (IZL=1, IZR=2, MROT=1)

 summary of all modes found
 --------------------------
 mode #   frequency/mhz     accuracy

  1         3898.878         1.3E-02
  2         6186.510         9.6E-03
  3         7707.002         2.0E-02
  4        10601.433         1.6E-02
  5        10883.906         8.1E-03
  6        11735.726         8.0E-03
  7        12697.915         1.3E-02
  8        13231.262         1.4E-02
  9        13775.642         1.7E-02
 10        14513.815         2.5E-02
 11        15666.807         2.0E-02
 12        15881.462         3.2E-02
 13        17229.137         2.5E-02
 14        17719.844         2.0E-02
 15        18473.004         1.6E-02
1++++++++++++++++++++++++++++++++++++++++++++++++++++++++++++++
 ++++++++++++++++++++++++++++++++++++++++++++++++++++++++++++++
 ++ results for the actual cavity as input to urmel +-
 ++ ***** not assuming any half cell symmetry ***** +-
 ++++++++++++++++++++++++++++++++++++++++++++++++++++++++++++++
 ++ mode type                =   1-em- 1             +-
 ++ frequency of mode        =   3898.878     mhz    +-
 ++ frequency/cut-off frequ. =  0.6657231            +-
 ++ wave length of mode      =  0.7689199E-01 m      +-
 ++ beam pipe cutoff te/tm   =  5857./*****   mhz    +-
 ++++++++++++++++++++++++++++++++++++++++++++++++++++++++++++++
 ++ particle speed b(beta)   =   1.000000            +-
 ++ int.(    ez           )dz=  0.1746822     v      +-
 ++ int.(    ez*cos(k*z/b))dz=  0.1165268     v      +-
 ++ int.(    ez*sin(k*z/b))dz=  0.1083852     v      +-
 ++ total stored field energy=  0.1342285E-13 vas    +-
 ++ k0    (=v*v/4*energy)    =  0.4716929     v/pc   +-
 ++ voltage taken at      r0 =  0.1499999E-01 m      +-
 ++ skin depth               =  0.1058367E-05 m      +-
 ++ q with all end plates    =      9501             +-
 ++ q without left  end plate=     14508             +-
 ++ q without right end plate=      9501             +-
 ++ q without both end plates=     14508             +-
 ++ p with all end plates    =  0.3460665E-07 w      +-
 ++ p without left  end plate=  0.2266352E-07 w      +-
 ++ p without right end plate=  0.3460665E-07 w      +-
 ++ p without both end plates=  0.2266352E-07 w      +-
 ++++++++++++++++++++++++++++++++++++++++++++++++++++++++++++++


 ++ full cell results  -  assuming p=v*v/2/rs  and  ++
 ++ that the input is the right half of a full cell ++
 ++++++++++++++++++++++++++++++++++++++++++++++++++++++++++++++
 ++ frequency                =   3898.878     mhz    ++
 ++ frequency/cut-off frequ. =  0.6657231            ++
 ++ voltage taken at     r0  =  0.1499999E-01 m      ++
 ++ k0    (=v*v/4*energy)    =  0.5057978     v/pc   ++
 ++ shunt impedance at r=r0  =  0.5991347     mohm   ++
 ++ (r/q)           at r=r0  =   41.29405     ohm    ++
 ++ (r/q)'=(r/q)/(k*r0)**2m  =   27.48576     ohm    ++
 ++ q without end plates     =     14508             ++
 ++++++++++++++++++++++++++++++++++++++++++++++++++++++++++++++
 ++++++++++++++++++++++++++++++++++++++++++++++++++++++++++++++

1quantity=er    scale= 1.86528E-02  dimension=v/m
1quantity=efi   scale= 5.15582E-03  dimension=v/m
1quantity=ez    scale= 1.94290E-02  dimension=v/m
1quantity=hr    scale= 5.41189E-05  dimension=a/m
1quantity=hfi   scale= 2.38878E-05  dimension=a/m
1quantity=hz    scale= 8.00659E-05  dimension=a/m
```

```
1,1,1   { (IZL=1, IZR=1, MROT=1)

 summary of all modes found
 --------------------------
 mode #   frequency/mhz     accuracy

  1         4102.236         5.5E-03
  2         7379.989         7.1E-03
  3         9013.504         7.7E-03
  4        10451.584         9.1E-03
  5        11414.814         5.8E-03
  6        11625.844         7.7E-03
  7        13144.903         4.4E-03
  8        13496.098         6.7E-03
  9        13586.391         7.2E-03
 10        15618.182         8.3E-03
 11        15991.607         9.5E-03
 12        16112.878         7.1E-03
 13        16717.930         1.3E-02
 14        18406.498         3.6E-02
 15        18406.498         3.6E-02
1++++++++++++++++++++++++++++++++++++++++++++++++++++++++
 ++++++++++++++++++++++++++++++++++++++++++++++++++++++++
 ++ results for the actual cavity as input to urmel +
 ++ ***** not assuming any half cell symmetry ***** +
 ++++++++++++++++++++++++++++++++++++++++++++++++++++++++
 ++ mode type                  =   1-ee- 1             +
 ++ frequency of mode          =   4102.236     mhz    +
 ++ frequency/cut-off frequ.   =  0.7004460            +
 ++ wave length of mode        =  0.7308026E-01 m      +
 ++ beam pipe cutoff te/tm     =  5857./*****   mhz    +
 ++++++++++++++++++++++++++++++++++++++++++++++++++++++++
 ++ particle speed b(beta)     =   1.000000            +
 ++ int.(    ez           )dz=  0.2076258     v      +
 ++ int.(    ez*cos(k*z/b))dz=  0.1423894     v      +
 ++ int.(    ez*sin(k*z/b))dz=  0.1245312     v      +
 ++ total stored field energy=  0.2250677E-13 vas    +
 ++ k0     (=v*v/4*energy)     =  0.3974666     v/pc   +
 ++ voltage taken at       r0 =  0.1499999E-01 m      +
 ++ skin depth                 =  0.1031801E-05 m      +
 ++ q with all end plates      =     10285              +
 ++ q without left  end plate=     18029              +
 ++ q without right end plate=     10739              +
 ++ q without both end plates=     19472              +
 ++ p with all end plates      =  0.5639914E-07 w      +
 ++ p without left  end plate=  0.3217524E-07 w      +
 ++ p without right end plate=  0.5401579E-07 w      +
 ++ p without both end plates=  0.2979189E-07 w      +
 ++++++++++++++++++++++++++++++++++++++++++++++++++++++++
 ........................


 ++ full cell results  -  assuming p=v*v/2/rs  and  ++
 ++ that the input is the right half of a full cell ++
 ++++++++++++++++++++++++++++++++++++++++++++++++++++++++
 ++ frequency                  =   4102.236     mhz    ++
 ++ frequency/cut-off frequ.   =  0.7004460            ++
 ++ voltage taken at      r0   =  0.1499999E-01 m      ++
 ++ k0     (=v*v/4*energy)     =  0.4504143     v/pc   ++
 ++ shunt impedance at r=r0    =  0.6805456     mohm   ++
 ++ (r/q)             at r=r0  =   34.94956     ohm    ++
 ++ (r/q)'=(r/q)/(k*r0)**2m    =   21.01358     ohm    ++
 ++ q without end plates       =     19472              ++
 ++++++++++++++++++++++++++++++++++++++++++++++++++++++++
 ++++++++++++++++++++++++++++++++++++++++++++++++++++++++

1quantity=hr    scale= 4.01929E-05  dimension=a/m
1quantity=hfi   scale= 3.28248E-05  dimension=a/m
1quantity=hz    scale= 2.42314E-05  dimension=a/m
```

```
1,2,0   { (IZL=1, IZR=2, MROT=0)

 summary of all modes found
 --------------------------
 mode #   frequency/mhz     accuracy

  1         2820.710         1.1E-02
  2         6207.518         1.2E-02
  3         9264.749         5.2E-03
  4        11186.189         4.1E-03
  5        11946.059         2.8E-03
  6        13416.229         2.6E-03
  7        14614.538         7.5E-03
  8        15921.156         8.7E-03
  9        17235.932         2.6E-03
 10        18638.850         1.4E-03
 11        19863.488         1.1E-03
 12        20133.268         1.1E-03
 13        21408.758         1.2E-03
 14        21881.635         3.9E-03
 15        22693.156         6.2E-03
1++++++++++++++++++++++++++++++++++++++++++++++++++++++++++
 ++++++++++++++++++++++++++++++++++++++++++++++++++++++++++
 ++ results for the actual cavity as input to urmel ++
 ++ ***** not assuming any half cell symmetry ***** ++
 ++++++++++++++++++++++++++++++++++++++++++++++++++++++++++
 ++ mode type                 =   tm0-em- 1           ++
 ++ frequency                 =   2820.710     mhz    ++
 ++ frequency/cut-off frequ.  =  0.3687441            ++
 ++ wave length of mode       =  0.1062826     m      ++
 ++ beam pipe cutoff tm-mode  =   7649.505     mhz    ++
 ++++++++++++++++++++++++++++++++++++++++++++++++++++++++++
 ++ particle speed b (b=beta)=   1.000000      c0     ++
 ++ int.(    ez           )dz=  -7016.583      v      ++
 ++ int.(    ez*cos(k*z/b))dz=  -6152.327      v      ++
 ++ int.(    ez*sin(k*z/b))dz=  -2786.341      v      ++
 ++ total stored field energy=  0.5581658E-04 vas    ++
 ++ k0       (=v*v/4*energy) =  0.2043068      v/pc   ++
 ++ voltage taken at     r0  =         0.      m      ++
 ++ skin depth               =  0.1244305E-05 m      ++
 ++ q with all end plates    =      8211              ++
 ++ q without left  end plate=     14665              ++
 ++ q without right end plate=      8211              ++
 ++ q without both end plates=     14665              ++
 ++ p with all end plates    =   120.4701      w      ++
 ++ p without left  end plate=   67.45233      w      ++
 ++ p without right end plate=   120.4701      w      ++
 ++ p without both end plates=   67.45233      w      ++
 ++++++++++++++++++++++++++++++++++++++++++++++++++++++++++


 ++ full cell results  -  assuming p=v*v/2/rs  and  ++
 ++ that the input is the right half of a full cell ++
 ++++++++++++++++++++++++++++++++++++++++++++++++++++++++++
 ++ frequency                 =   2820.710     mhz    ++
 ++ frequency/cut off frequ.  =  0.3687441            ++
 ++ voltage taken at     r0   =         0.     m      ++
 ++ k0       (=v*v/4*energy)  =  0.3390670     v/pc   ++
 ++ shunt impedance at r=r0   =  0.5611537     mohm   ++
 ++ r/q             at r=r0   =   38.26284     ohm    ++
 ++ q without end plates      =     14665              ++
 ++ peak surface e field at r=  0.1752469E-01 m      ++
 ++                      and z=  0.1581054E-01 m      ++
 ++ peak field strength there=   857937.6     v/m    ++
 ++ ratio peak/effecitve      =   2.677427            ++
 ++ peak surface h field at r=  0.3557355E-01 m      ++
 ++                      and z=  0.1336137E-01 m      ++
 ++ peak field strength there=   1136.058     a/m    ++
 ++++++++++++++++++++++++++++++++++++++++++++++++++++++++++
 ++++++++++++++++++++++++++++++++++++++++++++++++++++++++++
1quantity=er    scale= 8.44781E+02  dimension=v/m
1quantity=ez    scale= 9.26394E+02  dimension=v/m
1quantity=hfi   scale= 1.19152E+00  dimension=a/m
```

This program is to compute and understand URMEL outputs
and to get to superconducting paramaters

The 1st example will be Tm110 izl=1, izr=2 π mode with no pipes

Half cell results

constants

$c := 2.99792 \cdot 10^{8}$ m/sec

$\sigma := 5.8 \cdot 10^{7}$ a/vm [1/ohm-m] conductivity of Cu

$\mu := 4 \cdot \pi \cdot 10^{-7}$

Urmel inputs from half cell

$f := 3898.878 \cdot 10^{6}$ Hz freq of mode

$f\_over\_fco := 0.6657331$

$int\_ez\_dz := 0.1746822$ v

$int\_ez\_cos\_dz := 0.1165268$ v

$int\_ez\_sin\_dz := 0.1083852$ v

cos=cos(k*z/β), etc

define

$IEz := int\_ez\_dz$

$IEzC := int\_ez\_cos\_dz$

$IEzS := int\_ez\_sin\_dz$

intergrals of grad along z

$U := 0.1342285 \cdot 10^{-13}$ v·a·s [joules] stored field energy in 1/2 cell

$r0 := 0.015$ m radius at which voltage taken, Iris radius

$Q := 14508$ Q without end plates

These inputs come from detailed Urmel maps
Find Epeak and Hpeak and do scaleing

Epeak := ■ grid nr=219, nz=89

$Hpeak\_rad := 5.4 \cdot 10^{-2} \cdot 1$ @ r=77, z=75 [a/m]

$Hpeak\_azm := 2.39 \cdot 10^{-2} \cdot$ ■ @ r=195, z=0

$Hpeak\_z := 8.01 \cdot 10^{-2} \cdot 0.45$ @r=>78, z=~70

Misc derived parameters
Urmel results marked **

$\omega := 2\cdot\pi\cdot f$ $\omega = 2.44974\cdot 10^{10}$ rad/sec

** $\lambda := \frac{c}{f}$ $\lambda = 7.68919\cdot 10^{-2}$ m wave length of f

$L := \frac{\lambda}{2}$ $L = 0.03845$ m π mode cell length

$ncell := \frac{1}{L}$ $ncell = 26.01055$ m-1 number cells/m

$k := 2\cdot\frac{\pi}{\lambda}$ $k = 81.71457$ m-1 k=ω/c wave number

** $\delta := \sqrt{\left(\frac{2}{\mu\cdot\sigma\cdot\omega}\right)}$ $\delta = 1.05837\cdot 10^{-6}$ m skin depth Cu

$Rsur := \frac{1}{\delta\cdot\sigma}$ $Rsur = 0.01629$ ohm surface resistance Cu

$fco := \frac{f}{f\_over\_fco}$ $fco = 5.85652\cdot 10^{9}$ Hz cutoff freq

** $k0hc := \frac{\left(IEzC^2 + IEzS^2\right)}{4\cdot U}$ $k0hc = 4.71693\cdot 10^{11}$ v/as=v/coulomb

Q=U/P/ω Stored energy/power per omega
P=V^2/Rs = V^2/2Rsu where Rs, shunt resist, Rsu Urmel Rs
P=U*ω/Q

** $Phc := U\cdot\frac{\omega}{Q}$ $Phc = 2.26651\cdot 10^{-8}$ watts/half cell

Full cell results Voltage taken at r0=iris

$Ucell := 2 \cdot U$ $Pcell := 2 \cdot Phc$

** $k0fc := \frac{(2 \cdot IEzC)^2}{2 \cdot 4 \cdot U}$ $k0fc = 5.05798 \cdot 10^{11}$ v/coulomb

$Rs := \frac{(2 \cdot IEzC)^2}{2 \cdot Phc}$ $Rs = 1.19819 \cdot 10^{6}$ ohm/cell @r0 shunt resist

** $Rsu := \frac{Rs}{2}$ $Rsu = 5.99094 \cdot 10^{5}$ ohm/cell @r0 Urmel

$ROQ := \frac{Rs}{Q}$ $ROQ = 82.58808$ ohm/cell @r0

** $RuOQ := \frac{Rsu}{Q}$ $RuOQ = 41.29404$ ohm/cell @r0 Urmel

Transverse Kick Panofsky Wenzel

$ROQtrans := \frac{ROQ}{(k \cdot r0)^2}$ $ROQtrans = 54.97129$ ohm/cell

** $RuOQtrans := \frac{RuOQ}{(k \cdot r0)^2}$ $RuOQtrans = 27.48564$ ohm/cell

P*Rs_trans=Vtrans^2, P/ω=U/Q=U*ROQprime/Rs_tra

$Pcell \cdot Rs\_trans := Vtrans^2 \square \quad \frac{P}{\omega} := \frac{U}{Q} \square \frac{U}{Q} := U \cdot \frac{ROQtrans}{Rs\_trans} \square$

$Vtrans^2 := \omega \cdot Ucell \cdot ROQtrans \square$

$Vtrans := \sqrt{(\omega \cdot Ucell \cdot ROQtrans)}$ $Vtrans = 0.19014$ volts/cell @ U*2 specified

$vtran\_per\_m := Vtrans \cdot \frac{2}{\lambda}$ $vtran\_per\_m = 4.94555$ v/m

$Ucell = 2.68457 \cdot 10^{-14}$ joules/cell

OR also

$vtrans := 2 \cdot \frac{IEzC}{k \cdot r0 \cdot L}$ $vtrans = 4.94555$ v/m

Find Epeak and Hpeak and do scaleing to find operating gradient

Epeak :=

Hpeak_rad = 0.054 @ r=77, z=75 [a/m] grid nr=219, nz=89

Hpeak_azm = @ r=195, z=0

Hpeak_z = 0.03605 @r=>78, z=~70

$Hpeak\_surface := \sqrt{(Hpeak\_rad)^2 + (Hpeak\_z)^2}$ @ r=77, z=75

Hpeak_surface = 0.06492 this is peak field for the Urmel voltage and energy

We want to find scale factor for 1000gauss

$Hmax := \frac{0.1}{4 \cdot \pi \cdot 10^{-7}}$ $Hmax = 7.95775 \cdot 10^4$ Tesla Peak design H field

$F := \frac{Hmax}{Hpeak\_surface}$ $F = 1.22569 \cdot 10^6$

$Etrans := Vtrans \cdot \frac{F}{L}$ $Etrans = 6.06169 \cdot 10^6$ V/m kick

$W := Ucell \cdot \frac{F^2}{L}$ W = 1.04902 joules/m@grad

Try again Max field 1000 gauss $4 \cdot \pi \cdot 10^{-7} \cdot 10^4 = 0.01257$
H[a/m]*0.0125 -> B[gauss]

$Fnew := \frac{1000}{Hpeak\_surface} \cdot \frac{1}{0.01257}$ $Fnew = 1.22533 \cdot 10^6$

Surface resistance and Skin depth

$\sigma = 5.8 \cdot 10^7$ a/vm [1/ohm-m] conductivity of Cu

$\mu := 4 \cdot \pi \cdot 10^{-7}$

$\delta := \sqrt{\left(\frac{2}{\mu \cdot \sigma \cdot \omega}\right)}$ $\delta = 1.05837 \cdot 10^{-6}$ m skin depth

$Rsur := \frac{1}{\delta \cdot \sigma}$ $Rsur = 0.01629$ ohm surface resistance Cu

Geometry factors

P Wilson acc mode pg462 Cu cavities $L := \frac{\lambda}{2}$ $T := \left[\frac{\sin\left(\pi \cdot \frac{L}{\lambda}\right)}{\pi \cdot \frac{L}{\lambda}}\right]$

G1=Q*Rsur Q~ 1/ω^1/2

r/Q=ROQ/L=V^2/ωUL=G2*T^2/λ ~ω

r=R/L=V^2/P*L=G1*G2*T^2/(λ*Rsur) ~ω^1/2

$Q = 1.4508 \cdot 10^{4}$ $ROQtrans = 54.97129$ $T = 0.63662$

$G1 := Q \cdot Rsur$ $G1 = 236.34327$ ohm $\lambda = 0.07689$

$rOQtrans := \frac{ROQtrans}{L}$ $rOQtrans = 1.42983 \cdot 10^{3}$ ohm/m π mode cell length

$G2Tsq := ROQtrans \cdot 2$ $G2Tsq = 109.94258$ ohm

$g2tsq := rOQtrans \cdot \lambda$ $g2tsq = 109.94258$ $G2 := \frac{G2Tsq}{T^2}$ $G2 = 271.27244$ ohm

$G1G2Tsq := G1 \cdot G2Tsq$ $G1G2Tsq = 2.59842 \cdot 10^{4}$ ohm^2

$rtrans := \frac{G1G2Tsq}{\lambda \cdot Rsur}$ $rtrans = 2.0744 \cdot 10^{7}$ ohm/m for Cu

surface resistance superconducting

$Tc := 9.2$ K

@ Tc/T of 2 Rsur= 700 to 1000*10^-9 ohm for f=1.3*10^9
Rbcs=Aω^2/Tsc*e^(-1.76Tc/Tsc) TeslaLC pg 299

if $Tsc := .5\ Tc$ $Tsc = 4.6$ $TcOT := \frac{Tc}{Tsc}$ $TcOT = 2$

$exp := e^{-1.76\cdot\frac{Tc}{Tsc}}$ $exp = 0.0296$

We want to find A for 1.3GHz data

$$Rbcs(\omega sc, Tsc) := \frac{A\cdot\omega sc^2\cdot e^{-1.76\cdot\frac{Tc}{Tsc}}}{Tsc}$$

for TcOT of 2

$Rbcs := 800\cdot10^{-9}$ ohm

$fsc := 1.3\cdot10^9$

$\omega sc := 2\cdot\pi\cdot fsc$ $\omega sc = 8.16814\cdot10^9$

Find A

$A := Rbcs\cdot\frac{Tsc}{\omega sc^2\cdot exp}$ $A\cdot10^{20} = 1.86345\cdot10^{-4}$

$$Rbcs(fsc, Tsc) := \frac{A\cdot(2\cdot\pi\cdot fsc)^2\cdot e^{-1.76\cdot\frac{Tc}{Tsc}}}{Tsc}$$

find Rbcs(2K) at 1.3 GHz

$Rbcs(1.3\cdot10^9, 2) = 1.89446\cdot10^{-8}$

$Rbcs(3.9\cdot10^9, 2) = 1.70502\cdot10^{-7}$

$Tsc := 1, 1.25 .. 9$

$Rsur\_sc := Rbcs(3.9\cdot10^9, 2)$

$Rres(Tsc) := 3\cdot10^{-9}$

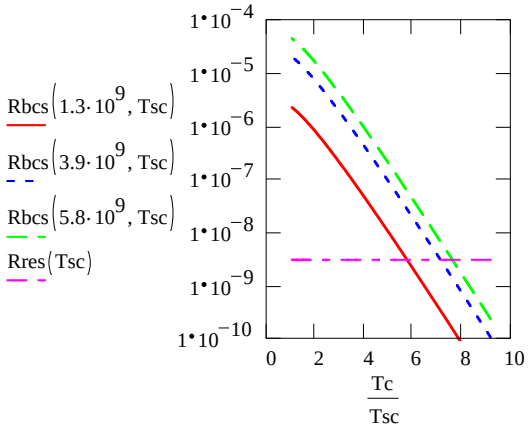
Rbcs(1.3·10^9, Tsc)
Rbcs(3.9·10^9, Tsc)
Rbcs(5.8·10^9, Tsc)
Rres(Tsc)
1•10^−4
1•10^−5
1•10^−6
1•10^−7
1•10^−8
1•10^−9
1•10^−10
0
2
4
6
8
10
Tc
Tsc

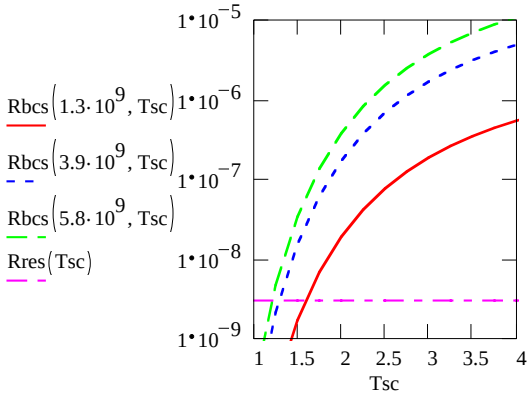
Rbcs(1.3·10^9, Tsc)
Rbcs(3.9·10^9, Tsc)
Rbcs(5.8·10^9, Tsc)
Rres(Tsc)
1•10^−5
1•10^−6
1•10^−7
1•10^−8
1•10^−9
1
1.5
2
2.5
3
3.5
4
Tsc

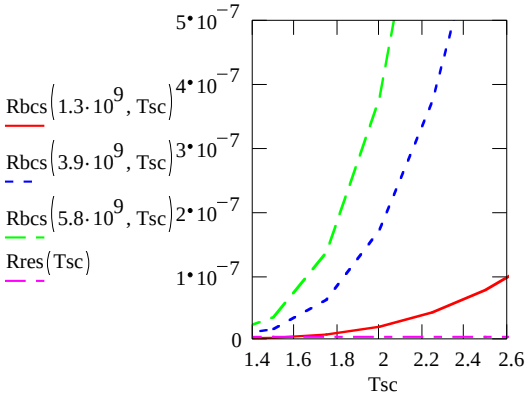
Rbcs(1.3·10^9, Tsc)
Rbcs(3.9·10^9, Tsc)
Rbcs(5.8·10^9, Tsc)
Rres(Tsc)
5•10^−7
4•10^−7
3•10^−7
2•10^−7
1•10^−7
0
1.4
1.6
1.8
2
2.2
2.4
2.6
Tsc

Get scrf parameters

$$Qsc := \frac{G1}{Rsur\_sc} \qquad Qsc = 1.38616 \cdot 10^{9}$$

$$Psc := W \cdot \frac{\omega}{Qsc} \qquad Psc = 18.53904 \qquad \text{watts/m @6 MV/m}$$

$$Pmachan := \frac{\left(5 \cdot 10^{6}\right)^{2}}{2 \cdot 715 \cdot 3.9 \cdot 10^{9}} \qquad Pmachan = 4.4827$$

$$Psc\_2 := \frac{\left(6.06 \cdot 10^{6}\right)^{2}}{\frac{ROQtrans}{L} \cdot Qsc} \qquad Psc\_2 = 18.52871$$

So 60MV deflection would need ~200 w*DF

Beam loss might be ~10^9/pulse or 1.6*10^-10amp
Power 25*10^9*1.6*10^-10= ~4w*DF

Cavity coupling $\omega 0 := 2 \cdot \pi \cdot 4.1022 \cdot 10^{9}$

$\omega = 2.44974 \cdot 10^{10}$ $\omega 0 = 2.57749 \cdot 10^{10}$

$$Kcup := \frac{\omega 0 - \omega}{\left(\frac{\omega 0 + \omega}{2}\right)} \qquad Kcup = 0.05082$$

A.3 Niobium Material Specifications

In metals at low temperatures the main contribution to thermal conductivity comes from the same electrons responsible for the electrical conductivity. Hence the Wiedemann-Franz-Lorenz Law relating them:

$$\bullet \times \text{‰} = L \times T$$

where • is the thermal conductivity, ‰ is the electrical resistivity, T is the absolute temperature and L = 2:443 $\times 10^{-8}$ V^2 K^{-2} is the Lorenz constant. These electrons are scattered by impurity atoms, lattice defects and phonons. At temperatures below 10 K the phonon population is negligible compared with the free electron quasiparticle population. So for metals at these temperatures impurities and defects (in which we include the boundaries between single crystallites) are the main determinants of the electrical resistivity and thermal conductivity. Alloys being "all defects" have such a high electrical resistivity that the phonon scatterers do not contribute much even at room temperature (300 K) hence stainless steel has low thermal conductivity and its RRR (ratio of electrical resistivity at 273 K to the electrical resistivity at 4 K) is only 1.4. Since the strength of a metallic element increases with its density of defects high thermal conductivity correlates with low strength. We use the RRR of a metallic element as an indicator of its thermal conductivity at low temperature.

For superconducting resonators high thermal conductivity is important so that the heat generated in the inner surface diffuses rapidly to the outer surface (which is in contact with liquid helium) preventing the resonator temperature from warming up. Also important is the microscopic uniformity and smoothness of the inner surface so that it can withstand the very high RF electric fields without field emission of electrons and the possible consequent electric breakdown. On the other hand, the external surface can benefit from some roughness that increases the actual surface in contact with the liquid helium reducing the effect of the Kapitza resistance. This thermal resistance reflects a temperature discontinuity between the solid and the liquid at the contact surface due to an acoustic mismatch.

Therefore the sheets of Niobium used in these resonators are specified for purity, defect free surface and bulk (since the surface etching process it undergoes exposes new surfaces from the bulk), RRR and grain size. The grain size reflects the size of the single crystals forming the metal. As indicated above smaller grain size corresponds to higher tension strength. An optimum combination might exist since the boundaries of the grains scatter electrons like defects and lower the RRR when they are the predominant type of defect.

Commercial standards for sheets of Niobium are described in the ASTM Specification B393-84 where reactor grade unalloyed niobium is referred to as R04200-Type 1. Individual laboratories have written their own specifications in which they include among others: chemical purity, RRR, yield strength, elongation, degree of recrystalization, grain size and surface finish. In what follows we present tables comparing specifications from DESY, CEBAF, some material purchased by Fermilab from Teledyne Wah Chang as well as from Cornell U.

Tab. A.1 presents a comparison of chemical purity specifications.

In the CEBAF specification designated RRR grade the RRR is required to be larger than 250, and no RRR requirements are made for the "reactor grade I. The DESY specifications also calls for two types: the "RRR 300 for which the aim is an RRR larger than 300 with a guaranteed minimum of 260 and the type "RRR 40 for structural (as opposed to current carrying) parts with a guaranteed minimum RRR of 40. The ASTM B393 specification has no RRR requirements

Metallurgical specifications involve grain sizes and degree of recrystallization. They are relevant for the press forming operations. So they refer to the material prior to their forming and incorporation into the cavity, since the electron beam welding and the heat treatments that follow it will change them. They are summarized in Tab. A.2.

Ultimate tensile strength, Yield strengths (0.2% offset) and Elongation in 1-in. gauge length are part of the ASTM B393 specification, which specify the minimum values 18 ksi,12 ksi and 25%

Table A.1: Niobium purity specifications.

Table I. Niobium Purity Specifications (ppm) by weight								
	ASTM-B393	DESY	(May 93)		CEBAF	890511	Wah Chang	Cornell
	R04200			(M.Foley)	reactor	RRR	980626	961025
		goal	guaranteed	RRR 300	grade I	grade	@FNAL	
C	100.0			10.0	50.0	25.0	30.0	50.0
N	100.0	5.5	40.0	10.0	50.0	10.0	20.0	50.0
O	150.0	20.0	40.0	10.0	*200.0*	25.0	50.0	200.0
H	15.0	1.3	5.0	2.0	*20.0*	*10.0*	3.0	10.0
Zr	200.0						50.0	
Ta	1,000.0	400.0	1,000.0	500.0	1,000.0	500.0	100.0	1,000.0
Fe	50.0	20.0	30.0	30.0	50.0	50.0	40.0	50.0
Si	50.0	20.0	30.0	30.0	50.0	50.0	50.0	50.0
W	300.0	50.0	70.0	70.0	100.0	100.0	30.0	100.0
Ni	50.0			30.0	*0.0*	20.0	20.0	
Mo	100.0	20.0	50.0	50.0	50.0	50.0	30.0	50.0
Hf	200.0						50.0	
Ti		10.0	50.0	50.0	40.0	10.0		30.0
Y						*2.0*		
B	2.0							
Al	20.0							
Be	50.0							
Cr	20.0							
Co	20.0							
other metals (each)					*30.0*	*20.0*		20.0

Table A.2: Grain size.

Table II. Grain size Specification								
	ASTM-B393	DESY		CEBAF			Wah Chang	Cornell
	R04200	(May 93)	(H. Kaiser)	(890511)			(980626)	(961025)
				reactor gradeI		RRR grade	@FNAL	
Material thickness				< .25"	>= .25"			
Minimum degree of recrystallization	> 90%			> 90%	> 70%	>90%		95%
Average grain size ASTM		#6 or finer	#6.5-#8.5	#6 or finer	#3 or finer	#5 or finer	#4 or finer	#6
Maximum grain size ASTM		local #4-#5		#3		#3		
grain size distribution		homogeneous					aim for uniform grain size	
Temper condition	Annealed	Deep drawing quality						

respectively. The DESY specification calls for these parameters to have the values >80 N/mm^2, >50 N/mm^2 and 30% also specifying a Young modulus (90 kN/mm^2. The CEBAF specifications do not mention Ultimate tensile strength but require the same Elongation of >25% and Yield strengths (0.2% offset) of 10.7 ksi and 12 ksi for the "RRR Grade and "Reactor Grade I respectively. This is summarized in Tab. A.3.

Table A.3: Mechanical properties.

Table III. Mechanical Properties								
					*expected values translated to practical units			
		ASTM-B393	DESY	(May 93)	CEBAF	(890511)	Wah Chang	Cornell
		R04200		(H.Kaiser)*	reactor grade I	RRR grade	(980626)	(961025)
Ultimate Tensile Strength	Kpsi	>18	>11.6	25.4			>18	>20
Yield Strength (0.2% offset)	Kpsi	>12	>7.2	7.7	>12	>10.7	>10.5	
Elongation in 1-in. gauge length		>25%	30%	54%	>25%	>25%	>25%	>60%
Young Modulus	Mpsi		>13	14				

Very relevant for the sheets to be formed the half-cells of the cavities is the surface condition. Again different laboratories specified them differently and the ASTM-B393 are not very specific about them.

DESY's specification[A.2] includes sentences on Fabrication and Treatment, Surface Quality, Mechanical Tolerances of the Final Product, Acceptance Tests and Defects. The inside surface (RF side) should have roughness ≤ 10 „m and be free of defects and contamination fingerprints, grease). Cracks, scratches, marks, shrink holes, blisters, oxide clusters, extraneous materials are considered defects if larger than 10 „m (RF side) or 50 „m (back side). Another specification[A.3] deals mostly with the fabrication of the resonators.

The CEBAF specifications[A.4,A.5] for both grades are identical with respect to surface finish, requiring it to be free of defects and with a metalic "as etched" finish without being quantitative.

The Wah Chang description[A.6] of the material sold to Fermilab just states that the surfaces must be free from scratches, blemishes and inclusions.

The Cornell U. Specification for Niobium Plate[A.7] describes the quality of finish by stating that the plate shall be free of injurious internal and external imperfections of a nature which would interfere in the manufacture of the drawn part and that the plate shall be shipped in the "surface etched" condition.

A.4 Cavity Fabrication and Processing Comments

This appendix is a collection of notes on welding parameters, weld chamber preparation, material handling procedures, plastics, and grinding information.

Welding
Welding parameters have been developed at a number of Labs. The list below represents a compilation. Clearly test welds are necessary and these numbers should be considered only a starting point.

- Weld parameters

[A.2] A. Matheisen and D. Proch, *Technical Specification for Niobium Applied for the Fabrication of 1.3 GHz Superconducting Cavities*, May 1993–Version 6, Lab–Note MHF 1/93.
[A.3] H. Kaiser, *Specification for 11 Niobium Resonators for the TESLA Test Facility*, Lab–Note 2/93
[A.4] Specification 11111S0143 NIOBIUM (Reactor grade I) Revision 3, May 11, 1989
[A.5] Specification 11111S0144 NIOBIUM (RRR grade) Revision 4, May 11, 1989
[A.6] Material Description in Fermilab Procard purchase TL685 (PO 511467 of May 21, 1998
[A.7] Cornell Electron Storage Ring SPEC: JK-4, Oct. 25, 1996 revision.

  - Material thickness – 1.2 mm (48 mil) for 1.5 mm (62 mil) material after machining weld prep area
  - Beam power – $\approx 1.5 - 1.8$ kwatts (i..e., 30 ma @ 500 kV or equivalent
  - Defocused beam – focus is 0.1 mm below surface (from gun side)
  - Eliptical motion – 3 mm wide by 1.5 mm in direction of weld seam
  - Rotation rate of beam – 10 kHz
  - Circumferential weld velocity – 5-10 mm/sec in weld direction
- Weld chamber preparation
  - Silicone oil – No silicone products (pump oil or lubricant) are to be used.
  - Lubricant of mechanical parts – only vacuum grease should be used where necessary.
  - Cleaning of chamber and internal parts – the inside should be wiped with alcohol prior to welding.
  - Pressure during welding – less than 5×10^{-5} mbar (5×10^{-5} Torr)
  - Venting chamber – clean nitrogen gas should be used to vent chamber only after temperature of Nb part has dropped to below 100 C at hottest spot.
  - Weld shields – Nb (≈ 0.3 mm thickness) must be used around the joint being welded in order to prevent Nb vapor from contaminating other weld preparations.

Material handling, Plastics, and Grinding

- Parts should never be handled without clean and lint-free gloves(e.g., latex or nylon).
- No process (e.g., grinding) should take place on the parts at any stage of fabrication without being followed by a complete cleaning and etch cycle.
- Parts, tools and work area should be in dirt and dust free areas and/or containers.
- Teflon is to be avoided on any surface to be etched because of its stability. Also no silicone or silicone based products.
- Polyethylene (HPPE best, LPPE soft) containers and wrap are good for storage of cavities and sub assemblies. Also can be used in chemistry for flanges and covers.
- Flanges can be protected during storage and handeling with PVC caps. (But PVC has hydrocarbons and should be avoided for vacuum components and RF surfaces because of multipacting.)
- Grinding–For small areas use "cartax" a rubber disk with 240 grain or finer (e.g., 500) ($240 \times 240 \text{grains/mm}^2$ of carbide) For big area use carbide floppy wheel - same grain size.

A.5 Cavity Cost Estimate Details

Table cavity cost model									
material									
Nb reactor grade	thickness	size	cost est$each	# per 13c cavi	tot$		tot cost hiRRR(RGX3)		
half cells	0.062"	6x6"	75	26	1950				
		4.5x4.5	45	26	1170		3510		
end tubes	0.062"	4.5x4.5	45	2	90		270		
coupler tubes	"	0.75x2	4	4	16				
NbTi									
end flanges 2.75D	0.62"	2.75x2.75	70	2	140				
coupler flanges1.3D		1.5x1.5	20	4	80				
helium vess flanges5D		5x5	220	2	440				
					small	large	small		
TOT small and large tiles					1936	2716	**4456**	**Material ~5K$**	
Nb weld shields	0.015"	6x6	150	6	900	reusable			
welding									
estimate based on 5 to 6 min per weld									
5 welds per hour									
5 welds per pump down									
45 min pump down									
45 min cool down and vent									
tot of 2.5 hr per pump down									
each weld series needs a tack sequence and a weld sequence for a tot of 5 hr									
also 2 hr of setup									
rate 200$/hr welding, 120$/hr engineering									
tot 7hr sequence=~ 1240$/5welds									
	#/cavity	number welds	Tot welds						
dumbells(2 hc)	12	1	12						
equator welds	13	1	13						
end half cells_iris	2	1	2						
end tubes	2	7	14						
TOT welds per cavity			41		est cost 8 sequences		9920		
end tubes									
tube		1							
end flange		1							
heliun v flange		1							
coupler port		2							
coupler flange		2							
Alternative Weld	#/cavity	numb welds ea	numb/weld cyc	numb weld cyc	Tot welds				
12 dumbells from half cells	12	1	4	3	12				
3 4cell cav sections	3	3	3	3	9				
2 beam tubes	2	8	~4	5	16				
2 beam tubes to end half cell	2	1	2	1	2				
end assemb to cavity center	2	1	2	1	2				
				13	41				
			cost@1240/cy	16120			**expect welding ~10-16K$**		
Snee est									
		each	number/cav	tot		tooling	welding each	number/cav	tot weld
Machining									
half cell stamp & machine		320	26	8320		have?			
weld iris, ends						700	400	14	5600
weld equator						1500	200	13	2600
end tubes machine and weld ?				2500					2500
flanges									
small		350	4	1400					
medium		400	2	800					
large		1000	2	2000					
weld tubes to flang							200	8	1600
				15020		2200			12300

Summary	RRR long	RG short	long Cu	short Cu					
material	5	2	0	0					
machining	15	11	7	5					
welding	13	9	13	9					
tooling/exp	2	2	2	2					
ToT	**35**	**24**	**22**	**16**					
	expensive mac	exp mach							
RG mat,	2-2.7								